

UNIVERSIDADE FEDERAL DE ALAGOAS
CENTRO DE TECNOLOGIA
PROGRAMA DE PÓS-GRADUAÇÃO EM ENGENHARIA CIVIL

SALVATORE VERDE

**NON-SORTED GENETIC ALGORITHM OPTIMIZATION OF COST-EFFICIENT
SYNTHETIC MOORING SYSTEMS UTILIZING POLYMER SPRINGS FOR 15 MW
FLOATING WIND TURBINES IN RELATIVELY SHALLOW WATERS**

MACEIÓ-AL

2024

SALVATORE VERDE

**NON-SORTED GENETIC ALGORITHM OPTIMIZATION OF COST-EFFICIENT
SYNTHETIC MOORING SYSTEMS UTILIZING POLYMER SPRINGS FOR 15 MW
FLOATING WIND TURBINES IN RELATIVELY SHALLOW WATERS**

Tese de Doutorado apresentada ao Programa de Pós-Graduação em Engenharia Civil da Universidade Federal de Alagoas, como requisito parcial para obtenção do título de Doutor em Engenharia Civil.

Área de concentração: Estruturas e Materiais.

Orientador: Prof. Dr. Eduardo Nobre Lages

MACEIÓ-AL

2024

Catálogo na fonte
Universidade Federal de Alagoas
Biblioteca Central
Divisão de Tratamento Técnico

Bibliotecária: Helena Cristina Pimentel do Vale CRB-4/661

- V483n Verde, Salvatore.
Non-sorted genetic algorithm optimization of cost-efficient synthetic mooring systems utilizing polymer springs for 15 mw floating wind turbines in relatively shallow waters / Salvatore Verde. – 2024.
99 f. : il.
- Orientador: Eduardo Nobre Lages.
Tese (doutorado em Engenharia Civil) – Universidade Federal de Alagoas, Centro de Tecnologia, Maceió, 2024.
- Bibliografia: f. 95-99.
1. Turbinas eólicas flutuantes. 2. Linhas sintéticas. 3. Águas rasas. 4. Otimização multiobjetivo.
5. Molas de polímero. I. Título.

CDU: 621.5



**NON-SORTED GENETIC ALGORITHM OPTIMIZATION OF COST-EFFICIENT
SYNTHETIC MOORING SYSTEMS UTILIZING POLYMER SPRINGS FOR 15 MW
FLOATING WIND TURBINES IN RELATIVELY SHALLOW WATERS**

SALVATORE VERDE

Tese de doutorado submetida à banca examinadora do Programa de Pós-Graduação em Engenharia Civil da Universidade Federal de Alagoas e aprovada no dia 26 do mês de março do ano de 2024.

Banca Examinadora:

Documento assinado digitalmente
 **EDUARDO NOBRE LAGES**
Data: 26/03/2024 20:26:26-0300
Verifique em <https://validar.iti.gov.br>

Prof. Dr. Eduardo Nobre Lages
(Orientador – PPGEC/UFAL)

Documento assinado digitalmente
 **ADEILDO SOARES RAMOS JUNIOR**
Data: 01/04/2024 12:47:39-0300
Verifique em <https://validar.iti.gov.br>

Prof. Dr. Adeildo Soares Ramos Júnior
(Avaliador Interno – PPGEC/UFAL)

Documento assinado digitalmente
 **FABIO MARTINS GONCALVES FERREIRA**
Data: 01/04/2024 10:32:17-0300
Verifique em <https://validar.iti.gov.br>

Dr. Fábio Martins Gonçalves Ferreira
(Avaliador Externo à Instituição – LCCV)

Documento assinado digitalmente
 **GUILHERME ROSA FRANZINI**
Data: 28/03/2024 13:40:10-0300
Verifique em <https://validar.iti.gov.br>

Prof. Dr. Guilherme Rosa Franzini
(Avaliador Externo à Instituição – USP)

Documento assinado digitalmente
 **THIAGO PONTIN TANCREDI**
Data: 27/03/2024 07:56:23-0300
CPF: ***.799.268-**
Verifique as assinaturas em <https://v.ufsc.br>

Prof. Dr. Thiago Pontin Tancredi
(Avaliador Externo à Instituição – UFSC)

Campus A. C. Simões, Av. Lourival de Melo Mota, S/N
Tabuleiro do Martins – CEP 57072-970 – Maceió – Alagoas
Tel/Fax: (82) 3214-1863
E-mail: ppgec@ctec.ufal.br
Homepage: www.ctec.ufal.br/posgraduacao/ppgec

A Deus sempre presente nos momentos difíceis.
Alla memoria di mia madre Aiello Maria
esempio di forza e ispirazione. A minha esposa
Rita de Cassia pela paciência e o suporte nessa
jornada.

ACKNOWLEDGMENTS

With heartfelt gratitude to God for His unwavering guidance, navigating the intricate roles of a professor and a doctoral candidate has been challenging yet gratifying. I acknowledge the role of divine providence in successfully reaching this significant academic milestone. My sincere appreciation extends to the diverse array of individuals and organizations whose support has contributed to a rich tapestry of achievements spanning the global landscape. Heartfelt thanks are extended to my esteemed advisor, Professor Eduardo Nobre Lages, and the exceptional community of students and professors at LCCV, Federal University of Alagoas. Gratitude is also expressed by the Brazilian National Council for Scientific and Technological Development (CNPq).

At this significant moment, I wish to express heartfelt gratitude to my parents, Ciro and Maria. My late mother's enduring love and guidance have been invaluable in my academic journey, and this achievement is a tribute to her influence. I am also grateful to my wife, Rita de Cassia, and her family for their unwavering support throughout this challenging yet rewarding endeavor.

RESUMO

A transição urgente para fontes de energia renovável, impulsionada pela necessidade de enfrentar desafios de segurança energética e mudanças climáticas, destaca o papel crucial da energia eólica offshore. Este estudo investiga os diversos aspectos dessa forma de energia, abordando tanto o potencial em instalações de águas rasas quanto a contínua evolução em direção a turbinas de maior porte. Ao analisar áreas de águas rasas, identificam-se locais economicamente viáveis para parques eólicos entre cinquenta e setenta metros de profundidade, utilizando conceitos de ancoragem compartilhada e sistemas de linha de amarração. A seleção do sistema adequado é crucial, com pesquisas anteriores destacando a eficiência das linhas de fibra sintética em comparação com as configurações tradicionais de correntes de aço. Este estudo conduz análises dinâmicas em uma turbina de quinze MW e na plataforma de referência VoltornUS-S no Mar Céltico. São avaliados os deslocamentos, rotações e cargas em uma âncora compartilhada, utilizando linhas de nylon e poliéster. Os resultados revelam uma redução significativa de trintásseis por cento na carga de pico na âncora com linhas de nylon em comparação com as de poliéster, embora com rotações maiores da plataforma, sugerindo possíveis melhorias no design de ancoragem. Considerando que o nylon é dez por cento mais econômico que o poliéster e que há pesquisas contínuas em conceitos eficientes de ancoragem, este estudo incentiva uma investigação mais aprofundada das aplicações de nylon em parques eólicos de águas rasas. Simultaneamente, o setor de energia eólica enfrenta o desafio de aumentar o tamanho das turbinas para reduzir o custo nivelado de energia, o que requer sistemas de plataforma e ancoragens menores, especialmente em instalações em águas rasas. Baseando-se em pesquisas anteriores que empregaram um framework de otimização multiobjetivo (MO) para projetar plataformas e sistemas de amarração com linhas sintéticas, este estudo amplia o framework existente incorporando estratégias de eficiência computacional. A utilização de um critério de término de algoritmo genético recentemente desenvolvido contribuem para a eficiência computacional. No cerne desta investigação acadêmica encontra-se a análise da otimização de custos dentro de um sistema alternativo de amarração que integra mola de polímero — um domínio inexplorado na literatura existente. A análise detalhada revela que a implementação do quadro de otimização produz resultados razoáveis; além disso, sua aplicação esclarece como o sistema alternativo pode efetivamente mitigar custos, especialmente notável para raios menores.

Palavras-chave: Turbinas eólicas flutuantes; Linhas sintéticas; Águas rasas; Otimização multiobjetivo; Molas de polímero.

ABSTRACT

The imperative transition to renewable energy sources, driven by the need to address energy security and climate change challenges, underscores the pivotal role of offshore wind energy. This study delves into the multifaceted aspects of wind energy, examining both the potential in shallow water installations and the ongoing paradigm shift towards larger turbine sizes. In exploring shallow water regions, economically viable locations for wind farms emerge between fifty and seventy meters in depth, employing shared anchor concepts and mooring line systems. The selection of an optimal system type is critical, and past research highlights the efficiency of synthetic fiber ropes over traditional chain catenary configurations. This work presents dynamic analyses of a fifteen MW turbine and the VoltturnUS-S reference platform in the Celtic Sea. A comprehensive comparative assessment of planar displacements, rotations, and loads on a shared anchor is conducted using nylon and polyester ropes. Results show a notable thirty-six percent reduction in peak resolved anchor load with nylon compared to polyester, albeit with larger rotations, suggesting potential improvements in mooring design. With nylon being ten percent more cost-effective than polyester and ongoing investigations into efficient shared anchor concepts, this study encourages further exploration of nylon applications in shallow-water wind farms. Simultaneously, the wind energy sector grapples with the challenge of escalating turbine sizes to reduce the levelized cost of energy. This necessitates smaller platform and mooring systems, especially in the context of shallow-water installations. Building upon prior research, which employed a multi-objective optimization (MO) framework for designing platforms and mooring systems with synthetic lines, this study extends the existing framework by incorporating computational efficiency strategies. Utilizing a running metric as a termination criterion for the MO contributes to computational efficiency. Most importantly, at the core of this academic inquiry lies the scrutiny of cost optimization within an alternative mooring system integrating spring polymer—an unexplored domain in extant literature. The thorough analysis reveals that implementing the optimization framework yields reasonable outcomes; furthermore, its application elucidates how the alternative system can effectively mitigate costs, particularly notable for smaller radii.

Keywords: Floating Wind Turbine; Synthetic Rope; Shallow Water; Multi-Objective Optimization; Spring Polymer.

LIST OF FIGURES

Figure 1 - Brazilian Bathymetry.....	14
Figure 2 - Type of foundations for different depths.....	15
Figure 3 - Layout of (A), single-line; (B), 3-line anchor; and (C), 6-line anchor systems.	16
Figure 4 - Model set-up indicating the platform mesh. The thicker lines denote the chain section.	23
Figure 5 - Windowing approach.....	26
Figure 6 - Plan view of the model indicating the line numbering.	27
Figure 7 - Details of mooring line geometry.	28
Figure 8 - Overview of the iterative process.....	31
Figure 9 - Decay Test.	32
Figure 10 - Euler angles definition.	35
Figure 11 - Rigid Body with forces applied in a connection point.....	36
Figure 12 - Rotation of the body about the L_x axis.	37
Figure 13 - Rotation of the body about the L_z axis.	38
Figure 14 - DLC 1.6 Time Series and Power Spectra Density.	43
Figure 15 - Blade Pitch time series for DLC 1.6.	43
Figure 16 - DLC 6.1 Time Series and Power Spectra Density.	44
Figure 17 - Surge and Sway motions for Chain - Nylon mooring System.....	45
Figure 18 - Surge and Sway motions for Chain - Polyester mooring System.	45
Figure 19 - Platform rotation for the taut mooring nylon system.....	46
Figure 20 - Platform rotation for the taut mooring polyester system.....	47
Figure 21 - Anchor Load distribution for taut mooring nylon system.	49
Figure 22 - Anchor Load distribution for taut mooring polyester system.	49
Figure 23 - Misalignment of the line 1 during the simulation.	50
Figure 24 - Example of a Polymer Spring Design.....	55
Figure 25 - Illustration of FOWT Mooring Load Behavior	55
Figure 26 - Impact of Polymer Spring on FOWT Mooring System Behavior	55
Figure 27 - Flowchart of the NSGA2 Framework.	59
Figure 28 - Graphical representation of the process to ascertain their placement within a Pareto frontier.	60
Figure 29 - Geometry constraint.	64
Figure 30 - Mooring system geometry.	70
Figure 31 - Dry chain mass and chain load capacity (left) and dry synthetic mass and	

synthetic load capacity (right).	70
Figure 32 - Mooring system with spring component.....	72
Figure 33 - Spring response curve.....	72
Figure 34 - Linear regression line for radius/SDTR relationship.	77
Figure 35 - Pareto frontier in mapped and cost-radius space: (a) West, (b) Statistical Learner, (c) Direct optimization and alternative mooring system optimization.....	82
Figure 36 - Radius – synthetic length: (a) West, (b) Statistical learner, (c) Direct optimization.....	84
Figure 37 - Radius – buoy displaced volume: (a) West, (b) Statistical learner, (c) Direct optimization.....	85
Figure 38 - Radius – chain diameter: (a) West, (b) Statistical learner, (c) Direct optimization.....	85
Figure 39 - Radius – Synthetic diameter: (a) West, (b) Statistical learner, (c) Direct optimization.....	86
Figure 40 - Radius vs (a) Target Load, (b) Spring length, (c) Buoy displaced volume, (d) Synthetic length, (e) Chain diameter, (f) Synthetic diameter.....	88

LIST OF TABLES

Table 1 - Brazilian Accumulated Potential Wind Energy	13
Table 2 - Design Load Case (DLC) Description and Environmental Conditions (ESS— Extreme Sea State; SSS—Severe Sea State).....	24
Table 3 - Quadratic Damping Coefficients	25
Table 4 - Largest wave height and subsample interval values.....	26
Table 5 - Mooring material properties.....	27
Table 6 - Initial configuration of the mooring lines	28
Table 7 - Nylon length section after the application of the pretension.....	28
Table 8 - Dynamic Stiffness [kN] comparison WF+LF vs WF	29
Table 9 - Convergent Dynamic Stiffness and updated length after performing the practical procedure considering WF+LF.	29
Table 10 - Mooring stiffness matrix for DLC 6.1 (Values kN, kN/rad or kN·m/rad).....	29
Table 11 - Mooring stiffness matrix for DLC 1.6 (Values kN, kN/rad or kN·m/rad)	30
Table 12 - Natural period of the floater motions	32
Table 13 - Structural Inertia Matrix of the platform and tower (Values in T_e or $T_e \cdot m^2$)	33
Table 14 - Added Mass Matrix for infinite period evaluated by OrcaWave (Values T_e , $T_e \cdot m$, or $T_e \cdot m^2$)	34
Table 15 - Hydrostatic Stiffness Matrix evaluated by OrcaWave (Values in kN, kN/rad or kN·m/rad).....	34
Table 16 - MSM for DLC 6.1 (Values kN, kN/rad or kN·m/rad)	34
Table 17 - Matrix showing asymmetric coefficients (Values kN, kN/rad or kN·m/rad)...	36
Table 18 - Connections and hydrostatic stiffness moment report (Value kN·m).....	36
Table 19 - Matrix that restores the symmetry in the stiffness matrix.....	39
Table 20 - Eigenvalues and eigenvectors obtained with the direct method.....	39
Table 21 - Eigenvalues and eigenvectors obtained with the Lanczos algorithm by OrcaFlex.	40
Table 22 - Natural periods [s] comparison for DLC 1.6.....	40
Table 23 - Natural periods [s] comparison for DLC 6.1.....	41
Table 24 - Summary of the Platform excursion statistics.	45
Table 25 - Summary of the platform rotation`s statistics	46
Table 26 - Mean load as % MBL.....	47
Table 27 - Summary of peak loads in the taut moored nylon system compared to the taut moored polyester system.	49

Table 28 - Peak resolved load % MBL.	50
Table 29 - Summary of tension statistic in the line 1	50
Table 30 – A tabular comparison of the solutions was conducted to ascertain their placement within a Pareto frontier.....	60
Table 31 - Design variables for the synthetic-based mooring system	62
Table 32 - Design variables for the alternative mooring system	62
Table 33 - Nylon – based mooring constant system properties.	70
Table 34 - Material nondimensionalized stiffness.....	71
Table 35 - Mooring system component costs.....	71
Table 36 - Reduction factor vs mudline angle.	71
Table 37 - Look up table varying with the Target Load.....	71
Table 38 - Spring component cost	72
Table 39 - IEA 15 MW reference turbine design requirements.....	74
Table 40 - Environmental Condition.....	75
Table 41 - List of the designs considered for the determination of the seed.....	76
Table 42 - Determination of the seed.....	76
Table 43 - list of designs for the calculation of the SDTR	76
Table 44 - Calculation of SDTR.....	77
Table 45 - Linear damping coefficient.	77
Table 46 - Quadratic damping coefficient.	78
Table 47 - Whole System Statics parameters.	78
Table 48 - OrcaFlex setup for nylon – based system.	78
Table 49 - OrcaFlex set up for the alternative mooring system.....	78
Table 50 - Parameters for the NSGA2.	79
Table 51 - Running metric parameters.....	80
Table 52 - Safety Factor for the predefined design A, B, and C.	80
Table 53 - Breakdown cost comparison.	81
Table 54 - Factor of Safety (FoS).....	83
Table 55 - List of representative design solutions from the statistical learner approach.	86
Table 56 - Constraint violation for representative design solutions of the statistical learner.	87
Table 57 - Representative Design Variable Values.....	88
Table 58 - Cost Breakdown.....	89

TABLE OF CONTENTS

1 INTRODUCTION	13
2 A COMPARISON OF ANCHOR LOADS, PLANAR DISPLACEMENT, AND ROTATION FOR NYLON AND POLYESTER MOORED SYSTEMS FOR A 15 MW FLOATING WIND TURBINE IN SHALLOW WATER	19
2.1 INTRODUCTION.....	19
2.1.1 Background.....	19
2.1.2 Nylon Rope.....	20
2.1.3 Taut mooring system.....	21
2.1.4 Mooring Stiffness Matrix	21
2.2 METHODOLOGY	21
2.2.1 Numerical Model.....	22
2.2.2 Case Study	23
2.2.2.1 Environmental Condition	23
2.2.2.2 Turbine.....	24
2.2.2.3 Floating Platform.....	24
2.2.2.4 Mooring System Configuration	25
2.2.3 Decay Test	31
2.2.4 Modal analysis.....	33
2.3 RESULTS.....	42
2.3.1 Time series and Power Spectral Density	42
2.3.2 Surge – Sway	44
2.3.3 Roll – Pitch – Yaw	46
2.3.4 Anchor Peak Load	47
2.4 DISCUSSION	50
2.4.1 Platform Offset Requirements	50
2.4.2 Line Tension Requirements	51
2.4.3 Design Improvements.....	51
2.5 CONCLUSION	52
3 OPTIMIZATION OF COST-EFFICIENT SYNTHETIC MOORING SYSTEMS UTILIZING POLYMER SPRINGS FOR 15 MW FLOATING WIND TURBINES IN RELATIVELY SHALLOW WATERS.	53
3.1 INTRODUCTION.....	53
3.1.1 Background.....	53

3.1.2 Polymer Spring	54
3.2 HARDWARE AND SOFTWARE	56
3.3 OPTIMIZATION FRAMEWORK	56
3.3.1 Constraint Handling.....	56
3.3.2 Termination Criteria.....	57
3.3.3 Definition of the optimization problem.....	57
3.3.3.1 Objective Function	59
3.3.3.2 Design variables.	61
3.3.3.3 Constraints.....	62
3.3.3.3.1 Geometric feasibility constraint.	63
3.3.3.3.2 Natural Period Constraints.	64
3.3.3.3.3 Touchdown constraint.....	66
3.3.3.3.4 DLC 6.1-time constraints.	66
3.3.3.3.5 Statistical Learner approach	68
3.4 INPUT DATA.....	69
3.4.1 Nylon mooring system configuration.....	69
3.4.2 Alternative mooring configuration with spring component.	71
3.4.3 Reference Turbine and Platform.....	73
3.4.4 Design code and requirements.....	73
3.4.5 Environmental conditions.....	74
3.4.6 Approach for modeling the extrapolation of peak load.	75
3.5 RESULTS.....	79
3.5.1 OrcaFlex Model Assessment.	80
3.5.2 Objective space analysis.....	81
3.5.3 Design space analysis.	83
3.5.3.1 Synthetic-base mooring system.....	83
3.5.3.2 Constraint assessment of the statistical learner approach.....	86
3.5.3.3 Alternative mooring system assessment.	87
3.6 CONCLUSION	89
4 CONCLUSIONS.....	91
4.1 SUMMARY OF CHAPTER 2	91
4.2 SUMMARY OF CHAPTER 3	92
4.3 SUGGESTION FOR FUTURE RESEARCH	93
5 BIBLIOGRAPHY.....	95

1 INTRODUCTION

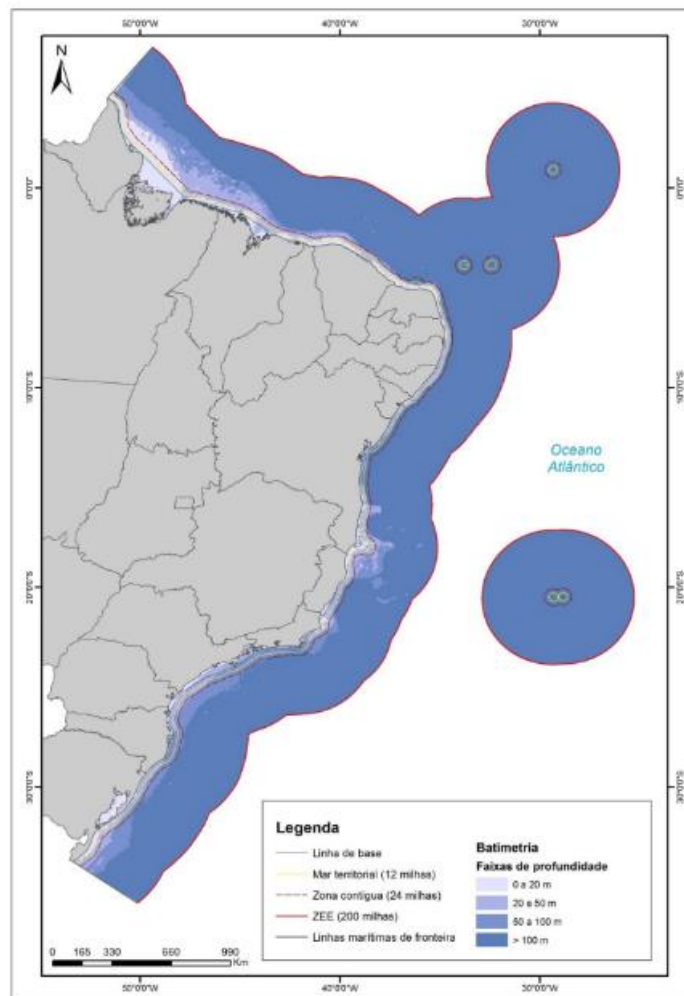
This dissertation seeks to contribute to the progression of knowledge concerning synthetic mooring systems, which constitute a vital element in the evolution of floating offshore wind turbine (FOWT) installations. The commitment of multiple governments to attain zero net emissions by the 2050s and 2060s underscores the pivotal role envisaged for wind energy in addressing environmental challenges. Presently, offshore wind capacity is 64.3 gigawatts GW, accounting for 7% of the cumulative global offshore wind installations. GWEC Market Intelligence anticipates the addition of over 380 gigawatts of new offshore wind capacity in the coming decade (2023-2032). This forecast is expected to raise the cumulative offshore wind capacity to 447 GW by the conclusion of 2032 (WILLIAMS; MARTINEZ PALACIO; ZHAO, 2023). Brazil introduced an OSS system through an information portal that manages offshore areas used for power generation (GOV.BR, 2023). According to Empresa de Pesquisa Energética (2020), Brazil possesses a substantial offshore wind potential estimated at approximately 700 GW, as shown in Table 1, in areas characterized by depths of up to 50 meters, as illustrated in Figure 1.

Table 1 - Brazilian Accumulated Potential Wind Energy

Velocidade /Batimetria	Áreas aproveitáveis (km ²)				Potencial (GW)				Potencial (TWh)			
	0 -20	20-50	50-100	>100	0 -20	20-50	50-100	>100	0 -20	20-50	50-100	>100
≥6,0	175.754	186.188	171.923	2.784.706	628	641	531	9.100	1.789	2.048	1.576	30.140
≥6,5	147.234	171.441	147.519	2.602.599	522	591	467	8.420	1.582	1.949	1.450	28.793
≥7,0	79.869	123.078	79.907	1.765.981	276	421	237	5.833	1.008	1.528	902	21.872
≥7,5	38.637	64.276	57.360	1.237.126	129	209	159	4.014	566	890	667	16.101
≥8,0	29.017	46.109	50.429	674.730	100	147	137	2.056	456	664	587	8.934
≥8,5	16.835	22.227	31.507	333.324	63	81	87	993	308	398	383	4.612
≥9,0	3.996	7.337	1.852	143.039	15	28	7	399	82	149	38	1.929
≥9,5	729	560	154	2.971	3	2	1	11	16	12	3	63
≥10,0	-	-	-	-	-	-	-	-	-	-	-	-

Source: (EMPRESA DE PESQUISA ENERGÉTICA, 2020)

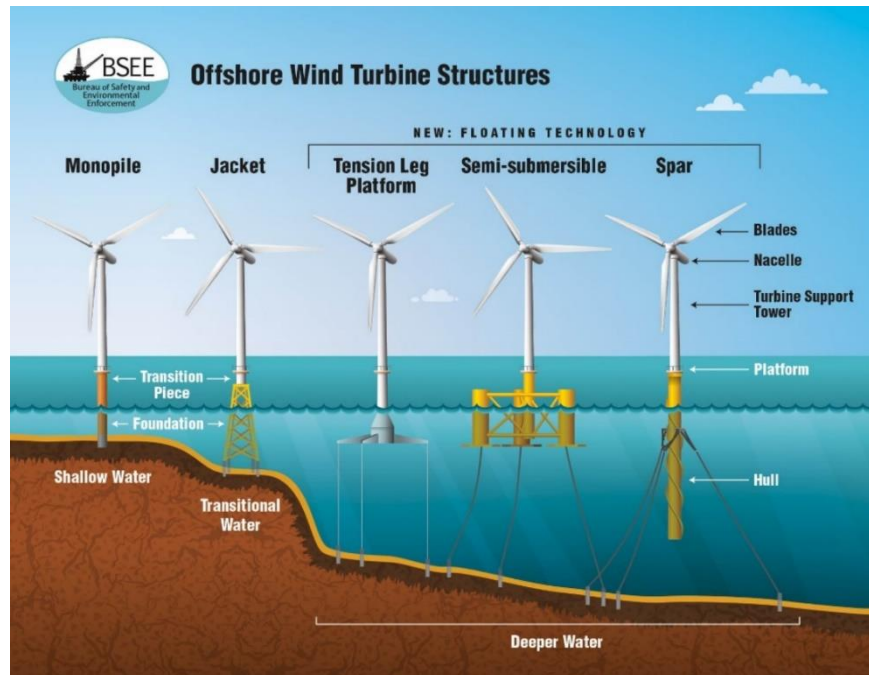
Figure 1 - Brazilian Bathymetry.



Source: (EMPRESA DE PESQUISA ENERGÉTICA, 2020)

The transition to greater depths introduces distinctive engineering complexities. In shallow water, typically up to approximately 30 or even 40 meters, conventional fixed-bottom technologies like monopiles or truss structures are applicable (ACHMUS et al., 2019). However, as water depth increases, the cost of engineering fixed-bottom structures becomes prohibitive. Beyond 85 meters, the preferred technology involves floating platforms using a chain catenary system for stability, as illustrated in Figure 2.

Figure 2 - Type of foundations for different depths.



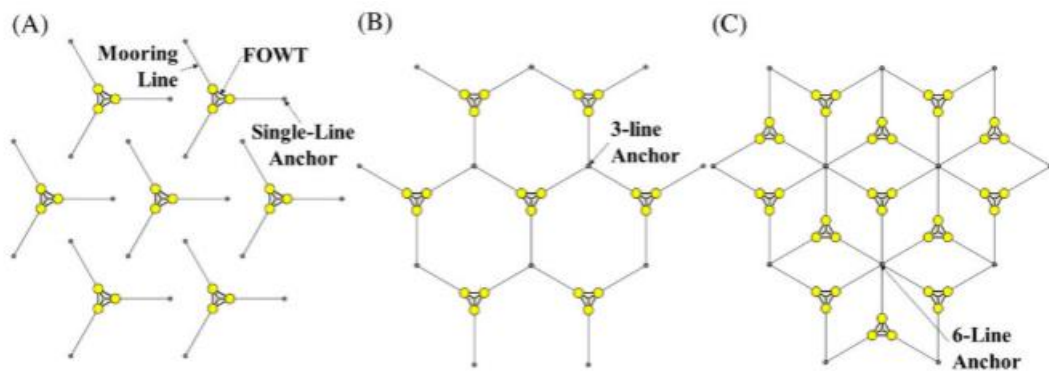
Source: (SPEHT, 2021)

Traditional chain catenary systems rely on chain weight for restoring force, but in shallow waters, their effectiveness requires a costly large chain mass. Synthetic moorings offer a promising solution for deploying Floating Offshore Wind Turbines (FOWTs) in transitional depths (PILLAI et al., 2022a, 2022b). Synthetic mooring systems generate a restoring force utilizing the extensional properties inherent in the fiber ropes. Despite the potential viability of synthetic ropes for deploying Floating Offshore Wind Turbine (FOWT) installations in intermediate water depths, substantial research is imperative before the technology can be considered commercially feasible. A significant challenge lies in accurately modeling the intricate behavior of synthetic ropes, given their complex viscoelastic properties. Many building and classing agencies recommend a simplified, conservative modeling approach, recognizing inherent complexities. However, these entities express openness to exploring more sophisticated solutions in future development phases. Polyester is the primary synthetic material extensively employed in the oil and gas industry, particularly in deep-water applications, due to its high stiffness. In shallow waters, using polyester results in substantial peak loads, leading to increased anchor costs and undesirable pitch oscillation, posing challenges in such environments (PILLAI et al., 2022b).

After this brief preamble, this study aims to address several noticeable gaps identified in existing literature.

To date, no comparative research has evaluated the performance of a chain-polyester line versus a nylon-based line for the 15 MW floating offshore wind turbine located on the VoltunUS-S platform in shallow waters. This investigation is of significant importance as it can potentially enhance the efficiency of wind farms utilizing shared anchor systems. Unlike traditional offshore oil and gas installations, offshore wind towers are arranged in arrays, presenting opportunities for cost reduction by connecting multiple mooring lines to a single anchor (Figure 3). This approach leads to direct cost savings and reduces the need for extensive offshore geotechnical site investigations (FONTANA et al., 2018). Therefore, the mitigation of vertical anchor loads is deemed essential, and it has been one of the primary focuses of inquiry in this thesis.

Figure 3 - Layout of (A), single-line; (B), 3-line anchor; and (C), 6-line anchor systems.



Source:(FONTANA et al., 2018)

Additionally, the optimization framework implemented with the open-source OpenFAST (Open-source Fatigue, Aerodynamics, Structures, and Turbulence) (NREL, 2020) coupled with MoorDyn (HALL, 2015), West et al. (2023) have proven effective in academic settings, its suitability for industrial applications may be limited. Therefore, implementing commercial software would be advantageous for the industry and could significantly enhance the practical application of the framework. In this work, the implementation has been executed using OrcaFlex (ORCINA, 2024), which required considerable effort and time due to the distinct features of the open-source software.

Furthermore, Load Reduction Devices (LRDs) installed along mooring lines have demonstrated promising results in mitigating loads on anchors and mooring lines (ARYAWAN et al., 2023; LOZON et al., 2022; MCEVOY; JOHNSTON; MARINE, 2019; MCEVOY; KIM, 2017). This innovation facilitates using smaller and lighter components, thereby reducing fatigue damage on the mooring system. While previous research has addressed load

optimization solutions (ARYAWAN et al., 2023), none have investigated a cost-effective solution tailored to this system, leveraging an automated tool based on multi-objective optimization. Additionally, evaluating whether the framework proposed by West et al. (2023) can effectively accommodate mooring systems integrating LRDs is crucial.

Lastly, West et al. (2023) did not propose integrating surrogate or statistical learner models into the optimization framework, as they do not guarantee finding the optimal solution. However, starting with basic statistical learner or surrogate modeling, such as linear regression, and comparing them with direct optimization could provide insights for refining and optimizing the approach. As George Box famously said, all the models are wrong, but some of them are useful.

The specific deliverables resulting from the research conducted in this dissertation are as follows:

- Implementing and validating the optimization framework using OrcaFlex for the synthetic-based mooring system.
- Assessment of the viability of applying the optimization framework to a more complex mooring system, such as one incorporating spring polymer, by investigating its behavior in the objective and design spaces.
- Evaluation of the efficacy of a basic statistical learner or surrogate, such as linear regression, through comparison with direct optimization to determine the viability of this approach.

This dissertation is structured as follows: Chapter 2 takes a good part of the work presented in the paper entitled "A Comparison of Anchor Loads, Planar Displacement, and Rotation for Nylon and Polyester Moored Systems for a 15 MW Floating Wind Turbine in Shallow Water," which has been published in the Journal of Ocean Engineering (VERDE; LAGES, 2023). It extends this investigation by exploring a mooring system that adjusts the diameter of the nylon rope to align with the minimum breaking load (MBL) of a polyester rope. Additionally, a modal analysis of the system is incorporated to provide further depth to the study. In this chapter, the primary focus is on scrutinizing a nylon-based mooring system engineered for a 15 MW reference turbine positioned on the VoltturnUS-S platform in the Celtic Sea at a water depth of 70 meters, mirroring the examination of a mooring system employing polyester rope (PILLAI et al., 2022b). Understanding the behavior of the nylon rope is pivotal for the development presented in Chapter 3, where optimization of a nylon-based mooring system is conducted. Chapter 2 outlines a specific procedure for modeling the nylon material and performs a thorough examination, including modal analysis, to understand the system's

behavior. Subsequently, key metrics such as anchor peak load, planar displacement, and rotation are calculated and compared with those of a similar polyester-based mooring system. The results indicate lower peak loads in the nylon system compared to polyester, suggesting significant potential for reducing capital expenditure (CAPEX) and thereby enhancing the feasibility of offshore wind power production.

With a more comprehensive understanding of the nylon rope's behavior established in Chapter 2, Chapter 3 serves as the cornerstone for the forthcoming manuscript titled "Optimization of Cost-Efficient Synthetic Mooring Systems Utilizing Polymer Springs for 15 MW Floating Wind Turbines in Relatively Shallow Waters" which is intended for submission to a suitable journal. In this chapter, the optimization framework outlined by West et al. (2023) is implemented using industry-standard software. Specifically, the commercial software OrcaFlex, designed for offshore structure analysis, is employed to develop a robust implementation. However, due to differences in the determination method of wave load seeds, comparing the results with OpenFAST + MoorDyn posed challenges, necessitating additional efforts to establish appropriate seed selection. Despite this, the results demonstrated satisfactory alignment, although the framework exhibited some sensitivity to seed selection.

Following this, the optimization framework is used to conduct a cost-effective optimization of a mooring system comprised of a synthetic line and a specific Load Reduction Device (LRD) such as the spring polymer. This application demonstrates the framework's ability to accurately model the mechanical behavior of the system and to seek optimized design configurations, representing the initial effort to conduct cost optimization for such systems.

Finally, a basic statistical learner, like linear regression, is incorporated into the optimization framework to replace time-domain simulations. This substitution aims to evaluate the learner's effectiveness. The results strongly correlated with direct optimization, but some inaccuracies in determining the constraint violation were observed.

2 A COMPARISON OF ANCHOR LOADS, PLANAR DISPLACEMENT, AND ROTATION FOR NYLON AND POLYESTER MOORED SYSTEMS FOR A 15 MW FLOATING WIND TURBINE IN SHALLOW WATER

2.1 Introduction

2.1.1 Background

Renewable energy is increasingly recognized as a critical solution for addressing geopolitical energy and climate change issues. Offshore wind installation has seen consistent growth, with 2021 experiencing an increase compared to 2020 (IEA, 2022). Shallow water sites for offshore wind turbines are being considered in the US (BULJANJAN, 2021) and the UK (THE CROWN ESTATE, 2022). However, despite this growth, mooring and anchor systems remain a subject of ongoing research, innovation, and optimization, as identified by academic and industrial partners (IKHENNICHEU et al., 2020). Prior research has focused on analyzing several types of platforms, such as semi-submersible, spar buoy, and tension leg platforms (PILLAI et al., 2022a). As horizontal axis turbines continue to increase in size, developers are turning to larger prototypes such as Vestas' first 15 MW turbine (BULJANJAN, 2022), for which NREL and the IEA have established a 15 MW reference turbine (GAERTNER et al., 2020). One example of a semi-submersible platform designed to support this reference turbine is the VoltturnUS-S, developed by the University of Maine (ALLEN et al., 2020). Recent work has investigated the impact of different mooring systems and shared anchor concepts in shallow waters, such as the Celtic Sea (PILLAI et al., 2022a). These investigations have confirmed the potential benefits of shared anchor concepts (DEVIN et al., 2021; DIAZ et al., 2016; FONTANA et al., 2018; GÖZCÜ; KONTOS; BREDMOSE, 2022). Part I of this work found that the peak load on a shared anchor could be reduced by up to 67%. The study also showed that increasing the platform footprint can further reduce peak loads by up to 56% in a catenary system. However, significant peak loads can still occur even when the wind and waves are not aligned. Part II of the same study focused on using a hybrid mooring line (PILLAI et al., 2022b) consisting of a chain polyester and a novel mooring tether. The results showed a peak load

reduction of up to 84% and 75%, respectively, for smaller footprints (293 m), and up to 80% and 59% for the largest footprint (838 m). However, using this hybrid line also resulted in a larger platform excursion that exceeded the design limit of 25 m. Additionally, the study investigated using a taut mooring system with a hybrid chain polyester line, which reduced platform excursion but came at the expense of higher peak anchor loads, including vertical loads and peak resolved loads that breached API design requirements. The authors suggested that more investigation of the taut-moored polyester system is needed. They recommended further optimization and improvements in mooring design systems, such as using nylon applications (PILLAI et al., 2022b).

2.1.2 Nylon Rope

For floating offshore wind turbines in shallow water, fiber ropes such as nylon and polyester can provide a compliant and cost-efficient solution (WELLER et al., 2015). Compared to polyester and chain, nylon lines have a lower unit length cost of approximately 10% and 75%, respectively, while possessing the same minimum breaking load (CASTILLO, 2020). Although methods for testing and modeling polyester have been incorporated into the design standard code DNV GL RP E305 (DET NORSKE VERITAS, 2015), they are not directly applicable to modeling nylon ropes since their stiffness depends on the mean and amplitude of the loads. Several stiffness models for nylon rope have been proposed, including a practical procedure that builds on an existing model developed for polyester (PHAM et al., 2019), a more sophisticated formulation of a constitutive law (CHEVILLOTTE, 2021), and a force-elongation formulation (WEST et al., 2020). The practical procedure is easier to implement in offshore analysis software. Recent work has demonstrated that the empirical formula, on which the practical procedure is based, is dependable for mean loads that are sufficiently large relative to the minimum breaking load (XU et al., 2021b). However, additional research on fatigue failure and prototype testing is required to validate the proposed models for using nylon ropes in mooring systems (DEPALO et al., 2022).

2.1.3 Taut mooring system

The use of a catenary chain system in shallow water is ineffective due to its weight, high tension, and cost (XU et al., 2021a). Additionally, the wave climate in shallow water requires a mooring system capable of adapting to depth changes caused by storm and tidal variations. These requirements are met by a taut mooring system using fiber rope, which allows for greater compliance and reduces the impact on the seabed, eliminating the need for long chain lines. However, a taut mooring system using fiber rope requires an anchor system capable of withstanding higher horizontal and primarily larger vertical loads (PILLAI et al., 2022b). To investigate the trade-off between using nylon rope and polyester rope in a taut mooring system, a dynamic analysis is conducted considering a 15 MW reference turbine supported by a semi-submersible platform deployed in shallow waters of the Celtic Sea. This analysis aims to replicate closely the simulation performed by Pillai et al. (2022b), which examined a taut mooring system using a polyester rope.

2.1.4 Mooring Stiffness Matrix

The mooring stiffness matrix is a critical parameter for floating offshore systems, especially in slow-drift motion, and it also affects the calculation of response amplitude operators to first-order wave forces. Analytical formulations for the mooring stiffness matrix of both catenary and taut mooring systems have been proposed using analytical mechanics methods (AMARAL; PESCE; FRANZINI, 2022) and the perturbation approach (AL-SOLIHAT; NAHON, 2016).

2.2 Methodology

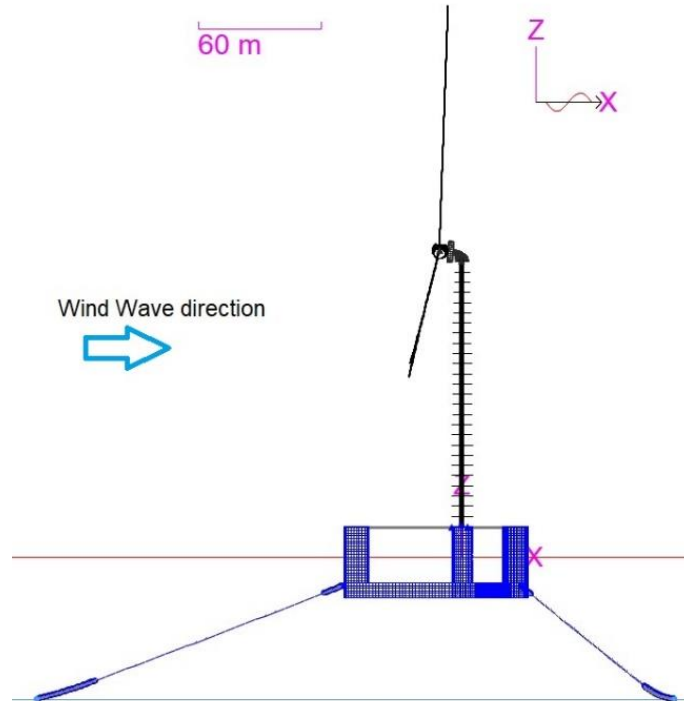
In this study, a 15 MW reference turbine is modeled and supported by the reference semi-submersible platform VoltturnUS-S using OrcaFlex. The aim of this numerical analysis

was to compare the results of a taut mooring polyester system presented in a recent study by Pillai et al. (2022b) with those obtained using a nylon rope. To ensure a direct comparison, the same numerical model is used as a case study as in the previous work, with the only difference being the replacement of the polyester rope with a nylon rope.

2.2.1 Numerical Model

OrcaFlex is a widely recognized industry-standard software tool for hydrodynamic analysis and dynamic mooring response. It includes an aerodynamic solver and blade element momentum (BEM) process, enabling simultaneous modeling of wind and wave loads. OrcaFlex also accepts floating body hydrodynamic data as input, which can be generated by other tools like WAMIT or OrcaWave, using potential flow theory to derive response amplitude operators (RAOs) and second-order quadratic transfer functions (QTFs). OrcaFlex has been extensively verified against various software packages, including FAST, MSC.ADAMS, Bladed, and HAWC2, demonstrating its reliability and accuracy (ROSS, 2018). The software's ability to model catenary and mooring systems has also been verified against FENRIS, Riflex, Ariane (QUIGGIN P.P., 2015), and OpenFast (PILLAI et al., 2022b), showing good agreement. A schematic model is presented in Figure 4. OrcaFlex offers the capability to calculate the mooring stiffness matrix required as input for diffraction analysis, and verifications of that matrix have been carried out, showing good agreement (AMARAL et al., 2022). To ensure a fair comparison, the present study used the Turbsim stochastic full-field turbulence simulator software (JONKMAN, 2016) to generate a three-dimensional wind field according to the current standard (IEC, 2019). Similarly, wave conditions were simulated using OrcaFlex with JONSWAP spectrum parameters. The simulations were run for 3600 s, including a start-up time of 1000 s, during which environmental conditions were smoothly ramped up to allow the transient response enough time to settle. Multiple wind and wave conditions were generated using different seeds. The same numerical model and case study were used in this paper as in a recent work by Pillai et al. (2022a), except that the taut mooring polyester system was replaced with a nylon rope. The numerical analysis used OrcaFlex to model a 15 MW reference turbine supported by the reference semi-submersible platform VoltturnUS-S, enabling a direct comparison of results.

Figure 4 - Model set-up indicating the platform mesh. The thicker lines denote the chain section.



Source: (VERDE; LAGES, 2023)

2.2.2 Case Study

The Celtic Sea, at a depth of 70 m, has been chosen as a representative location for comparison with previous work (PILLAI et al., 2022b).

2.2.2.1 Environmental Condition

The previous study of the taut mooring system only analyzed two dynamic load cases, as listed in Table 2. Typically, one of these cases represents the most critical ultimate limit state (ULS), which governs the design of the mooring components and anchors (WEST et al., 2021). Additionally, Pillai et al. 2022a pointed out that a misalignment between wind and waves could

result in the most severe anchor load case.

Table 2 - Design Load Case (DLC) Description and Environmental Conditions (ESS—Extreme Sea State; SSS—Severe Sea State).

DLC	Sea state	Wind Speed [ms⁻¹]	Wind Direction [°]	Significant Wave height (H_s) [m]	Mean Zero-Crossing Wave Period (T_z) [s]	Wave Direction [°]
1.6	SSS	22.00	0	12.5	17.5	0
6.1	ESS	33.00	0	14.4	14.1	0

Source: (VERDE; LAGES, 2023)

2.2.2.2 Turbine

The IEA-15-240 RWT (v1.0) is a representative example of the next generation of larger offshore wind turbines developed by Gaertner et al. (2020). This turbine features advanced structural design and control systems, reflecting real-world applications. The Reference Open-Source Controller (ROSCO v2.4.1) toolbox has been implemented to regulate generator torque and blade pitch, following industry standards (ABBAS et al., 2021). As Pillai et al. (2022b) explain, ROSCO ensures proper blade regulation during turbine operation while the blades are feathered in the parked position, as specified in the turbine manual.

2.2.2.3 Floating Platform

A previous study on platform optimization found that a design with three outer cylinders is optimal for costs below \$6 million, while a design with six outer cylinders is optimal at a cost of \$6 million (HALL, 2013). However, semi-submersible structures and spar buoys are currently the most mature concepts in the market (IKHENNICHEU et al., 2020). It is worth noting that semi-submersible platforms are particularly suitable for shallow water applications due to their limited draft. The University of Maine has developed a reference platform (ALLEN

et al., 2020) that reflects the industry standard practice used in the work by Pillai et al. (2022a, 2022b). However, the potential flow analysis implemented in OrcaWave does not account for drag contributions, which are significant for this type of floating platform. Therefore, quadratic damping coefficients are added using the diagonal entries given in Table 5 of the reference platform report (ALLEN et al., 2020), as shown in Table 3.

Table 3 - Quadratic Damping Coefficients

Surge N/(m/s) ²	Sway N/(m/s) ²	Heave N/(m/s) ²	Roll Nm/(rad/s) ²	Pitch Nm/(rad/s) ²	Yaw Nm/(rad/s) ²
9.225E+05	9.225E+05	2.296E+03	1.676E+10	1.676E+10	4.798E+10

Source: Author adapted from Allen et al. (2020)

2.2.2.4 Mooring System Configuration

To enable a comparison with the chain-polyester taut mooring system described in Pillai et al. (2022b), a chain-nylon taut system is analyzed using the dynamic stiffness empirical formula proposed by Pham et al. (2019), which is based on experimental data collected by Huntley (2016):

$$K_{rd} = 0.39L_m - 0.21L_a + 2.08 \quad (1)$$

where L_m and L_a represent the mean load and the load amplitude, respectively, both expressed as a percentage of the minimum breaking load (MBL). The static modulus is expressed by (VARNEY A. S.; TAYLOR R.; SEELIG W, 2013):

$$\frac{K_{rs}}{MBL} = 3.05 \quad (2)$$

The MBL [kN] of nylon in wet conditions was estimated using the statistical formula provided in OrcaFlex, which was obtained through the least squares fitting and demonstrated good agreement with the manufacturer's data:

$$MBL = 13957 \cdot d^2 \cdot 1.67 \quad (3)$$

Where d is the nylon rope nominal diameter [m] and 1.67 is a safety factor adopted by Pillai et al. (2022b). The practical procedure suggested by Pham et al. (2019) is used to estimate the convergent dynamic stiffness for each DLC case, which was implemented in a Python script using equation (1) coupled with OrcaFlex. It is important to note that Pillai et al. (2022b) fine-

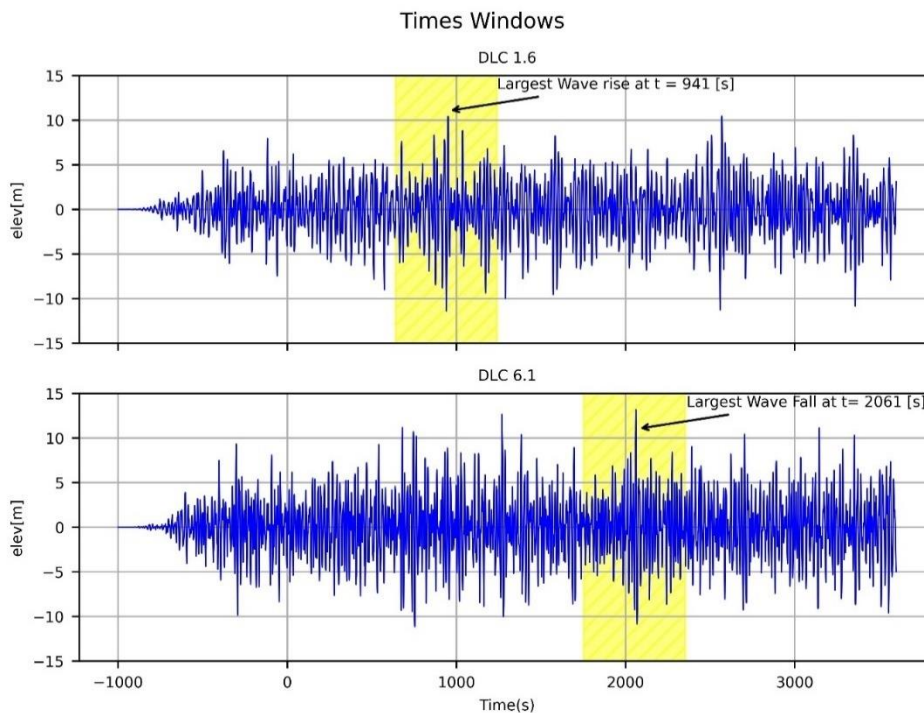
tuned the taut polyester moored system using only the DLC 6.1 case. In this work, the windowing approach is adopted by Pillai et al. (2022b), which involves subsampling the 3600 s surface elevation to select a 600 s extract that includes the largest wave event. This approach was chosen to ensure a fair comparison between our results and those reported in Pillai et al. (2022b). Table 4 and Figure 5 summarize the values used in our simulations, with the highlighted yellow regions indicating the 600 s interval used for estimating the dynamic stiffness.

Table 4 - Largest wave height and subsample interval values.

DLC	Significant Wave Height (Hs) [m]	Mean Zero-Crossing Wave Period (Tz) [s]	Largest Wave Event [m]	Sample Time Interval [s]	Simulation time origin [s]	Largest Wave Event localization [s]
1.6	12.5	17.5	21.82	600	641	941
6.1	14.4	14.1	22.45	600	1753	2061

Source: (VERDE; LAGES, 2023)

Figure 5 - Windowing approach.



Source: (VERDE; LAGES, 2023)

From this point onward, the analysis in this work deviates slightly from that outlined in

the associated published paper (VERDE; LAGES, 2023). To ensure a more equitable comparison, the nylon nominal diameter was adjusted to align with the Maximum Breaking Load (MBL) of the polyester and chain sections, resulting in a different outcome. However, the main findings of the aforementioned paper are largely preserved. Material properties are detailed in Table 5.

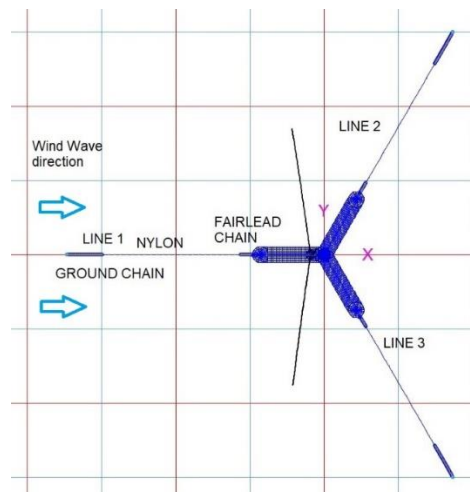
Table 5 - Mooring material properties.

Section	Description	MBL [kN]	Nominal diameter [mm]	Mass per unit length [kg/m]
Chain	R3 studless mooring chain	22286	185	685
Polyester	Bridon MoorLine Polyester	20601	266	46.2
Nylon	wire-lay nylon	20667	298	55.7

Source: Author (2024)

The three mooring lines consisted of three sections each – a chain near the fairlead, a nylon rope in the middle, and a ground chain at the bottom, as shown in Figure 6, and were adjusted to achieve a convergent dynamic stiffness for each load case, with a pretension of 800 kN.

Figure 6 - Plan view of the model indicating the line numbering.



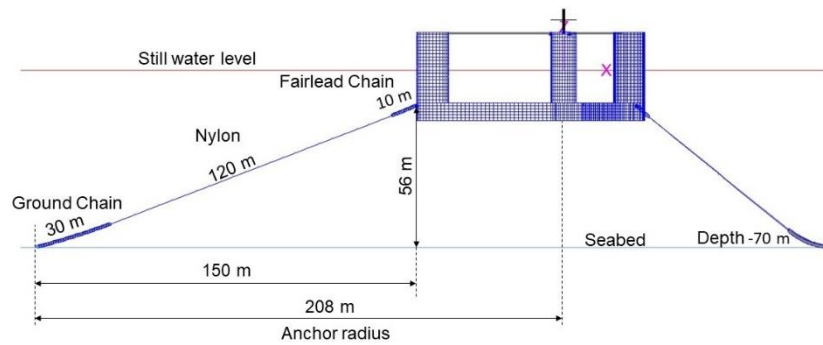
Source: (VERDE; LAGES, 2023)

Before pre-tensioning, the lines were configured uniformly, as demonstrated in Table 6 and Figure 7, which depicts the numerical modeling.

Table 6 - Initial configuration of the mooring lines

Section	Diameter [m]	Length [m]	Target segment length [m]	Number of segments
Fairlead Chain	0.185 (Studless)	10	1	10
Nylon rope	0.298	120	5	24
Ground Chain	0.185 (Studless)	30	1	30

Source: Author (2024)

Figure 7 - Details of mooring line geometry.

Source: (VERDE; LAGES, 2023).

After applying the pretension, the length of the nylon section of the mooring lines changed, as shown in Table 7.

Table 7 - Nylon length section after the application of the pretension

Nylon length of line 1 [m]	Nylon length of line 2 [m]	Nylon length of line 3 [m]
119.136	118.955	118.955

Source: Author (2024)

Once the pretension was applied, the mooring stiffness was calculated and inputted into the OrcaWave program for a diffraction analysis. After that, the resultant tables were supplied to OrcaFlex to perform the static analysis of the practical procedure. Moreover, according to Pham et al. (2019), the practical procedure applied to a semi-submersible does not need to update the mooring stiffness matrix to obtain the convergent dynamic stiffness since, in the semi-submersible case, the low-frequency motions are small compared to the wave frequency responses, and the matrix should not play a relevant role. This assumption was investigated by running two simulations for DLC 6.1, one considering the wave frequency (WF) and low

frequency (LF) contribution and another without the LF. The summary presented in Table 8 shows that the dynamic stiffness exhibits a relatively small difference of 7%, indicating that the LF does not significantly affect this system property. It is worth noting that the simulation, including the LF contribution, took longer, for instance, more than 1800 s. Since the inclusion of LF should better capture the underlined physics, the dynamic stiffness estimated with the simulation that includes both WF and LF has been used to run the 3600 s simulation; thus, for each DLC, the dynamic stiffness and the updated nylon section length are presented in Table 9.

Table 8 - Dynamic Stiffness [kN] comparison WF+LF vs WF

DLC	6.1		
Line	1	2	3
WF+LF	68585	44287	42770
WF	66415	46027	45604
Relative change	3.16%	3.93%	6.63%

Source: Author (2024)

Table 9 - Convergent Dynamic Stiffness and updated length after performing the practical procedure considering WF+LF.

DLC	Nylon section Line 1		Nylon section Line 2		Nylon section Line 2	
	Dynamic Stiffness [kN]	Updated Length [m]	Dynamic Stiffness [kN]	Updated Length [m]	Dynamic Stiffness [kN]	Updated Length [m]
1.6	61542	123.07	44398	120.71	45022	120.54
6.1	68585	123.02	44287	120.62	42770	120.58

Source: Author (2024)

Before performing the 3600 s simulation for the two DLC cases, the mooring stiffness matrix was calculated by conducting a static analysis in OrcaFlex without considering any environmental load, as presented in Table 10 and Table 11.

Table 10 - Mooring stiffness matrix for DLC 6.1 (Values kN, kN/rad or kN·m/rad)

	Surge	Sway	Heave	Roll	Pitch	Yaw
Surge	185.91	0.61	-6.19	-6.37	1824.6	-1.24
Sway	0.6	173.87	0.53	-1706.43	6.65	-106.32
Heave	-6.32	0.53	66.57	-5.27	-23.06	-0.3
Roll	-6.36	-1710.43	-5.28	50145.98	-67.78	858.13
Pitch	1820.82	6.63	-24.89	-67.47	50690.28	-10.91
Yaw	-1.18	-89.52	-0.25	847.31	-11.96	48672.57

Source: Author (2024)

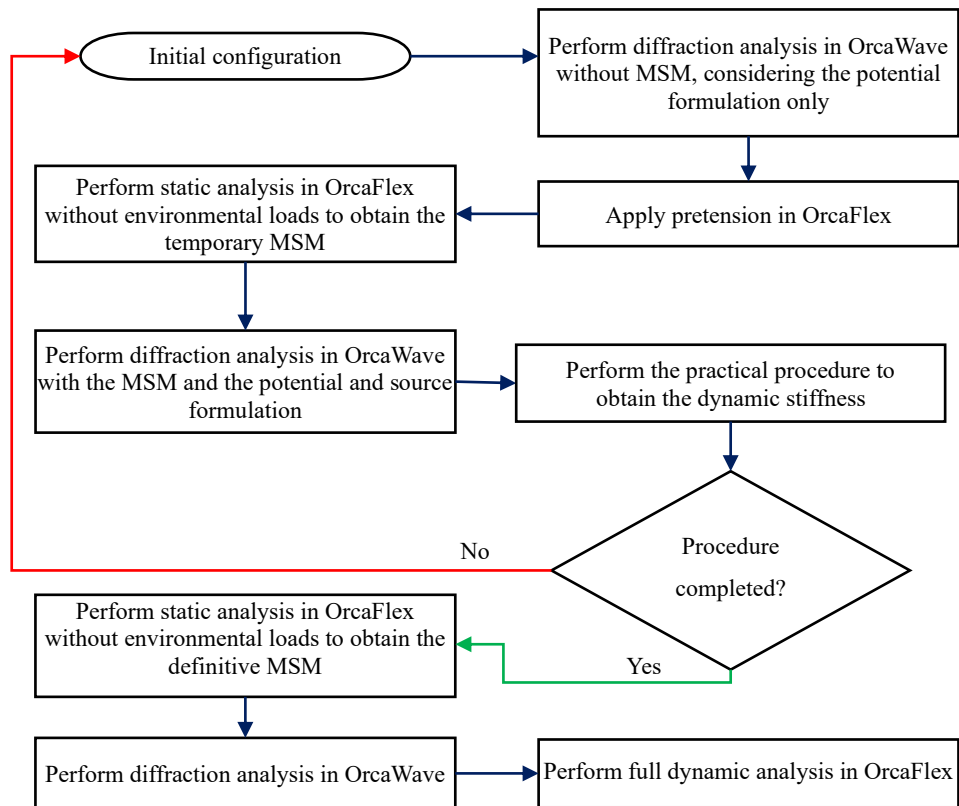
Table 11 - Mooring stiffness matrix for DLC 1.6 (Values kN, kN/rad or kN·m/rad)

	Surge	Sway	Heave	Roll	Pitch	Yaw
Surge	187.96	-0.45	-9.55	4.24	1868.83	-8.46
Sway	-0.45	169.45	-0.26	-1663.4	-4.85	-108.67
Heave	-9.55	-0.26	66.41	5.69	-65.02	0.61
Roll	4.24	-1663.4	5.69	49007.73	65.87	875.02
Pitch	1868.83	-4.85	-65.02	65.86	50782.33	-70.22
Yaw	-8.46	-108.67	0.61	1077.87	-83.84	47691.93

Source: Author (2024)

Once calculated, the mooring stiffness matrices were fed into OrcaWave software to perform two diffraction analyses. The resultant hydrodynamic tables were then used to perform two complete dynamic analyses for each DLC. It is important to emphasize that several attempts were made to adjust pretension, chain section length, nylon section length (while keeping the total length of the line constant), and diameter to achieve the convergent dynamic stiffness. The dynamic stiffness convergence was also found to be strongly sensitive to changes in the diameter and length of the chain and nylon sections, indicating the potential for further optimization of the mooring system. Figure 8 shows an overview of the whole iterative manual process in which MSM stands for mooring stiffness matrix.

Figure 8 - Overview of the iterative process.



Source: Author (2024)

2.2.3 Decay Test

The decay simulations were conducted to understand the system's behavior better. Simulations were conducted for the six degrees of freedom for each DLC, as the mooring stiffness varies. During the simulations, the wind turbine was parked, the wind loads were excluded, and the blade degrees of freedom were fixed. An initial offset of 10 meters or 10° was used. The natural periods were calculated by averaging the oscillation periods over the decays shown in Figure 9 and are presented in Table 12. The natural periods, as the eigenvalues are ordered in descending order to facilitate a comparison with the shape modes, which are calculated later in the modal analysis. The natural yaw period was found to be much greater

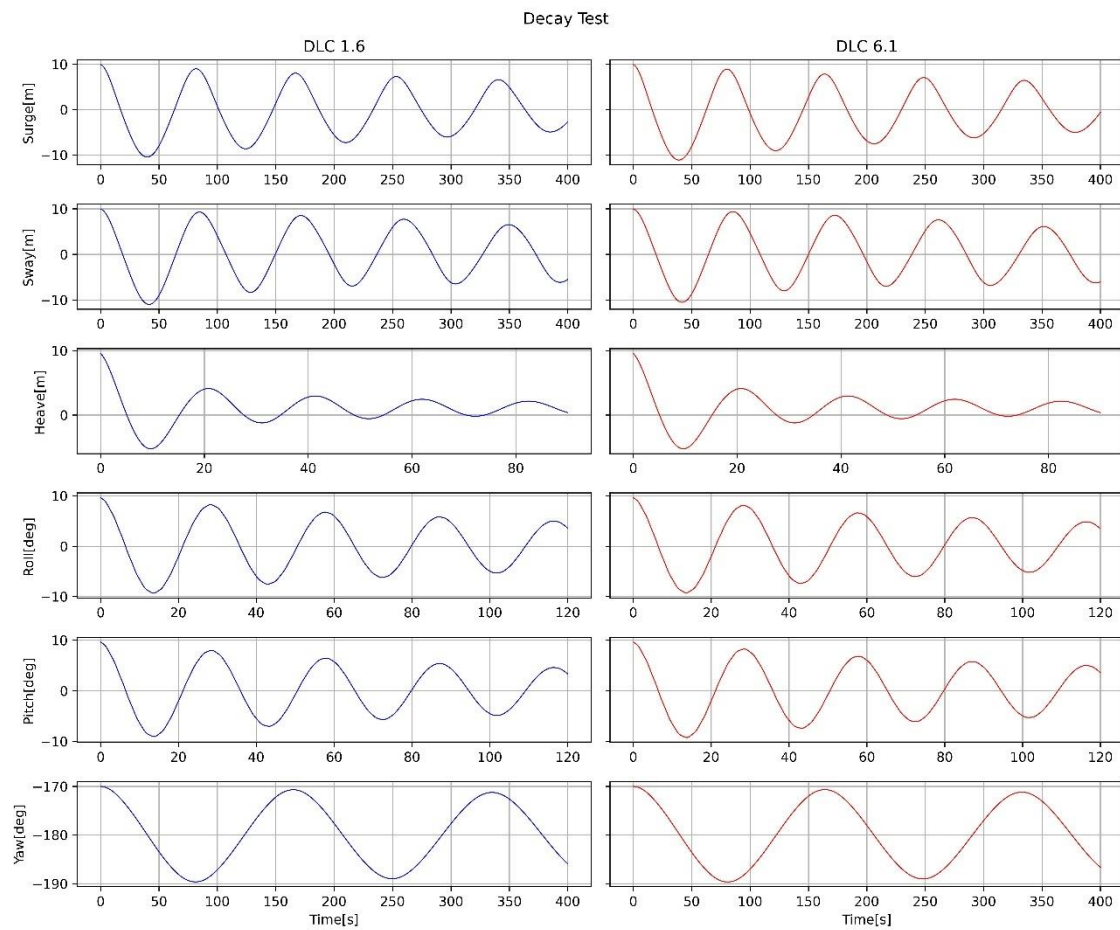
than what is typical for a semi-submersible platform, which should be greater than 50–60 s according to table 7.1 of DNV-RP-C205 (DET NORSE VERITAS, 2010). A possible explanation for this behavior is the softer response of the leeward lines 2 and 3.

Table 12 - Natural period of the floater motions

Mode	Natural Periods [s]		
	DF	DLC 1.6	DLC 6.1
1	Yaw	168.45	167.30
2	Sway	87.96	88.51
3	Surge	86.31	84.83
4	Roll	29.30	29.30
5	Pitch	29.30	29.25
6	Heave	20.85	20.85

Source: Author (2024).

Figure 9 - Decay Test.



Source: Author (2024).

2.2.4 Modal analysis

Modal analysis is crucial following a decay test as it provides a deeper understanding of a mechanical system's dynamic behavior. While the decay test reveals damping properties and transient response, modal analysis uncovers natural frequencies, mode shapes, and modal participation factors. This information aids in identifying resonance risks, predicting dynamic performance under different loads, and facilitating structural health monitoring. Therefore, modal analysis enhances engineers' ability to optimize designs, implement effective vibration control measures, and ensure the long-term reliability of mechanical systems.

For the reference platform VoltturnUS-S in a moored condition, with the reference turbine IEA 15 MW mounted on top and each modeled as a rigid body, the corresponding eigenvalue problem is formulated as follows:

$$\omega^2 \mathbf{M} \mathbf{x} = \mathbf{K} \mathbf{x} \quad (4)$$

where \mathbf{M} is the inertia matrix, \mathbf{K} is the stiffness matrix, ω is the natural frequency and \mathbf{x} is the associated mode shape. In this problem, six natural frequencies and six mode shapes are described in the local body coordinate system, as well as their surge, sway, heave, roll, pitch, and yaw components.

The inertia matrix \mathbf{M} is composed as follows:

$$\mathbf{M} = \mathbf{M}_s + \mathbf{M}_a \quad (5)$$

where \mathbf{M}_s is the structural inertia matrix of the platform and tower (Table 13), and \mathbf{M}_a is the added mass matrix for the infinite period (Table 14).

Table 13 - Structural Inertia Matrix of the platform and tower (Values in Te or Te·m²)

	Surge	Sway	Heave	Roll	Pitch	Yaw
Surge	29782.2	0.0	1.1	0.0	-100910.7	0.0
Sway	0.0	29782.8	0.0	100762.8	0.0	-7.4
Heave	1.1	0.0	45213.5	0.0	-41.9	0.0
Roll	0.0	100762.8	0.0	56184847.5	0.0	-1151837.3
Pitch	-100910.7	0.0	-41.9	0.0	56100571.1	0.0
Yaw	0.0	-7.4	0.0	-1151837.3	0.0	44098863.1

Source: Author (2024).

Table 14 - Added Mass Matrix for infinite period evaluated by OrcaWave (Values T_e , $T_e \cdot m$, or $T_e \cdot m^2$)

	Surge	Sway	Heave	Roll	Pitch	Yaw
Surge	9650.9	0.0	1.1	0.0	-100910.7	0.0
Sway	0.0	9651.5	0.0	100762.8	0.0	-7.4
Heave	1.1	0.0	25082.2	0.0	-41.9	0.0
Roll	0.0	100762.8	0.0	11614291.0	0.0	-316.2
Pitch	-100910.7	0.0	-41.9	0.0	11611344.1	0.0
Yaw	0.0	-7.4	0.0	-316.2	0.0	20161729.2

Source: Author (2024).

The stiffness matrix K is composed as follows:

$$K = K_H + K_M \quad (6)$$

where K_H is the hydrostatic stiffness matrix (Table 15), and K_M is the mooring stiffness matrix (MSM).

Table 15 - Hydrostatic Stiffness Matrix evaluated by OrcaWave (Values in kN, kN/rad or kN·m/rad)

	Surge	Sway	Heave	Roll	Pitch	Yaw
Surge	0	0	0	0	0	0
Sway	0	0	0	0	0	0
Heave	0	0	4469.186	0	-127.749	0
Roll	0	0	0	2631118	0	0
Pitch	0	0	-127.749	0	2643558	0
Yaw	0	0	0	0	0	0

Source: Author (2024).

Following the outlined procedure, the modal analysis will be conducted for DLC 6.1. The MSM for DLC 6.1 was calculated by OrcaFlex, excluding hydrostatic stiffness. Additionally, the lateral and axial coefficients of the chain section in OrcaFlex are set to zero to exclude non-conservative forces such as friction. Thus, for DLC 6.1, the MSM in the local coordinate system is shown in Table 16.

Table 16 - MSM for DLC 6.1 (Values kN, kN/rad or kN·m/rad)

	Surge	Sway	Heave	Roll	Pitch	Yaw
Surge	185.91	0.61	-6.37	-6.37	1827.58	-1.13
Sway	0.61	173.55	0.53	-1710.89	6.64	-96.81
Heave	-6.37	0.53	66.59	-5.29	-25.30	-0.27
Roll	-6.37	-1710.89	-5.29	50068.86	-67.65	760.73
Pitch	1827.58	6.64	-25.30	-67.65	50686.00	-9.82
Yaw	-1.13	-96.81	-0.27	951.94	-11.45	47202.96

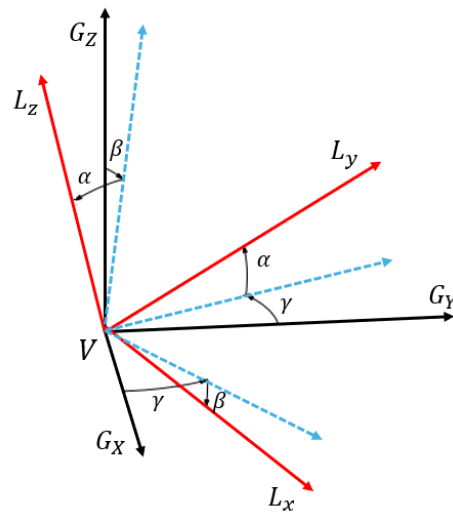
Source: Author (2024).

Analyzing the MSM, it is instructive to check the asymmetric coefficients by performing the following operation:

$$\mathbf{C}_{asym} = \mathbf{K}_M - \mathbf{K}_M^T \quad (7)$$

The asymmetric coefficients are displayed in bold in Table 17, given that the mooring stiffness coefficients were calculated using a method that considers only the unbalanced mooring system forces. This condition does not guarantee the symmetry of the stiffness matrix. Defined the Euler angles as shown in the Figure 10 , where α is defined as rotation about the current L_x axis, β is defined as rotation about the current L_y axis, γ is defined as rotation about the current L_z axis, these results can be verified by observing Table 16, where the terms Roll/Yaw ($dM_x/d\gamma$) and Yaw/Roll ($dM_z/d\alpha$) are **760.73** kN·m and **951.94** kN·m, respectively. From the vessel static results in Table 17, it can be noticed that the connections moment M_y is **-191.2** kN·m, which exactly matches the difference in the off-diagonal terms, i.e., $760.73 - 951.94 = -191.2$ kN·m. Similarly, Table 18 shows that the connection moments about the L_y axis and L_x axis are balanced by the hydrostatic stiffness moment about the respective axes.

Figure 10 - Euler angles definition.



Source: Author (2024).

Table 17 - Matrix showing asymmetric coefficients (Values kN, kN/rad or kN·m/rad)

	Surge	Sway	Heave	Roll	Pitch	Yaw
Surge	0.0	0.0	0.0	0.0	0.0	0.0
Sway	0.0	0.0	0.0	0.0	0.0	0.0
Heave	0.0	0.0	0.0	0.0	0.0	0.0
Roll	0.0	0.0	0.0	0.0	0.0	-191.2
Pitch	0.0	0.0	0.0	0.0	0.0	1.6
Yaw	0.0	0.0	0.0	191.2	-1.6	0.0

Source: Author (2024).

Table 18 - Connections and hydrostatic stiffness moment report (Value kN·m)

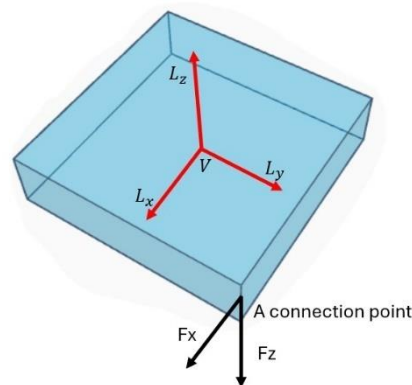
Variable	Value
VolturnUS-S semisub Connections L_x moment (kN·m)	-1.6
VolturnUS-S semisub Connections L_y moment (kN·m)	-191.2
VolturnUS-S semisub Hydrostatic stiffness L_x moment (kN·m)	1.6
VolturnUS-S semisub Hydrostatic stiffness L_y moment (kN·m)	191.2

Source: Author (2024).

It is highly instructive to elucidate these results from a physical standpoint. Considering a rigid body with only two forces applied at connection A (Figure 11). The moment acting on the body about the y-axis can be expressed as:

$$M_y = F_x \Delta z + F_z \Delta x \quad (8)$$

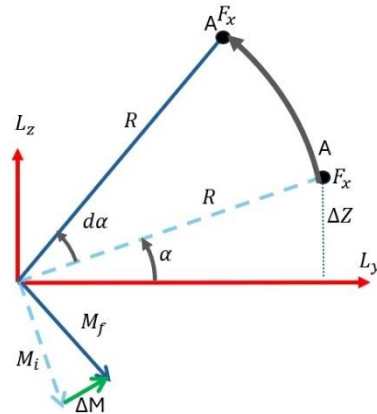
Figure 11 - Rigid Body with forces applied in a connection point.



Source: Author (2024).

Rotating anticlockwise the body about the L_x axis, a change in the location of the connection point A is observed according to Figure 12.

Figure 12 - Rotation of the body about the L_x axis.



Source: Author (2024).

The initial total moment M_i , and its component along the z-axis, holding the F_x constant (acting in the direction of the reader), can be calculated as follows:

$$M_i = F_x R \quad (9)$$

$$M_{i_z} = -F_x R \cos(\alpha) \quad (10)$$

The final total moment M_f and its component along the z-axis can be calculated as follows:

$$M_f = F_x R \quad (11)$$

$$M_{f_z} = -F_x R \cos(\alpha + d\alpha) \quad (12)$$

Hence, the change of moment acting about the z-axis can be calculated as follows:

$$dM_z = M_{f_z} - M_{i_z} = -F_x R [\cos(\alpha + d\alpha) - \cos\alpha] \quad (13)$$

Now considering that $\cos(\alpha + d\alpha) = \cos(\alpha)\cos(d\alpha) - \sin(\alpha)\sin(d\alpha)$ and $\cos(d\alpha) \cong 1$, $\sin(d\alpha) \cong d\alpha$, substituting in the previous equation follows:

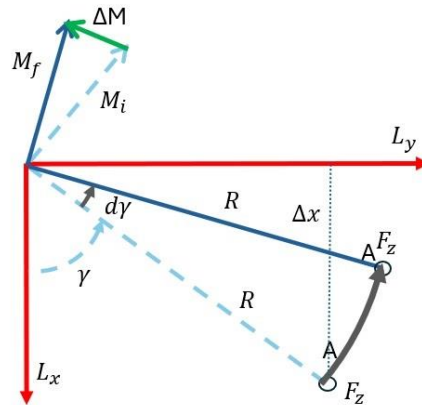
$$dM_z = F_x R \sin(\alpha) d\alpha = F_x \Delta Z d\alpha \quad (14)$$

Then the change of the moment M_z w.r.t $d\alpha$ can be calculated as follows:

$$\frac{dM_z}{d\alpha} = F_x \Delta Z \quad (15)$$

Now rotating anticlockwise the body about the L_z axis by an angle $d\gamma$, a change in the location of the connection point A is observed. Now, the force F_z is acting in the opposite direction of the reader, according to Figure 13.

Figure 13 - Rotation of the body about the L_z axis.



Source: Author (2024).

The change of moment acting about the L_x axis w.r.t $d\gamma$ can be found with the procedure seen above, holding the following equation:

$$\frac{dM_x}{d\gamma} = -F_z \Delta x \quad (16)$$

Using the equation (15) and (16), the connection moment M_y can be expressed by the algebraic sum of the off-diagonal terms as follows:

$$M_y = F_x \Delta z + F_z \Delta x = \frac{dM_z}{d\alpha} - \frac{dM_x}{d\gamma}$$

Since in this case $M_y = -191.2 \text{ kN} \cdot \text{m}$ follows that $\frac{dM_z}{d\alpha} \neq \frac{dM_x}{d\gamma}$ which explains the asymmetry in the MSM and shows the mooring system loads are balanced by the hydrostatic stiffness loads.

To perform a modal analysis is amenable to work with symmetric matrices, thus the stiffness matrix of the whole system can be obtained by the following equation:

$$\mathbf{K} = \mathbf{K}_H + \mathbf{K}_M + \mathbf{A}$$

where \mathbf{A} is the matrix in Table 19.

Table 19 - Matrix that restores the symmetry in the stiffness matrix.

	Surge	Sway	Heave	Roll	Pitch	Yaw
Surge	0,000	0,000	0,000	0,000	0,000	0,000
Sway	0,000	0,000	0,000	0,000	0,000	0,000
Heave	0,000	0,000	0,000	0,000	0,000	0,000
Roll	0,000	0,000	0,000	0,000	0,000	-191.2
Pitch	0,000	0,000	0,000	0,000	0,000	1.6
Yaw	0,000	0,000	0,000	0,000	0,000	0,000

Source: Author (2024).

After symmetrizing the stiffness matrix, the eigenvalue problem can be solved using a direct method already implemented in the NumPy package. The frequencies and mode shapes obtained with this direct method are summarized in Table 20. For comparison, results from the OrcaFlex modal analysis are presented in Table 21. The frequencies match very well, although there are differences in the sign of the mode shape of the sway, roll, and pitch. These discrepancies are primarily due to algorithmic variations, and while the norms differ due to normalization, the overall agreement is noteworthy.

Table 20 - Eigenvalues and eigenvectors obtained with the direct method.

Mode	Direct Method					
	1	2	3	4	5	6
Period (s)	192.183	82.841	80.072	28.572	28.482	19.837
Frequency (Hz)	0.005	0.012	0.012	0.035	0.035	0.050
X	-0.004	-0.049	-0.999	-0.008	0.983	-0.003
Y	-0.562	0.999	-0.049	0.982	0.010	0.000
Z	0.000	0.000	-0.001	-0.001	0.015	1.000
α	0.000	0.001	0.000	-0.189	-0.002	0.000
β	0.000	0.000	0.001	-0.002	0.184	0.000
γ	-0.827	0.000	0.000	-0.005	0.000	0.000

Source: Author (2024).

Table 21 - Eigenvalues and eigenvectors obtained with the Lanczos algorithm by OrcaFlex.

Mode	Lanczos algorithm (OrcaFlex)					
	1	2	3	4	5	6
Period (s)	192.457	83.08	80.326	28.489	28.397	19.858
Frequency (Hz)	0.005	0.012	0.012	0.035	0.035	0.05
X	0.0	0.034	-0.529	0.001	-0.101	-0.002
Y	-0.012	-0.689	-0.026	-0.116	-0.001	0.0
Z	0.0	0.0	-0.001	0.0	-0.001	0.74
α	0.0	-0.001	0.0	0.017	0.0	0.0
β	0.0	0.0	0.001	0.0	-0.014	0.0
γ	-0.017	0.0	0.0	0.0	0.0	0.0

Source: Author (2024).

In addition to the undamped modal analysis performed by both the DLCs, the effect of seabed friction is also investigated by setting the lateral coefficient to 0.5 and the axial coefficient to zero of the chain section in OrcaFlex. It is crucial to emphasize that during modal analysis in OrcaFlex, nodes on the seabed are restrained by a linear stiffness derived from the seabed's shear stiffness and the node's contact area. This limitation of movement along the seabed plane is essential for precise modal analysis of systems involving seabed contact. This adaptation yields a symmetric, conservative system well-suited for modal analysis. The results are compared with the natural periods calculated by the decay test and summarized in Table 22 and Table 23.

Table 22 - Natural periods [s] comparison for DLC 1.6.

Mode	DF	Decay test	Modal Analysis undamped	Modal Analysis with friction
1	Yaw	168.45	191.49	194.68
2	Sway	87.96	84.05	84.21
3	Surge	86.31	79.91	79.89
4	Roll	29.30	28.50	28.50
5	Pitch	29.30	28.39	28.39
6	Heave	20.85	19.86	19.86

Source: Author (2024).

Table 23 - Natural periods [s] comparison for DLC 6.1.

Mode	DF	Decay test	Modal Analysis undamped	Modal Analysis with friction
1	Yaw	167.30	192.46	189.37
2	Sway	88.51	83.08	82.93
3	Surge	84.83	80.33	80.34
4	Roll	29.30	28.49	28.49
5	Pitch	29.25	28.40	28.40
6	Heave	20.85	19.86	19.86

Source: Author (2024).

An initial comparison reveals that the natural periods obtained from a decay test, except for the yaw, exceed those derived from modal analysis under undamped conditions. In both Design Load Cases (DLCs), the surge and sway periods are longer in the decay test results, likely due to the inherent damping effects. However, disparities in the heave, roll, and pitch periods are notably smaller, suggesting reduced susceptibility to damping effects in these modes. Discrepancies in the yaw period suggest the influence of the lines and/or the frequency-dependent added mass since the modal analysis performed here used only the added mass for the infinity period. Besides this discrepancy, these findings are consistent with the modal analysis results, including friction, as depicted in the respective table columns.

To conclude this paragraph, according to DNV C205 (DET NORSKE VERITAS, 2010), the natural periods T_j , $j=1, 2, \dots, 6$, of a moored offshore structure are approximately given by

$$T_{jj} = \frac{2\pi}{\sqrt{\frac{K_{Mjj} + K_{Hjj}}{M_{Sjj} + M_{ajj}}}} \quad (17)$$

The natural surge period is determined using this approximated formula:

$$T_{11_{Surge}} = \frac{2\pi}{\sqrt{\frac{K_{M11}}{M_{S11} + M_{a11}}}} = \frac{2\pi}{\sqrt{\frac{185.91}{20131,3 + 9650,95}}} = 79.55 \text{ s} \quad (18)$$

and the result aligns very well with the surge natural period obtained from the modal analysis for DLC 6.1, which is $T_{11_{Surge}} = 80.33 \text{ s}$. This illustrates that the approximate formula can be safely utilized in the optimization problem to be addressed in the following chapter.

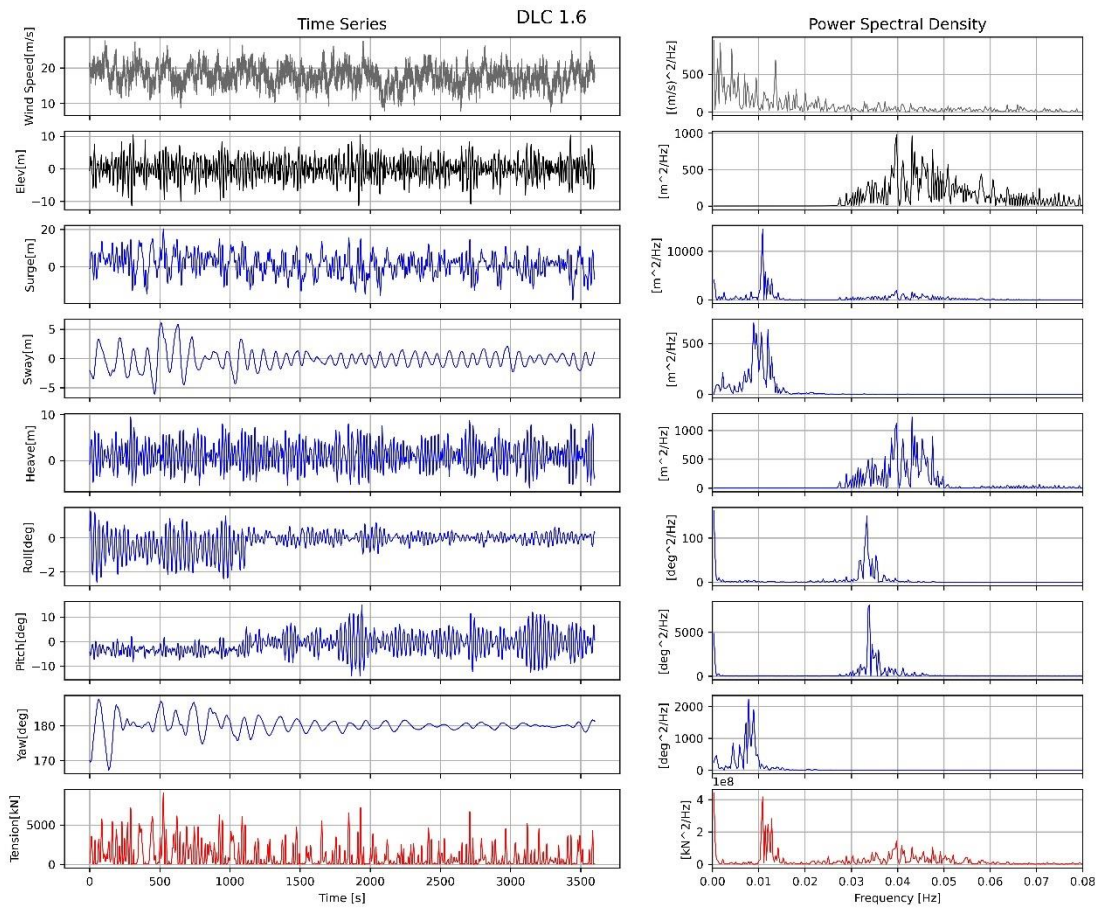
2.3 Results

To better understand the system's behavior, the time series of platform motions and power spectral density analysis are compared with the wave elevation for both DLCs. Additionally, the response of the platform motion and anchor loads for the chain-nylon mooring system under the two DLC load cases is compared with those obtained by Pillai et al. (2022b).

2.3.1 Time series and Power Spectral Density

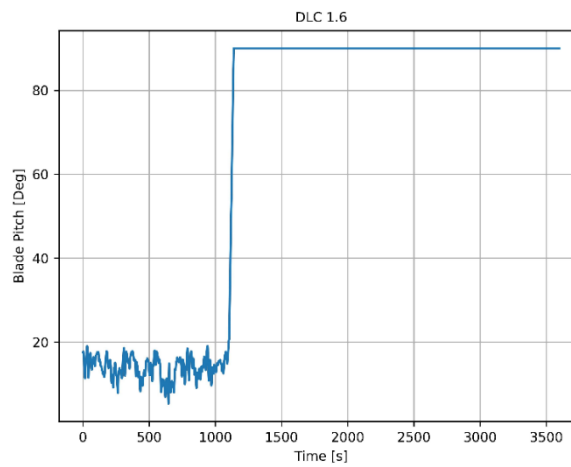
The time series and power spectral density plots of wind speed, wave elevation, surge, sway, roll, pitch, yaw, and tension in line 1 are shown in Figure 14 for DLC 1.6 and Figure 16 for DLC 6.1. In DLC 1.6, the wave frequencies (WF) major contribute is to heave, roll, pitch, and less to surge and tension, while low frequencies (LF) contribute to surge, sway, roll, pitch, yaw, and tension in line 1. This is expected for surge, sway, and yaw to have a natural period near or greater than 100 s, and for the tension, roll, and pitch, the turbine is in operational condition, transmitting the wind effect in LF to the line and the platform. In DLC 6.1, WF's major contribution is to heave, roll, and pitch, and less to surge and tension, while LF contributes to surge, sway, yaw, and tension, but in a smaller magnitude than in DLC 1.6. This is also expected since sway and yaw have a natural period greater than 100 s, and the turbine is in the parked condition, transmitting less wind effect in LF than in DLC 1.6 to line 1. For DLC 1.6, it is fascinating to observe the increase in the pitch angle after the blade has been pitched to shut down the rotor, reaching a blade pitch of 90° at approximately 1000 seconds, as depicted in the time series data of the blade pitch in Figure 15.

Figure 14 - DLC 1.6 Time Series and Power Spectra Density.



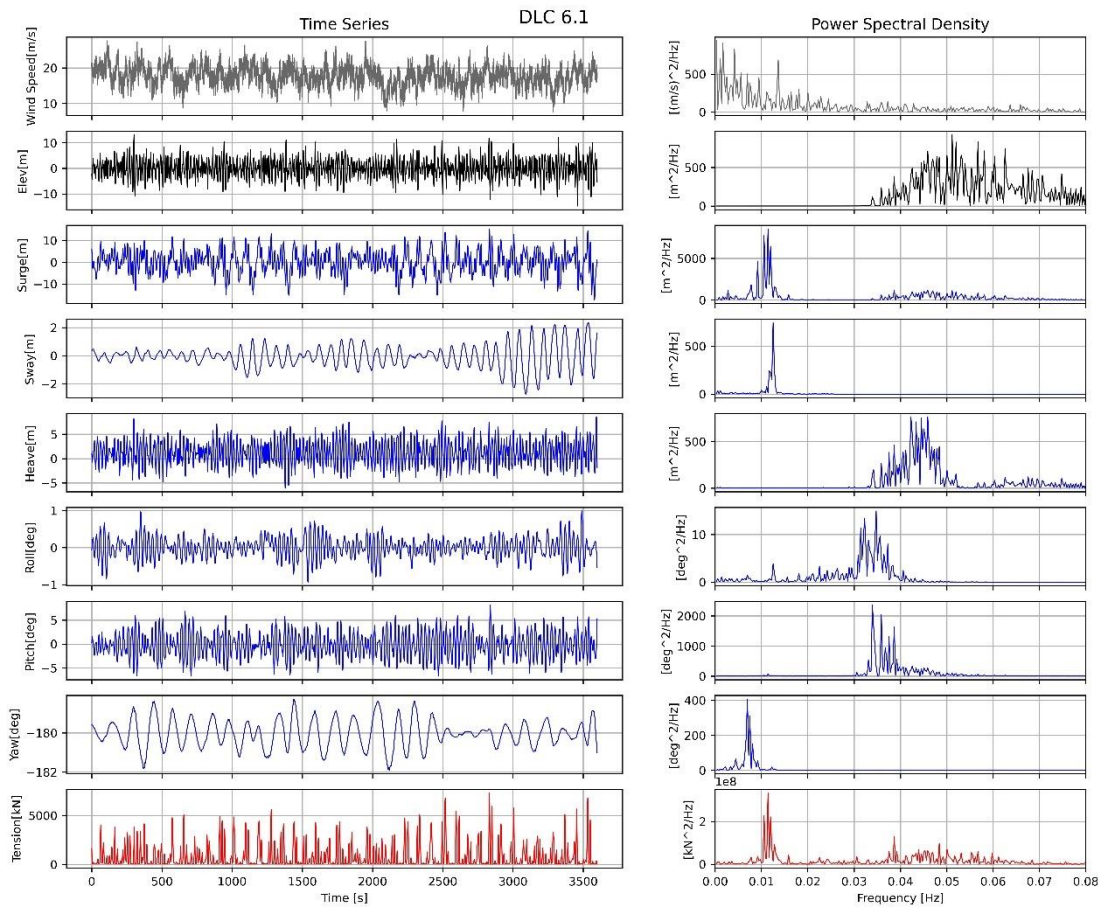
Source: Author (2024).

Figure 15 - Blade Pitch time series for DLC 1.6.



Source: Author (2024).

Figure 16 - DLC 6.1 Time Series and Power Spectra Density.



Source: Author (2024).

2.3.2 Surge – Sway

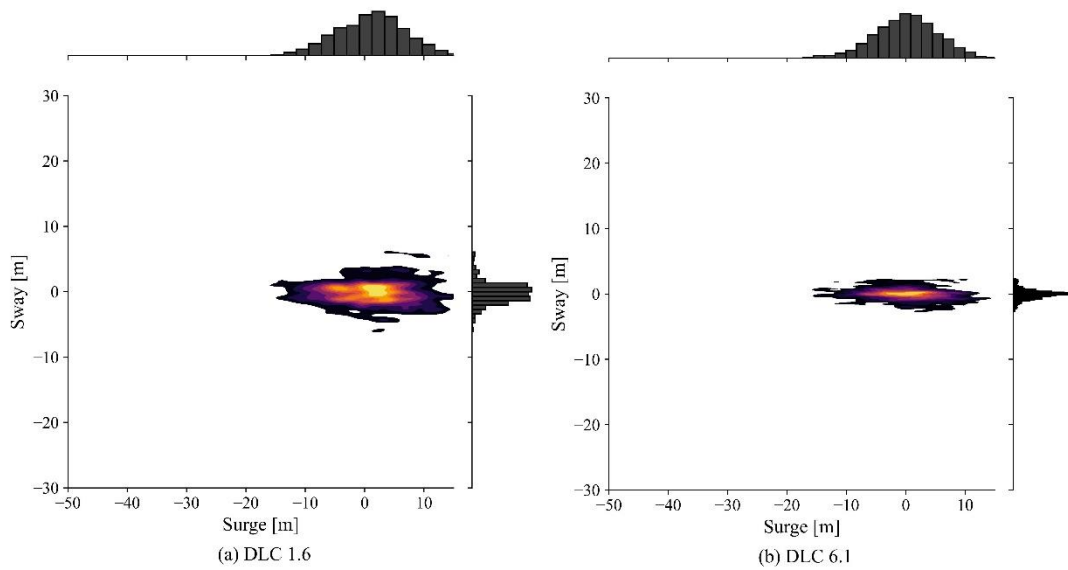
Figure 17 shows the surge-sway motions of the taut mooring nylon system as a heatmap, along with kernel density plots for each axis, to facilitate comparison with the results obtained for the polyester system (Figure 18). In DLC 1.6, surge ranged from -17.89 m to 20.32 m, staying within the prescribed limit of ± 25 m, while sway varied from -6.09 m to 6.10 m. In DLC 6.1, surge ranged from -17.38 m to 15.38 m, also staying below the prescribed limit, while sway varied from -2.37 m to 2.34 m. Surge and sway motions for the nylon system were comparable to those reported for the polyester system by Pillai et al. (2022a). However, both were generally smaller than those obtained for the chain catenary system. The platform motion statistics are summarized in Table 24.

Table 24 - Summary of the Platform excursion statistics.

	DLC 1.6				DLC 6.1			
	Min	Max	Mean	STD	Min	Max	Mean	STD
Surge [m]	-17.89	20.32	1.05	5.81	-17.38	15.38	0.10	5.27
Sway [m]	-6.09	6.10	-0.18	1.62	-2.73	2.34	-0.06	0.80

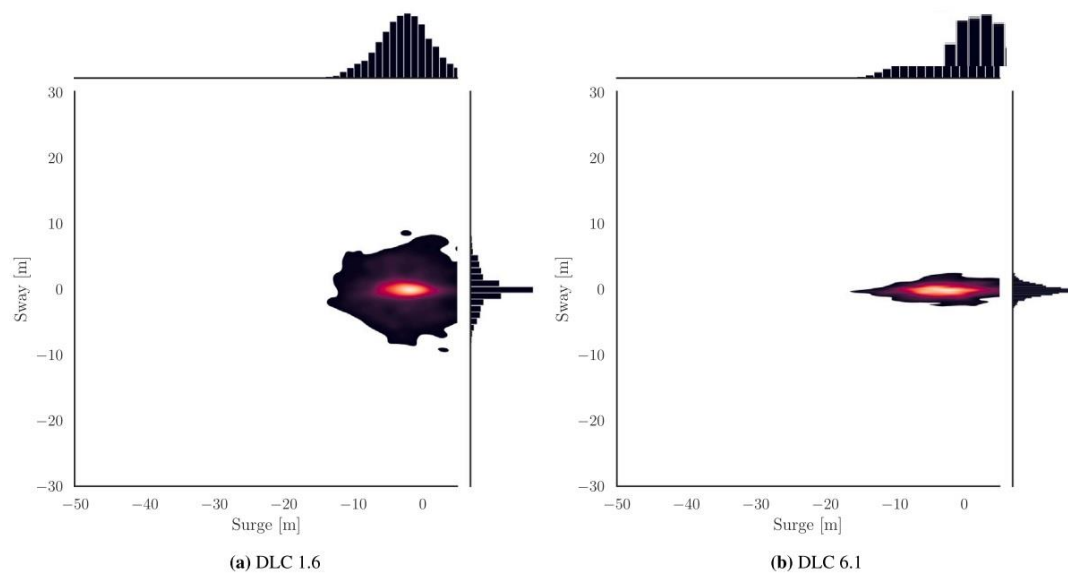
Source: Author (2024).

Figure 17 - Surge and Sway motions for Chain - Nylon mooring System.



Source: Author (2024).

Figure 18 - Surge and Sway motions for Chain - Polyester mooring System.



Source: (PILLAI et al., 2022b)

2.3.3 Roll – Pitch – Yaw

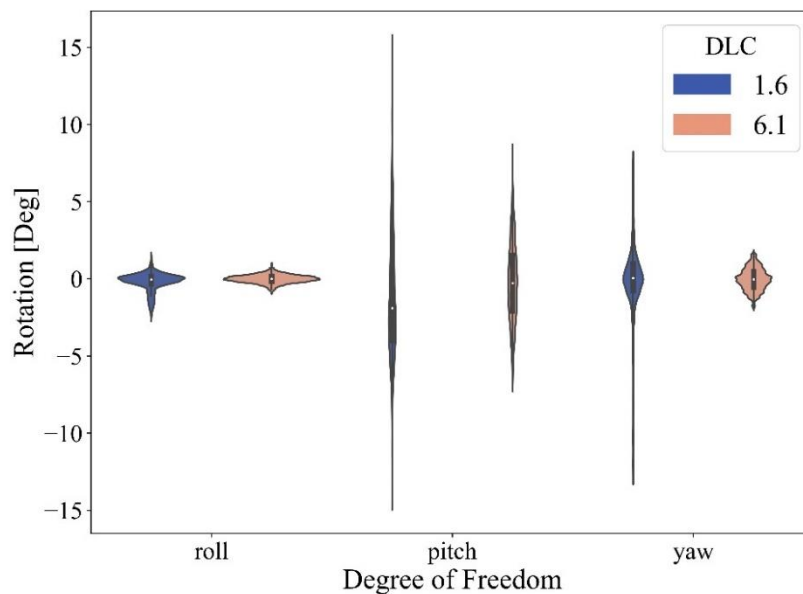
Figure 19 presents the rotations as a violin plot, depicting the median value at the white point and the kernel density distribution of the rotations during the time domain simulation. In contrast to the polyester case (Figure 20), the median value for all rotations is not aligned with zero. Additionally, the pitch and yaw observed in the parked condition (DLC 6.1) are greater than those observed in the operational case (DLC 1.6). This result may be due to the asymmetric response of the nylon lines, as well as the simultaneous effects of reduced aero damping (since the rotor is shut down) and frequency loads near the pitch and yaw natural frequencies that could potentially excite these rotations. Notably, the parked condition exhibits a smaller pitch of 8.18° compared to 14.94° for the operational condition. The statistics for the platform's rotations are summarized in Table 25.

Table 25 - Summary of the platform rotation's statistics

	DLC 1.6				DLC 6.1			
	Min	Max	Mean	STD	Min	Max	Mean	STD
Roll [Deg]	-2.62	1.60	-0.18	0.60	-0.93	0.99	0.00	0.27
Pitch [Deg]	-14.09	14.94	-1.25	4.10	-6.74	8.18	-0.23	2.57
Yaw [Deg]	-12.82	7.75	0.12	2.37	-1.90	1.73	-0.03	0.71

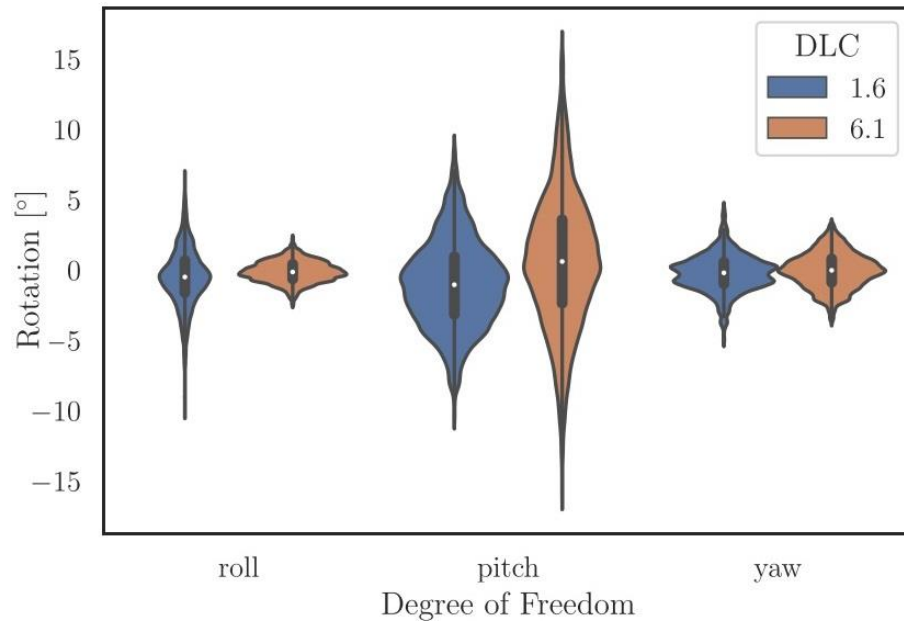
Source: Author (2024).

Figure 19 - Platform rotation for the taut mooring nylon system.



Source: Author (2024).

Figure 20 - Platform rotation for the taut mooring polyester system.



Source: (PILLAI et al., 2022b).

2.3.4 Anchor Peak Load

According to Xu et al. (2021b), equation (1) from the experiment can be used in preliminary design when the mean load is sufficiently greater than the MBL, but they did not provide a specific threshold for this condition. Table 26 shows the mean loads experienced by the mooring lines in each DLC. For both DLCs, increasing the mean load magnitude may be necessary to ensure the validity of applying the equation (1).

Table 26 - Mean load as % MBL.

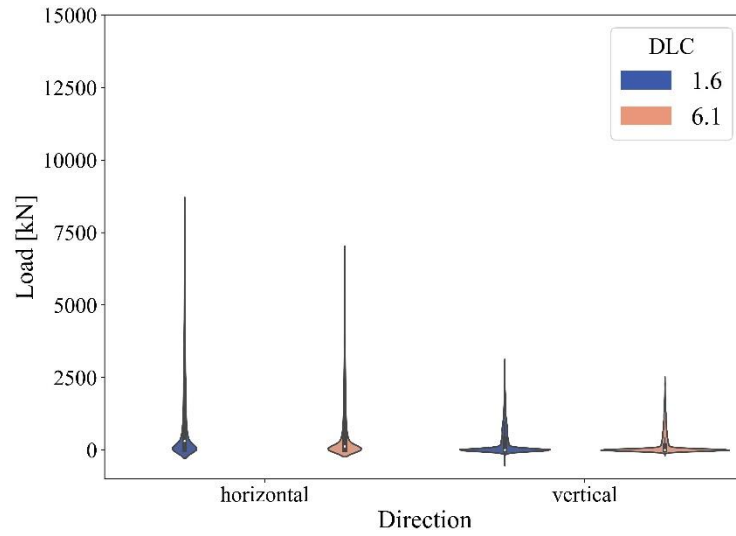
DLC	6.1	1.6
Mean load [kN]	778	978
MBL [kN]	20667	20667
%MBL	4%	5%

Source: Author (2024).

After verifying the applicability of equation (1) and assuming its validity for the purpose of this study, a comparison between the two systems was further explored. Figure 21 presents a violin plot that details the kernel density distributions of the horizontal and vertical anchor

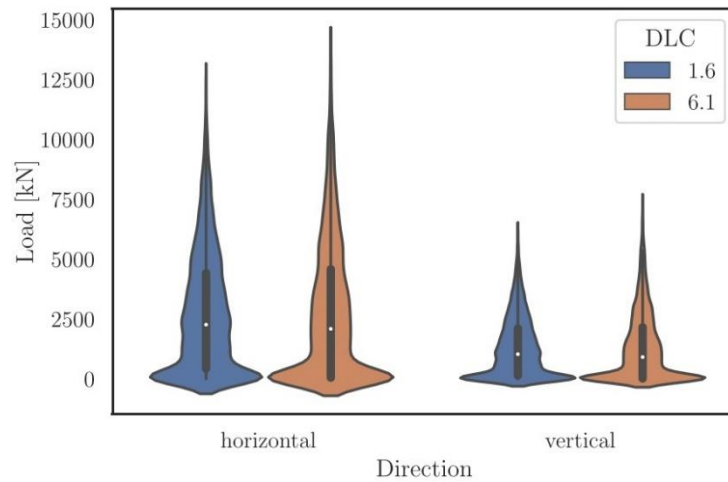
loads related to line 1. As shown, the loads remain reasonably low and stay below the pretension value in both operational and parked conditions. Furthermore, the simulation results indicate that the line for DLC 6.1 remained taut throughout the operation, without becoming slack at any point, while for DLC 1.6, the line became slack at the same point. The median vertical load is below the initial pretension for both conditions, but in the parked condition, it is smaller than in the operational one. However, the horizontal load, and consequently the resolved load, is greater than the initial pretension. The horizontal loads in both conditions dominate the vertical loads. The anchor loads of nylon and a polyester mooring system (as reported by Pillai et al. (2022b)), are compared and illustrated in Figure 22 and summarized in Table 27. Under load case DLC 1.6, the nylon system exhibited 49% and 67% of the vertical and horizontal anchor loads, respectively, compared to the polyester system. Table 28 compares the ratio of peak resolved load (PRL) and the minimum breaking load (MBL) between the two systems, indicating that the polyester system exceeded standard code limits while the nylon system remained within them. However, given that worst-case scenarios can occur with misaligned waves and wind (PILLAI et al., 2022a), it is advisable to consider a broader spectrum of load cases, including fatigue and accidental limit states. Although the nylon moored system is still in its early stages, our findings showed that it resulted in a smaller anchor load, less surge, roll, and pitch, but larger sway and yaw platform motions than the polyester system. Line 1 frequently experienced misalignment with the wave direction due to environmental conditions, as seen in Figure 23, likely reducing the tension acting on that line. Furthermore, the anchor loads exceeded those of the pure chain catenary. Table 29 summarizes the tension statistics of line 1.

Figure 21 - Anchor Load distribution for taut mooring nylon system.



Source: Author (2024).

Figure 22 - Anchor Load distribution for taut mooring polyester system.



Source: (PILLAI et al., 2022b)

Table 27 - Summary of peak loads in the taut moored nylon system compared to the taut moored polyester system.

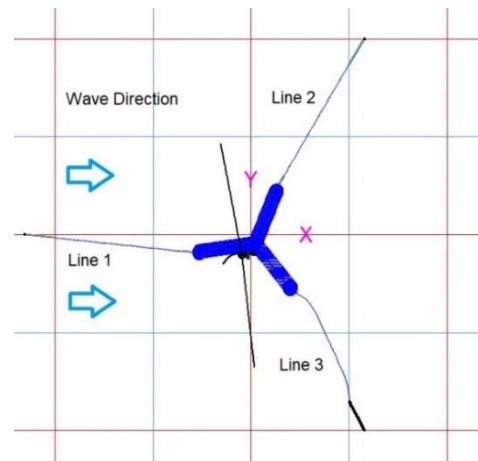
DLC	Peak vertical load [kN]		Relative to Poly.	Peak horizontal load [kN]		Relative to Poly.	Peak resolved load (PRL) [kN]		Relative to Poly.
	<i>Poly.</i>	<i>Nylon</i>		<i>Poly.</i>	<i>Nylon</i>		<i>Poly.</i>	<i>Nylon</i>	
1.6	6222	3028	49%	12560	8435	67%	14017	8962	64%
6.1	7360	2439	33%	13980	6803	49%	15799	7227	46%

Source: Author (2024).

Table 28 - Peak resolved load % MBL.

	Diameter [m]	MBL [kN]	PRL/MBL
<i>Polyester</i>	0.266	20601	0.77
<i>Nylon</i>	0.298	20667	0.35

Source: Author (2024).

Figure 23 - Misalignment of the line 1 during the simulation.

Source: Author (2023).

Table 29 - Summary of tension statistic in the line 1

	DLC 1.6				DLC 6.1			
	Min	Max	Mean	STD	Min	Max	Mean	STD
Tension [kN]	-3	8953	978	1397	5	7300	778	1180

Source: Author (2024).

2.4 Discussion

2.4.1 Platform Offset Requirements

To ensure a fair comparison between the taut-moored nylon system and the polyester system, the same requirements framework is employed as described in Pillai et al. (2022b), which was based on the studies by Allen et al. (2020) and Ma et al. (2019). According to the

requirements framework, maintaining the umbilical cable's integrity is achievable if the maximum excursions are within ± 25 meters. In the simulation of the taut-moored nylon system for DLC 1.6, the surge never exceeded the limit, with a maximum value of 20.32 m. The sway also remained within the limit, reaching a maximum of 6.10 m. However, it is important to note that equation (1) may not be applicable for both DLCs and special attention should be given to it. The requirements framework sets a limit of 6° for pitch rotations. The response of the nylon moored system exceeded this limit, reaching an absolute maximum pitch of 8.18° in DLC 6.1 and 14.94° in DLC 1.6.

2.4.2 Line Tension Requirements

Limiting the loads on anchors and lines is crucial to ensure reliable station-keeping of a platform. Following the American Petroleum Institute (API) guidelines, Pillai et al. (2022b) recommend a safety factor of 1.67 for the ultimate state limit (ULS), corresponding to a peak load limit of 60% of the minimum breaking load (MBL). The use of a nylon-moored system reduces both the horizontal and vertical loads on the anchor in both design load cases (DLCs), resulting in a lower peak load limit of 35% MBL. However, further optimizations are required to ensure that a more efficient nylon line can meet the API's recommended limit.

2.4.3 Design Improvements

As previous studies have pointed out (PHAM et al., 2019; PILLAI et al., 2022b), using a nylon-moored system can reduce peak loads on anchors and lines but can also result in larger rotations due to the system's more compliant behavior. To mitigate these excessive rotations, Pillai et al. (2022a) suggested replacing the nacelle fore-aft acceleration feedback with the platform pitch in the control loop, as proposed by Abbas et al. (2021) and Fleming et al. (2014). Despite concerns about fatigue and water absorption, which have historically limited the use of nylon in permanent mooring systems, recent results have shown that modifications to rope construction and improvements in fiber coatings can significantly enhance the lifetime of nylon

(CHEVILLOTTE et al., 2020).

2.5 Conclusion

The offshore wind industry's focus on exploring the potential energy in shallow water is rapidly increasing. This work builds upon previous research and extends the assessment of the mooring and anchor system for the 15 MW reference turbine, supported by the VoltturnUS-S platform in the shallow waters of the Celtic Sea. Specifically, this study examines a taut moored chain-nylon system using the mooring stiffness matrix and compares the results of anchor loads and platform motions with the taut moored chain-polyester system analyzed by Pillai et al. (2022b). The main findings of this paper are:

Smaller anchor load: The use of nylon results in a significant reduction in the peak anchor load of approximately 64% compared to polyester. This finding, combined with the development of new, more cost-efficient anchor concepts, suggests that a nylon-taut moored system has the potential to significantly reduce the cost of the foundations for a shallow water wind farm using the shared anchor concept.

Peak resolved loads: The taut moored system using nylon exhibited a peak load of only 35% MBL, whereas the polyester system had a peak load of 77% MBL. Furthermore, since nylon has the same MBL as polyester but is 10% less expensive, using a nylon-based taut moored system in a shallow water wind farm with a shared anchor could result in significant cost savings for the mooring system.

Platform offsets and rotations: To optimize the performance of the taut moored chain-nylon system, variables, including the length of the sections, chain and nylon diameter, lay angle, pretension, and anchor radius, must be fine-tuned. Moreover, improvements in mooring design, such as the application of distributed loads and control system strategies, can mitigate excessive responses and improve system performance.

Additional findings indicate that dynamic stiffness estimation should be conducted for each load case, and a suitable equation modeling nylon behavior needs validation through prototype investigations. To comprehensively investigate the nylon taut-moored system, future work should evaluate a wide range of design load cases, including accidental limit state (ALS) and fatigue limit state (FLS).

3 OPTIMIZATION OF COST-EFFICIENT SYNTHETIC MOORING SYSTEMS UTILIZING POLYMER SPRINGS FOR 15 MW FLOATING WIND TURBINES IN RELATIVELY SHALLOW WATERS

3.1 Introduction

3.1.1 Background

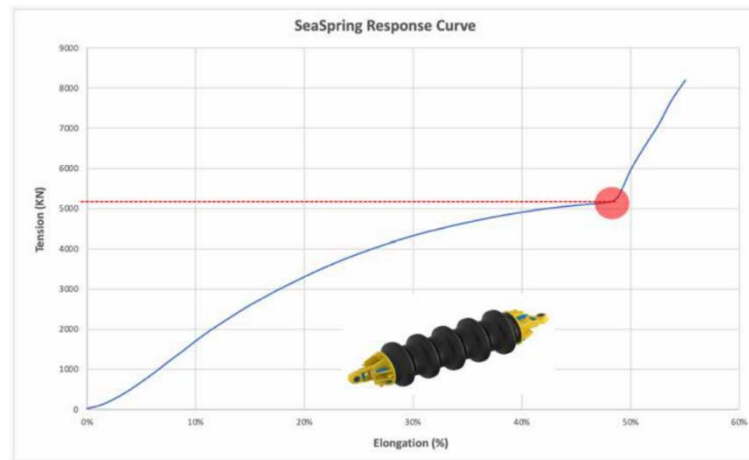
The renewable energy industry is rapidly advancing into open seas through the use of floating offshore wind technology. With a growing interest in shallow waters, the industry faces the challenge of adapting mooring systems to these environments (PILLAI et al., 2022b). Despite the increasing size of turbines, the issue of mooring systems in shallow waters persists. Recent studies have illuminated the potential for reducing peak loads and, consequently, Capital Expenditure (CAPEX) through the implementation of synthetic ropes (PILLAI et al., 2022b; VERDE; LAGES, 2023; WEST et al., 2023). Furthermore, incorporating spring polymer components has demonstrated promising CAPEX reduction prospects (ARYAWAN et al., 2023; LOZON et al., 2022). Various optimization methodologies have been proposed to address the need for viable mooring systems. Previous researchers have focused on optimizing mooring systems by analyzing mooring lines in the frequency domain (BENASSAI et al., 2015; BROMMUNDT et al., 2012). However, while efficient, this approach tends to underestimate the magnitude of tension within the lines. Another approach involves using metamodel techniques, where mooring lines are represented by surrogate models or statistical learners integrated into the optimization process (LI et al., 2019). Despite reducing the need for time-domain simulations, this method does not guarantee the accurate prediction of optimal designs. Alternatively, direct time-domain simulations can be conducted, but they come at a high computational cost (FERREIRA et al., 2017). Recently, a tiered constraint screening method has been introduced for a multi-objective optimization genetic algorithm, which aims to obtain mooring radius-lowest cost designs over a range of radii simultaneously (MOGA) (WEST et al., 2021, 2023). The validation of the optimization framework developed by West et al. (2023), using OpenFast and MoorDyn, began by comparing it with an implementation in OrcaFlex.

This step facilitated cross-validation and spurred the framework's adoption within the industry, filling a significant gap. Subsequently, the OrcaFlex-based framework was validated for a mooring system incorporating polymer springs, a mechanical complexity beyond the original scope of West et al. (2023). This validation process was challenging and required meticulous execution. Notably, there was no prior work optimizing the cost of this alternative mooring system, making this effort pioneering. The research established robust validation procedures to ensure realistic results and automated cost optimization processes. Most importantly, optimizing the alternative mooring system led to a substantial reduction in CAPEX, which is crucial for the viability of Offshore Wind Energy.

3.1.2 Polymer Spring

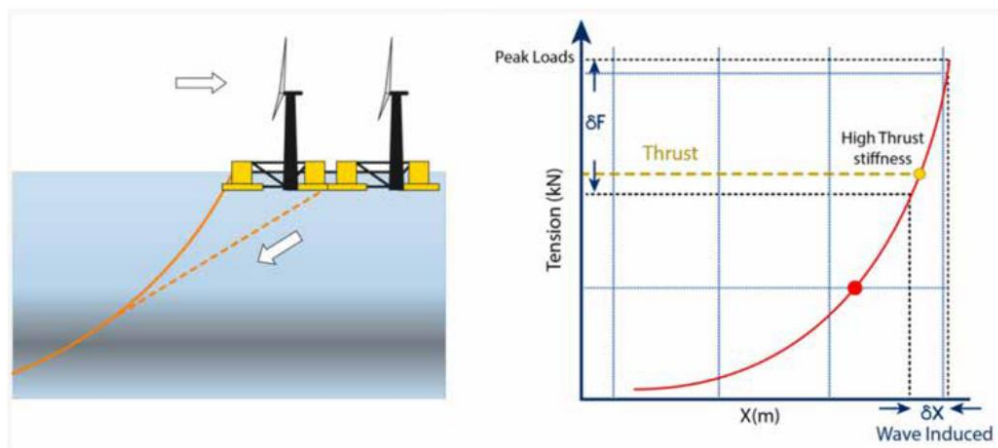
Polymer springs are versatile mooring line components. McEvoy and Kim (2017) applied them to floating tidal devices. Additional insights, including cost-benefit analyses for FOWT mooring systems, can be found in references (ARYAWAN et al., 2023; LOZON et al., 2022; MCEVOY; JOHNSTON; MARINE, 2019). These studies collectively show that polymer springs notably reduce maximum mooring loads and offer broader design benefits, including enhancing fatigue life, reducing mooring footprint, and optimizing platform motion. The spring can be designed with tailored stress-strain response curves. This paper, however, focuses on a spring design with a degressive axial stiffness response curve, as illustrated in Figure 24. Typically, the spring is defined by its "Target Load," which is the load or tension causing approximately 50% compression or 50% elongation when the polymer spring is pulled at both ends. For example, the polymer spring in Figure 24 has a target load of approximately 5,000 kN. Figure 25 shows the typical mooring load-excursion behavior of a FOWT due to forces from waves, wind, and currents. In this scenario, the mooring line is stiff near the turbine's thrust load. Peak mooring loads can be notably reduced by selecting the right polymer spring response curve, target load, and quantity or length of the polymer spring component. Figure 26 below illustrates the potential impact of using this spring. In this example, the polymer spring is designed to be stiff at lower tension levels and compliant with the turbine's thrust load.

Figure 24 - Example of a Polymer Spring Design.



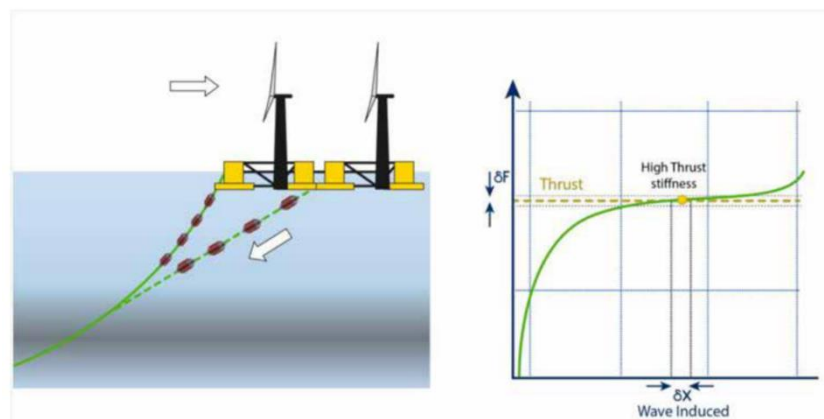
Source: (ARYAWAN et al., 2023).

Figure 25 - Illustration of FOWT Mooring Load Behavior



Source: (ARYAWAN et al., 2023).

Figure 26 - Impact of Polymer Spring on FOWT Mooring System Behavior



Source: (ARYAWAN et al., 2023).

3.2 Hardware and Software

The outcomes presented in this paper were derived utilizing computational resources featuring a laptop equipped with a central processing unit (CPU) comprising six cores, 16 GB RAM, and a 237 GB solid-state drive (SSD). The analysis involved the utilization of OrcaFlex and OrcaWave suites for offshore dynamic and diffraction analysis, the Pymoo Python package for NSGA2 optimization, Scipy for Savitzky-Golay filtering, Openturns for generating the Generalized Extreme Distribution, Joblib for parallel computation, and Numpy and Panda for additional computational tasks.

3.3 Optimization Framework

The optimization framework employed in this study follows a similar approach to that utilized by West et al. (2023). For the reader's convenience, their multi-objective routine is presented in Figure 27. It utilizes the Non-Sorted Genetic Algorithm II (NSGA2) to discover a Pareto Frontier encompassing two competing objectives: the minimum cost and the mooring system radii.

3.3.1 Constraint Handling

In this paper, a penalty-free niched approach is employed, eliminating the need for penalty parameters (DEB; AGRAWAL, 1999). The penalty function induces selective pressure toward the feasible region, and niching ensures diversity among feasible solutions, aiding the genetic recombination operator in discovering new feasible solutions. The penalty term, where infeasible solutions are solely compared based on their constraint violation values:

$$F(\mathbf{x}) = \begin{cases} f(\mathbf{x}), & \text{if } g_j(\mathbf{x}) \geq 0, \forall j \in J \\ f_{max} + \sum_{j=1}^J \langle g_j(\mathbf{x}) \rangle, & \text{otherwise} \end{cases} \quad (19)$$

where $f(\mathbf{x})$ is an objective function and $g_j(\mathbf{x})$ are constraints.

3.3.2 Termination Criteria

The running metric, a relatively recent approach (BLANK; DEB, 2020), analyzes a run when the true Pareto front is unknown. Generally, multi-objective algorithms aim to improve convergence based on the dominance relation or the diversity in the solution set. The running metric leverages this by monitoring indicators concerning extreme points and the non-dominated solution set each generation, deriving measures of convergence and diversity. Pymoo adopts this metric for terminating a multi-objective optimization algorithm in the absence of predefined criteria. Three parameters require definition: "tol" represents the allowable difference between specific metrics of non-dominated solutions in consecutive generations; "period" denotes the final number of generations for analysis, and "skip" specifies the number of excluded generations.

3.3.3 Definition of the optimization problem

As highlighted by West et al. (2023) for a broader system, it remains unclear whether the mooring system and cost are in competition, but it is crucial to comprehend their relationship. To ensure the competitiveness of relevant objectives, the mooring system radius and cost are mapped into competing criteria, as shown in the next section. Figure 27 depicts the operation of the NSGA2 algorithm within this framework. The mathematical expression of the optimization problem in question, accounting for the constraints, closely resembles the one presented by West et al. (2023). For the reader's convenience, it is reiterated here:

$$\begin{aligned}
& \text{Maximize } -L(\mathbf{x}) \text{ and } \varphi(\mathbf{x}) \\
& \text{Subject to } g_i(\mathbf{x}) \geq 0, i = 1, 2, \dots, 7 \\
& R_{min} \leq R \leq R_{max} \\
& L_{syn_{min}} \leq L_{syn} \leq L_{syn_{max}} \\
& d_{syn_{min}} \leq d_{syn} \leq d_{syn_{max}} \\
& d_{chain_{min}} \leq d_{chain} \leq d_{chain_{max}} \\
& V_{min} \leq V \leq V_{max}
\end{aligned} \tag{20}$$

wherein the symbols hold the following significance:

$L(\mathbf{x})$ the vector length defining a design in the domain mooring radio – lowest cost.

$\varphi(\mathbf{x})$ the angle defining a design in the domain mooring radio – lowest.

R is the mooring system radius.

L_{syn} is the length of the nylon line.

d_{syn} is the diameter of the nylon line.

d_{chain} is the diameter of the chain line and V is the volume of the buoy.

$g_1(\mathbf{x})$ is the mooring system geometric constraint violation.

$g_2(\mathbf{x})$ is the platform heave natural period constraint.

$g_3(\mathbf{x})$ is the platform pitch natural period constraint.

$g_4(\mathbf{x})$ is the platform surge natural period constraint.

$g_5(\mathbf{x})$ is the synthetic touchdown constraint.

$g_6(\mathbf{x})$ is the time-domain chain ultimate strength constraint.

$g_7(\mathbf{x})$ is the time-domain synthetic ultimate strength constraint.

R_{min} is the minimum mooring radius.

R_{max} is the maximum mooring radius.

$L_{syn_{min}}$ is the minimum synthetic length.

$L_{syn_{max}}$ is the maximum synthetic length.

$d_{syn_{min}}$ is the minimum synthetic diameter.

$d_{syn_{max}}$ is the maximum synthetic diameter.

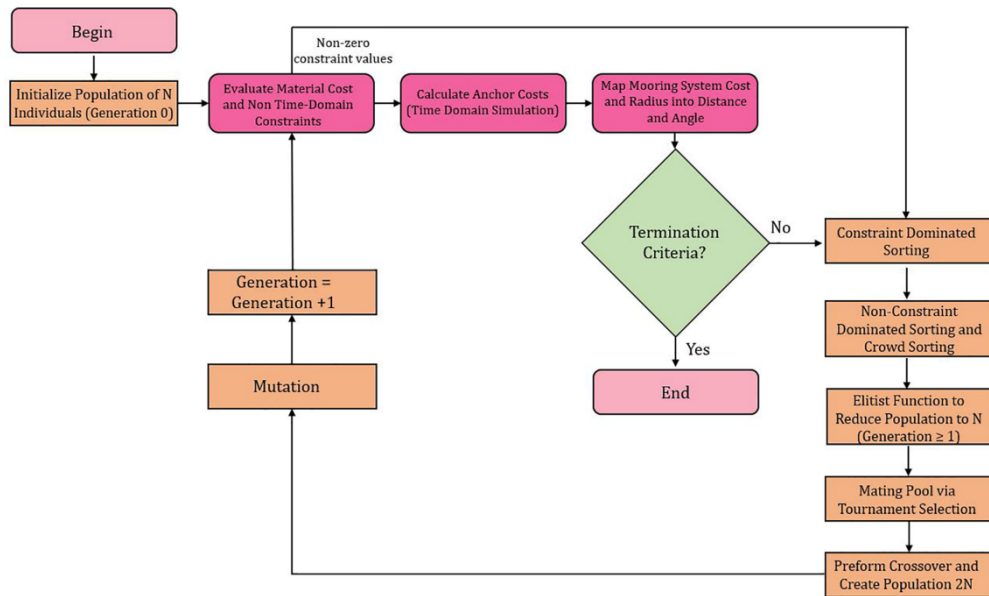
$d_{chain_{min}}$ is the minimum chain diameter.

$d_{chain_{max}}$ is the maximum chain diameter.

V_{min} is the minimum buoy displaced volume.

V_{max} is the maximum buoy displaced volume.

Figure 27 - Flowchart of the NSGA2 Framework.



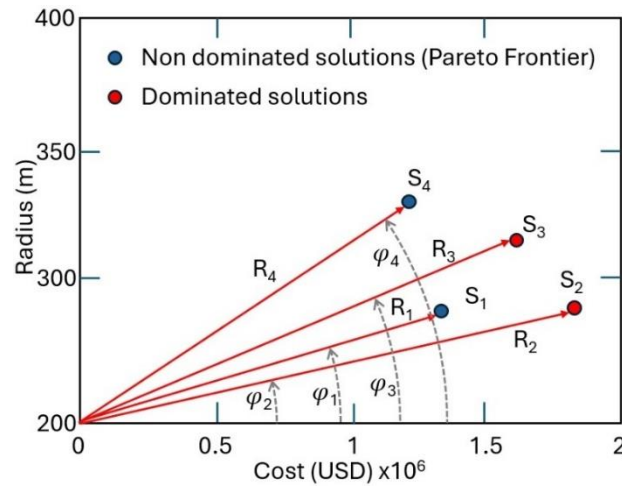
Source: (WEST et al., 2023)

3.3.3.1 Objective Function

This paragraph delves into the mapping function employed by West et al. (2023) within their optimization framework. In the realm of general mooring systems, it remains uncertain whether the system's radius and cost engage in direct competition, yet understanding their relationship is pivotal. Incorporating competing objectives within a multi-objective framework is essential to navigate this relationship and prevent solutions from converging into a single solution. To ensure that pertinent objectives are in contention, both the mooring system's radius and cost are translated into competing objectives. This process entails mapping the mooring radius and system cost, thereby establishing two opposing objectives. For each feasible design, a vector is formulated, ranging from zero mooring cost to the optimizer's lower bound of selectable radii, serving as a design variable. The objective serves a dual purpose: firstly, to minimize the vector length, directing the optimizer towards lower-cost designs, and secondly, to maximize the vector angle, ensuring a diverse range of designs across the solution space. This mapping process is visually depicted in Figure 28 and Table 29, which illustrates the comparison of the objective functions. A solution dominates another if the radius is superior

(smaller) and the angle is better (greater), is dominated when the reverse is true, and is nondominated if the radius is superior (smaller) and the angle is inferior (smaller), or vice versa. If a solution dominates or is nondominated in all comparisons, then it is permitted to be part of the Pareto frontier.

Figure 28 - Graphical representation of the process to ascertain their placement within a Pareto frontier.



Source: Author (2024)

Table 30 – A tabular comparison of the solutions was conducted to ascertain their placement within a Pareto frontier.

Solutions	Objective comparison	Classification
$S_1 : S_2$	$R_1 < R_2 \rightarrow S_1$ is better than S_2 $\varphi_1 > \varphi_2 \rightarrow S_1$ is better than S_2	S_1 dominates S_2
$S_1 : S_3$	$R_1 < R_3 \rightarrow S_1$ is better than S_3 $\varphi_1 < \varphi_3 \rightarrow S_1$ is worse than S_3	S_1 does not dominates S_3
$S_1 : S_4$	$R_1 < R_4 \rightarrow S_1$ is better than S_3 $\varphi_1 < \varphi_4 \rightarrow S_1$ is worse than S_3	S_1 does not dominates S_4
$S_2 : S_3$	$R_2 > R_3 \rightarrow S_2$ is worse than S_3 $\varphi_2 < \varphi_3 \rightarrow S_2$ is worse than S_3	S_2 is dominated by S_3
$S_2 : S_4$	$R_2 > R_4 \rightarrow S_2$ is worse than S_4 $\varphi_2 < \varphi_4 \rightarrow S_2$ is worse than S_4	S_2 is dominated by S_4
$S_3 : S_4$	$R_3 > R_4 \rightarrow S_3$ is worse than S_4 $\varphi_3 < \varphi_4 \rightarrow S_3$ is worse than S_4	S_3 is dominated by S_4

Source: Author (2024)

To precisely determine the vector length and angle, the cost is normalized to align with the radius's order of magnitude, enabling meaningful adjustments in both parameters. Equations

(21) and (22) provide detailed calculations for vector length and angle, respectively. At the end of each generation, the length and angle vectors describing each design's position are utilized to map the designs back into the mooring radius-lowest cost space. It is worth noting that while these angle and length values may not hold direct physical significance, they serve as tools to elucidate the relationship between the mooring footprint and cost.

$$L(\mathbf{x}) = \sqrt{\left(\frac{C(\mathbf{x})}{M_{norm}}\right)^2 + (R - R_{min})^2} \quad (21)$$

$$\varphi(\mathbf{x}) = \tan^{-1}\left(\frac{R - R_{min}}{\frac{C(\mathbf{x})}{M_{norm}}}\right) \quad (22)$$

where $C(\mathbf{x})$ is the total component cost of the mooring system, including the anchor cost, and M_{norm} is the mooring cost normalization constant.

3.3.3.2 Design variables

In the optimization problem of the mooring system with a synthetic line, five distinct variables encompass the system: mooring radius, synthetic line length, synthetic line diameter, chain diameter, and buoy displaced volume, as outlined in the table. From these quantities, all other attributes of the mooring system, including cost and performance, can be derived (Table 31). However, in optimizing the mooring system with a spring polymer, two additional variables are introduced: spring length and target load, as indicated in the table. Additionally, the synthetic line length is redefined to incorporate the length of the spring (Table 32).

Table 31 - Design variables for the synthetic-based mooring system

Design variable	Description	Variable Type	Range
R	Mooring system radius	Continuous	250 m – 400 m
L_{syn}	Length of the nylon line (as fraction of radius)	Continuous	0.42 - 0.65 (105 m – 260 m)
d_{syn}	Diameter of the nylon line	Continuous	175 mm – 240 mm
d_{chain}	Diameter of the chain line	Continuous	135 mm – 178 mm
V	Buoy displaced volume	Continuous	0 m ³ – 10 m ³

Source: Author (2024)

Table 32 - Design variables for the alternative mooring system

Design variable	Description	Variable Type	Range
L_{syn}	Length of the nylon line (as fraction of radius)	Continuous	0.4 - 0.61 (100 m – 244 m)
L_{spring}	Length of the spring (as fraction of radius)	Continuous	0.02 - 0.04 (5 m – 16 m)
<i>Target load</i>	Target load of the spring component	Continuous	3000 (kN) – 6000 (kN)

Source: Author (2024)

3.3.3.3 Constraints

The constraints in this optimization problem are carefully selected to guarantee the proper performance of the mooring system. These constraints are derived using the same tiered constraint methodology as described in West et al. (2023), which helps avoid the need for computationally intensive analyses on subpar designs. Many of these constraints are rooted in the IEC/ABS guidelines, which govern the construction and classification of floating offshore wind turbines. The tiered-constraint method proposed by West et al. (2023) aims to eliminate design variables that violate specific requirements. It operates as a cascade process, with the design moving through a stack of layers, each representing a constraint function. A constant is

added to each constraint function, tailored to filter out slightly unfeasible designs. This constant decreases as the design progresses through the layers.

3.3.3.3.1 Geometric feasibility constraint

This constraint serves to filter out extreme designs where mooring line lengths are impractical. The upper bound represents a line that goes directly from the fairlead to the seafloor and then horizontally to the anchors, lacking stiffness due to the mooring system's geometry. Conversely, excessively short lines are deemed non-functional, with a minimum length set at 85% of the straight-line anchor-to-fairlead distance. It is important to note that this threshold may require adjustment depending on the chosen mooring line materials. A schematic depicting this geometry is shown in Figure 29. The geometric constraints employed in the optimization routine are detailed as follows, according to West et al. (2023):

$$\begin{aligned}
 & \text{if: } L_T \leq 0.85 \sqrt{(R - R_f)^2 + (D_w - D_f)^2} \\
 \text{Then: } g_1 &= 100 \frac{0.85 \sqrt{(R - R_f)^2 + (D_w - D_f)^2} - L_T}{0.85 \sqrt{(R - R_f)^2 + (D_w - D_f)^2}} + 46 \\
 & \text{Else if: } (R - R_f) + (D_w - D_f) \leq L_T \\
 \text{Then: } g_1 &= 100 \frac{L_T - (R - R_f) + (D_w - D_f)}{[(R - R_f) + (D_w - D_f)]} + 46 \\
 & \text{Else: } g_1 = 0
 \end{aligned} \tag{23}$$

Where:

L_T is the total line length.

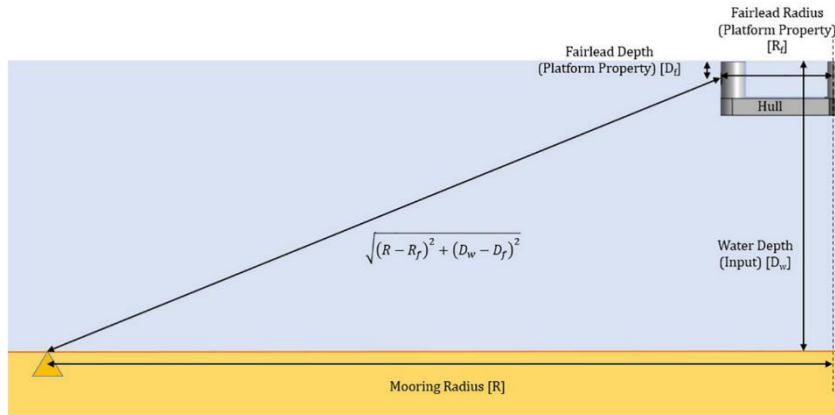
R is the design variable radius.

R_f the distance from the center of the platform to the fairlead connection point.

D_w is water depth.

D_f is the depth from the mean water line (MWL) to the fairlead connection point.

Figure 29 - Geometry constraint.



Source: (WEST et al., 2023).

3.3.3.3.2 Natural Period Constraints

The purpose of these constraints is to identify designs susceptible to resonance issues, which could potentially influence the time-domain response of the platform. Employing this analytical approach allows us to avoid costly time-domain simulations by utilizing the static calculations provided by OrcaFlex for the assessment of the mooring stiffness matrix (ORCINA, 2023). The approximate formulas for the calculation of the natural period, verified in the previous chapter, are used in the constraints employed in the optimization routine and are detailed as follows according to West et al. (2023):

$$T_{nHeave} = \frac{2\pi}{\sqrt{\frac{K_{33} + K_{33Mooring}}{m_{platform} + a_{33}}}}$$

if $T_{nHeave} \leq T_{Heave_{min}}$:

$$\text{Then } g_2 = 30 \frac{T_{Heave_{min}} - T_{nHeave}}{T_{Heave_{min}}} + 16$$

Else: $g_2 = 0$

Where:

K_{33} is the platform heave stiffness.

$K_{33Mooring}$ is the mooring system heave stiffness.

$m_{platform}$ is the mass of the platform.

a_{33} is the infinite period added mass of the platform in heave.

T_{nHeave} is the platform heave natural period.

$T_{Heave_{min}}$ is the minimum acceptable platform heave period.

$$T_{nPitch} = \frac{2\pi}{\sqrt{\frac{K_{55} + K_{55Mooring}}{I_{platform} + a_{55}}}}$$

$$\text{if } T_{nPitch} \leq T_{Pitch_{min}}:$$

$$\text{Then } g_3 = 30 \frac{T_{Pitch_{min}} - T_{nPitch}}{T_{Pitch_{min}}} + 16$$

$$\text{Else: } g_3 = 0$$
(25)

Where:

K_{55} is the platform pitch stiffness.

$K_{55Mooring}$ is the mooring system pitch stiffness.

$I_{platform}$ is platform pitch inertia.

a_{55} is the infinite period added inertia of the platform in pitch.

T_{nPitch} is the platform pitch natural period.

$T_{Pitch_{min}}$ is the minimum acceptable platform pitch period.

$$T_{nSurge} = \frac{2\pi}{\sqrt{\frac{K_{11Mooring}}{m_{platform} + a_{11}}}}$$

$$\text{if } T_{nSurge} \leq T_{Surge_{min}}:$$

$$\text{Then } g_4 = 30 \frac{T_{Surge_{min}} - T_{nSurge}}{T_{Surge_{min}}} + 16$$

$$\text{if } T_{nSurge} \geq T_{Surge_{max}}:$$

$$\text{Then } g_4 = 30 \frac{T_{nSurge} - T_{Surge_{max}}}{T_{Surge_{max}}} + 16$$

$$\text{Else: } g_4 = 0$$
(26)

Where:

$K_{11Mooring}$ is the mooring system surge stiffness.

a_{11} is the infinite period added mass of the platform in surge.

$T_{n_{surge}}$ is the platform surge natural period.

$T_{surge_{min}}$ is the minimum allowable surge period.

$T_{surge_{max}}$ is the maximum allowable surge period.

3.3.3.3.3 Touchdown constraint

The "touchdown constraint" ensures that the nylon line does not make contact with the seabed. To achieve this, static calculations are performed in OrcaFlex for environmental loads acting in 0° and 180° directions. Afterward, the top and bottom positions of the line are determined, and the catenary equation is applied to calculate the line's position. Subsequently, equation (27) is employed to verify that the synthetic section remains at least 1.0 meter above the seafloor for each unique loading scenario.

$$\begin{aligned}
 & Z_{min} = \min[z_i(s)] \\
 & \text{if } Z_{min} \leq Z_{syn_{allowable}}: \\
 & \text{Then } g_5 = 10 \frac{Z_{syn_{allowable}} - Z_{min}}{Z_{syn_{allowable}}} + 6 \\
 & \text{Else: } g_5 = 0
 \end{aligned} \tag{27}$$

Where:

Z_{min} is the minimum distance from the seabed of the synthetic section of the mooring line.

z_i is the vertical position of line in 0° and 180° loading cases.

$Z_{syn_{allowable}}$ is the allowable synthetic distance from the seafloor (1.0 m).

3.3.3.3.4 DLC 6.1-time constraints

The constraints $\mathbf{g}_6(\mathbf{x})$, $\mathbf{g}_7(\mathbf{x})$ pertains to DLC 6.1-time constraints, ensuring the mooring lines' ability to withstand dynamic loading. Just as in West et al. (2023), the ABS upper-lower bound stiffness model is used to determine the tension in the synthetic mooring

lines in this study (ABS, 2021). The maximum line tension constraints for both the chain and synthetic sections of the mooring line are expressed in the following equations, respectively:

$$\begin{aligned}
 & \text{if } F_{fchain} T_{fairlead_{max}} \geq MBS_{chain}: \\
 \text{Then } g_6 &= 3 \frac{F_{fchain} T_{fairlead_{max}} - MBS_{chain}}{MBS_{chain}} \\
 & \text{Else: } g_6 = 0
 \end{aligned} \tag{28}$$

Where:

$T_{fairlead_{max}}$ is the maximum tension at the fairlead.

F_{fchain} is the chain fatigue factor.

MBS_{chain} is the minimum breaking strength of the chain.

$$\begin{aligned}
 & \text{if } F_{syn} T_{syn_{max}} \geq MBS_{syn}: \\
 \text{Then } g_7 &= 3 \frac{F_{syn} T_{syn_{max}} - MBS_{syn}}{MBS_{syn}} \\
 & \text{Else: } g_7 = 0
 \end{aligned} \tag{29}$$

Where:

$T_{syn_{max}}$ is the maximum tension in the synthetic line.

F_{syn} is the ABS synthetic factor of safety (FoS) for a synthetic mooring line.

MBS_{syn} is the minimum breaking strength of the synthetic mooring line in dry condition.

The last constraint $g_8(\mathbf{x})$ will be used solely for the optimization of the alternative mooring system with the inclusion of the spring component and is expressed by the following equation:

$$\begin{aligned}
 & \text{if } T_{fairlead_{max}} \geq T_{target\ load}: \\
 \text{Then } g_8 &= 3 \frac{T_{fairlead_{max}} - T_{target\ load}}{T_{target\ load}} \\
 & \text{Else: } g_8 = 0
 \end{aligned} \tag{30}$$

3.3.3.3.5 Statistical Learner approach

As previously emphasized, the tension imposed on the mooring line presents a constraint within the design domain, necessitating assessment through time-domain simulation. An alternative to the computationally intensive time-domain simulation method within an optimization framework is the utilization of statistical learning techniques. Although it is recognized that such methods may not ensure precise prediction of optimal designs, there is merit in investigating their effectiveness. Various statistical learning models, ranging from basic linear regression to more complex ones such as polynomial regression, neural networks, random forests, and Extreme Gradient Boosting (XGB), are available for consideration (KUNAPULI, 2023). However, it is paramount to evaluate the trade-offs in terms of deployment time and the time saved by employing these models. Six-hour simulations were conducted to determine the appropriate wave seed for the optimization framework, encompassing wave loads, mean wind loads, mean current loads, and mean wave drift loads, in addition to utilizing the ABS method for synthetic line modeling. Analysis of the resultant data revealed a linear relationship between the design radius variable and the ratio of dynamic tension to static tension (SDTR). Consequently, a pragmatic approach was adopted, employing linear regression as a surrogate for time-domain simulation. This approach simplifies by overlooking the influence of other design variables and the non-linearity of physics since the primary objective was to assess the performance of a basic statistical learner compared to direct optimization results while also considering the trade-off between the time consumed to deploy the learner and the time saved in its usage. Consequently, the constraints $\mathbf{g}_6(\mathbf{x})$ and $\mathbf{g}_7(\mathbf{x})$ can be formulated using Equations (28) and (29), taking into account the following expressions:

$$T_{fairlead_{max}} = SDTR T_{Static\ fairlead} \quad (31)$$

$$T_{Syn_{max}} = SDTR T_{Static\ Syn} \quad (32)$$

$$T_{anchor_{max}} = SDTR T_{Static\ Anchor} \quad (33)$$

$$Mudline\ Angle_{max} = SDTR\ Mudline\ Angle_{Static} \quad (34)$$

$$SDTR = A\ radius + B \quad (35)$$

In the equation (34) the $Mudline\ Angle_{max}$, is the angle formed by the bottom chain line with the seabed in the dynamic simulation, while $Mudline\ Angle_{Static}$ is calculated during

the static simulation. In the equation (35) the coefficients A and B are to be determined considering predefined sets of design configurations as shown in the section 3.4.6.

3.4 Input data

The necessary inputs for conducting the optimization in this study are outlined in the following sections. They are consistent with those employed by West et al. (2023). For a more detailed explanation of the data inputs, readers should refer to the mentioned work.

3.4.1 Nylon mooring system configuration

The mooring system's geometry for optimization is depicted in Figure 30. The mooring system properties are contained in Table 33. The stiffnesses and breaking strengths of the chain and nylon lines, consistent with West et al. (2023), are displayed in Figure 31. The specific gravity of the synthetic lines is 1.15 gr/cm^3 , and the mass density of the steel chain is 8050 kg/m^3 . The nondimensionalized stiffness values for both the chain and synthetic mooring components are provided in Table 34. The material cost data used for estimating the mooring cost can be found in Table 35. As West et al. (2023) highlighted, estimating the anchor's cost is complicated because it can only be determined after a time-domain simulation. In contrast, the costs of the other mooring system components can be predetermined. Like West et al. (2023), the Vryhof Stevmantis Mk 5 drag embedment anchor is also examined (VRYHOF, 2018). Its ultimate holding capacity is determined in relation to its weight using the following equation:

$$UHC = AW^{0.92} \quad (36)$$

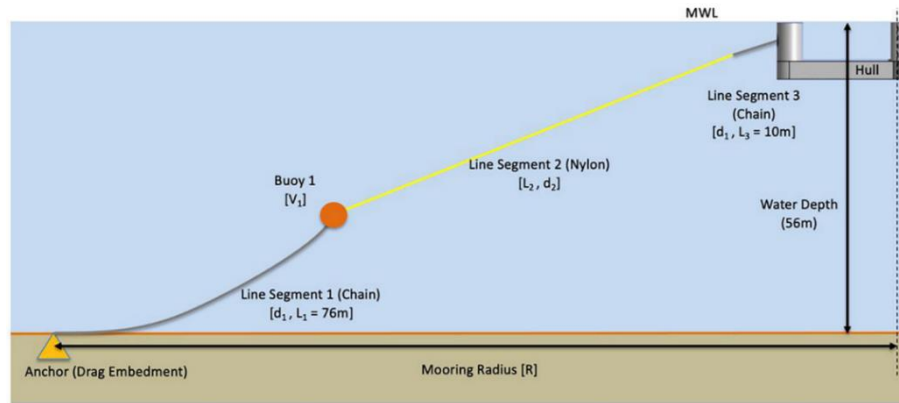
where UHC is the ultimate holding capacity of the anchor (in t), W is the weight of the anchor (in t), and A is a parameter that depends on soil and can vary from 24 to 110 (lower for mud/silt; higher for sand and hard clay). Drag embedment anchors are primarily engineered to withstand horizontal loads on the seafloor. According to API guidelines (API, 2018), there is some flexibility for accommodating minor vertical loads, as long as the recommended load reduction factors for a specific load relative to the seafloor, as outlined in Table 36, are applied.

Rearranging equation (36) and considering the relevant safety and load reduction factors results in an equation that relates the maximum anchor tension to the anchor weight, as shown below:

$$W = e^{\ln\left(\frac{F_{s_{anchor}} T}{R_f A}\right)/0.92} \tag{37}$$

where $F_{s_{anchor}}$ is the anchor safety factor and R_f is the mudline angle reduction factor.

Figure 30 - Mooring system geometry.



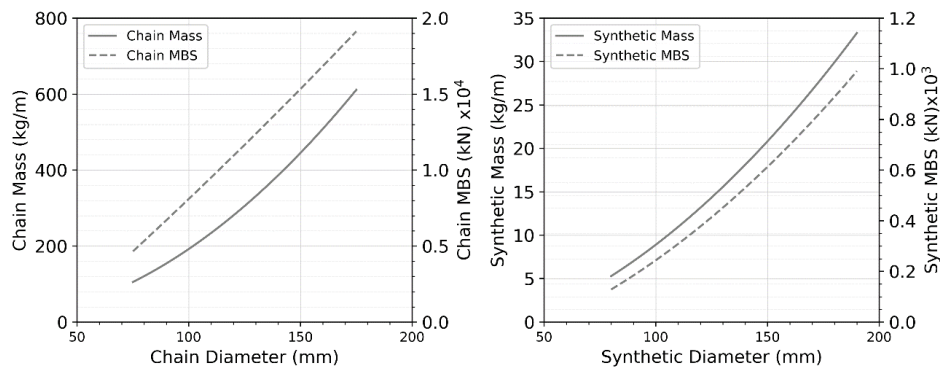
Source: (WEST et al., 2023).

Table 33 - Nylon – based mooring constant system properties.

Number of mooring lines	3
Angle of mooring lines	60°, 180°, 300°
Depth to anchors below SWL (water depth)	56 m
Depth to fairleads below SWL	14 m
Radius to fairleads from platform centerline	58 m
Unstretched chain length (leader)	10 m
Unstretched chain length (anchor)	76 m

Source: Author adapted from West et al. (2023).

Figure 31 - Dry chain mass and chain load capacity (left) and dry synthetic mass and synthetic load capacity (right).



Source: Author adapted from West et al. (2023).

Table 34 - Material nondimensionalized stiffness.

Material	Stiffness
Steel chain	43xMBS
Nylon (quasi-static stiffness)	5xMBS
Nylon (dynamic stiffness)	10xMBS

Source: Author adapted from West et al. (2023).

Table 35 - Mooring system component costs.

Material	Cost (USD/kg)
Steel chain	1.5
Nylon	17
Buoy	22.3
Anchor	155
Mooring cost normalization constant	3.3×10^4

Source: Author adapted from West et al. (2023).

Table 36 - Reduction factor vs mudline angle.

Mudline angle (°)	0	5	10	15	20
Reduction factor	1	0.98	0.95	0.89	0.81

Source: Author adapted from West et al. (2023).

3.4.2 Alternative mooring configuration with spring component

Figure 32 illustrates the mooring system for optimization with the inclusion of the spring component. Figure 33 depicts the spring response curves with a Target Load ranging from 2500 to 7500 kN. These curves enable the creation of a load-elongation Table 37 in OrcaFlex, dependent on the designated target load.

$$c = \text{Target Load}/2500 \quad (38)$$

Table 37 - Look up table varying with the Target Load.

Elongation [%]	0	5	10	15	20	25	30	35	40	45	46.5	50
Tension [kN] $\times 10^2$	c*0	c*5	c*9	c*12	c*16	c*19	c*21	c*22	c*24	c*25	c*26	c*32

Source: Author (2024).

The linear mass of the spring was estimated using data from Lozon et al. (2022), where a spring with a target load of 4000 kN has a linear mass of 1759.9 [kg/m]. The spring's linear

mass is estimated by scaling the linear mass of the polymer spring with a target load of 4000 kN, according to the following equation:

$$linear\ mass = \frac{1759.9}{4000} Target\ Load \tag{39}$$

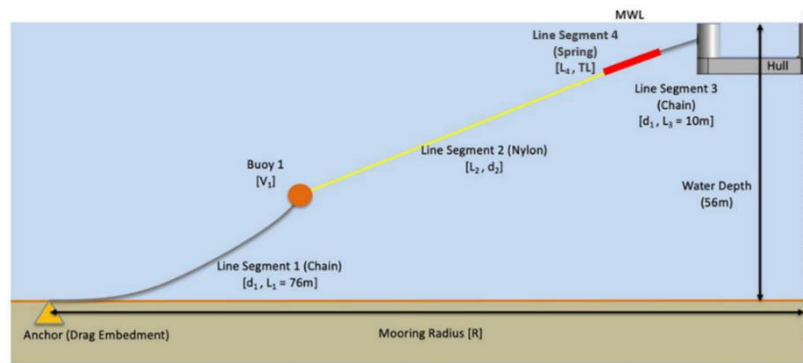
The cost of the spring component was sourced from McEvoy et al. (2019), who estimated the spring's price to be 20% higher than that of the chain. The spring price is detailed in the Table 38:

Table 38 - Spring component cost

Material	Cost (USD/kg)
Spring component	1.5*1.2 = 1.8

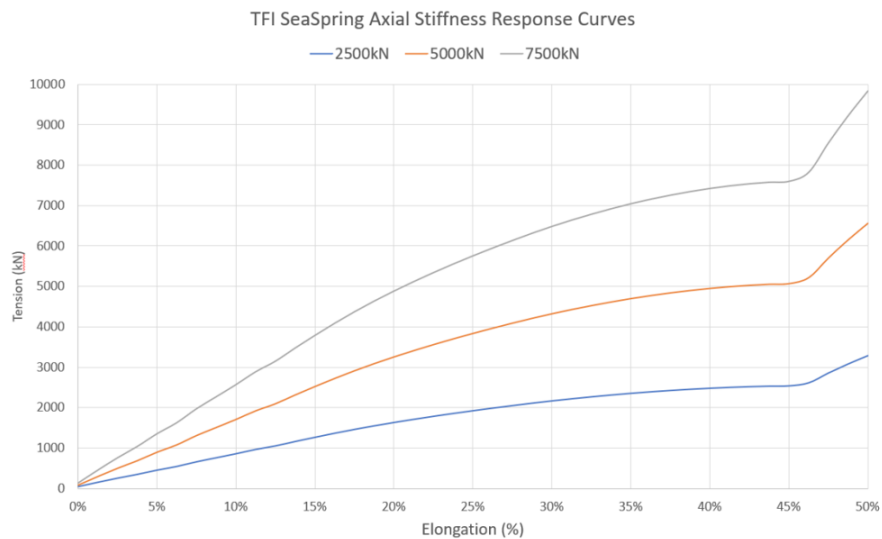
Source: Author (2024).

Figure 32 - Mooring system with spring component.



Source: Author adapted from West et al. (2023).

Figure 33 - Spring response curve.



Source: (ARYAWAN et al., 2023).

3.4.3 Reference Turbine and Platform

The VoltturnUS-S is a reference floating offshore wind platform created by the University of Maine, USA (ALLEN et al., 2020), in support of the International Energy Agency's (IEA) 15-megawatt (MW) reference wind turbine. This platform is of the semisubmersible type and consists of four columns, including three radial ones and a central column, linked by pontoon structures. All technical specifications of this platform design, including information about the wind turbine system, are available from Gaertener et al. (2020). The OrcaFlex model for this platform is accessible through Orcina as a part of their examples database under the designation "K03 15MW semi-sub FOWT" in which are also found the files necessary to run the hydrodynamics analysis with OrcaWave (ORCINA, 2023b).

3.4.4 Design code and requirements

The study's design criteria, following the approach of West et al. (2023), incorporate recommendations from ABS, IEC, and API, (ABS, 2023; API, 2014; IEC, 2019) along with the University of Maine's prior design work. These criteria cover anchor safety, synthetic material strength, and chain safety in line with ABS guidelines. The minimum chain safety factor is determined for 25-year DLC 1.2 fatigue conditions. The minimum synthetic safety factor considers the system to have no redundancy. Additional criteria focus on keeping the platform's natural period out of the wave energy region, with heave and pitch periods set at 18 s and 25 s, respectively. A surge period constraint of 55 to 350 s prevents excessively rigid or flexible mooring systems, avoiding the need for time-domain simulations. Moreover, the design ensures the synthetic mooring line stays above the seafloor. A conservative soil parameter is used for anchor sizing due to limited geotechnical data. Compliance with ABS regulations mandates a minimum 1.0 m clearance for the synthetic section, with the potential for larger clearances in more conservative designs. See Table 39 for a summary of these design requirements.

Table 39 - IEA 15 MW reference turbine design requirements.

Synthetic minimum breaking factor of safety	2.18
Chain minimum breaking factor of safety	3.3
Anchor factor of safety (non-redundant)	1.8
Soil parameter (—)	50
Maximum synthetic depth from Still Water Line (SWL) (m)	55
Maximum platform surge period (s)	350
Minimum platform surge period (s)	55
Minimum platform heave period (s)	18
Minimum platform pitch period (s)	25

Source: Author adapted from West et al. (2023).

3.4.5 Environmental conditions

Environmental data was extracted from West et al. (2023). Those authors obtained this data from a lease site near New York, including significant wave height and peak period (8.4 m and 11.65 s) as per DNV guidelines (DET NORSE VERITAS, 2010). These parameters facilitated estimating the JONSWAP spectrum's shape factor. Additionally, DNV's method for estimating mean drift force on a floating structure was applied using the JONSWAP spectrum and diagonal terms of the difference frequency quadratic transfer function. Current loading on the platform was determined by multiplying the surge term of the quadratic damping function for the 15-MW VoltturnUS-S platform by the squared current velocity at the site. The mean wind load on the turbine was calculated based on the 15 MW IEA turbine's thrust in the parked configuration and the site's wind speed. Table 40 summarizes the environmental loading data for the FOWT site. The combined wave, current, and wind loads are applied to the platform to expedite simulations and ensure computational feasibility. West et al. (2023) found that this approximate approach, while underpredicting dynamic line tension of 16%, was still deemed acceptable for a screening design.

Table 40 - Environmental Condition

1st Wave effect	H(m)	T(s)	γ
	8.4	11.65	3.09
2nd order Wave effect	Mean Load (kN)		
	64.2		
Current	Current velocity (m/s)		Mean Load (kN)
	1.39		1780
Wind	Wind velocity (m/s)		Mean Load (kN)
	39		896

Source: Author adapted from West et al. (2023).

3.4.6 Approach for modeling the extrapolation of peak load

For this work, a specific procedure guided the selection of the wave load seed. Three designs (A, B, C see Table 41) underwent six 1-hour simulations each, following ABS recommendations. These simulations accounted for wave loads, as well as mean loads for drift wave, current, and wind actions, calculating the average maximum tension for each simulation. Subsequently, each design underwent 24 simulations of 1000 seconds, each with a different seed. Peaks of the maximum tension derived from these simulations were fitted to a generalized extreme value distribution to estimate the expected number of peaks in a 1-hour simulation, providing the maximum probability of maximum tension. The maximum tension in the line was estimated using this probability and the GEV distribution. A comparison was made between this extrapolated maximum tension and the average maximum tension for each design to determine the seed that best approximated the extrapolated tension to the average tension. Subsequently, the three seeds were used to run 1000-second simulations for each of the three designs, and the extrapolated tension was compared to the average tension for each one. The seed with the lowest root mean square error among the three was selected as the optimal seed, see Table 42.

Table 41 - List of the designs considered for the determination of the seed.

Design	Radius (m)	Synthetic Length (m)	Chain Diameter (mm)	Synthetic Diameter (mm)	Buoy Displaced Volume (m ³)
A	278	138	167	208	7.24
B	340	194	159	201	4.63
C	397	248	154	195	4.69

Source: Author (2024).

Table 42 - Determination of the seed

1000 sec extrapolated tension T_{1k} (kN)							6 hours averaged tension T_{avg} (kN)
$(T_{avg} - T_{1k})/T_{1k}$	-0.5%		0.6%		0.4%		
Seed	747140245		1258363098		-214526383		
Design	A	Relative Change	B	Relative Change	C	Relative Change	
A	5122	0.55%	5260	-1.57%	5091	1.69%	5150
B	5235	1.51%	5354	-0.75%	5217	1.86%	5313
C	5096	-1.09%	5182	-2.73%	5062	-0.42%	5041
Root Mean Squared Error	0.019		0.032		0.025		

Source: Author (2024).

In the context of utilizing the statistical learner, the static-to-dynamic tension ratio (SDTR) is computed for each pre-defined design outlined in Table 43, as detailed in Table 44. Subsequently, the linear regression model parameters were determined to characterize the association between the radius and SDTR, as illustrated in Figure 34 and expressed by

$$SDTR = -0.004 \text{ radius} + 2.8727 \quad (40)$$

Other regression models, though potentially improving precision, were deemed beyond the study's scope.

Table 43 - list of designs for the calculation of the SDTR

Design	Radius (m)	Synthetic Length (m)	Chain Diameter (mm)	Synthetic Diameter (mm)	Buoy Displaced Volume (m ³)
A	278	138	167	208	7.24
B	340	194	159	201	4.63
C	397	248	154	195	4.69
D	317	173	160	196	2.93

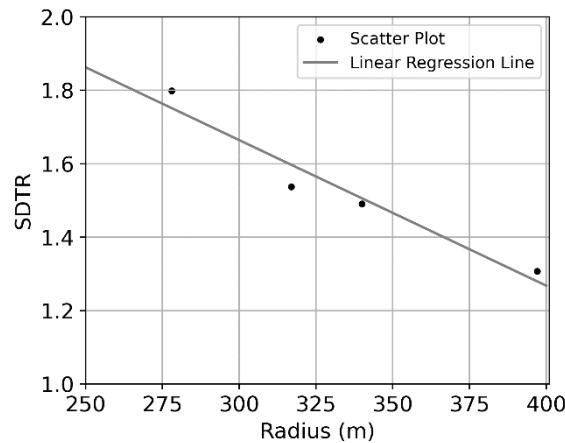
Source: Author (2024).

Table 44 - Calculation of SDTR.

Radius (m)	ABS Maximum Tension (kN)	Static Tension (kN)	Dynamic to Static Tension Ratio SDTR
397	5041	3857	1.307
340	5313	3564	1.491
317	4931	3209	1.537
278	5150	2862	1.799

Source: Author (2024).

Figure 34 - Linear regression line for radius/SDTR relationship.



Source: Author (2024).

To expedite the determination of mean offsets, linear and quadratic damping coefficients are adjusted in the OrcaFlex input files. This modification results in an overdamped system, enabling faster attainment of steady-state displacements and mooring line tensions. In the initial IEA 15-MW files, linear damping relies solely on coefficients from the potential flow analysis. To improve damping in the model for mean offset simulations, the linear damping matrix is implemented as defined in Table 45 in OrcaFlex.

Table 45 - Linear damping coefficient.

Surge kN/(m/s)	Sway kN/(m/s)	Heave kN/(m/s)	Roll kN·m/(rad/s)	Pitch kN·m/(rad/s)	Yaw kN·m/(rad/s)
5.00E+02	5.00E+02	1.00E+04	1.00E+07	1.00E+07	1.00E+06

Source: Author adapted from West et al. (2023).

The quadratic damping matrix is enhanced for mean offset simulations. The surge and sway degrees of freedom are increased tenfold in magnitude, while the heave degree of freedom

and all rotational degrees of freedom are increased by a factor of 100. Other components of the quadratic matrix remain unaltered. The modified quadratic damping matrix used for the mean offset simulations is defined in Table 46:

Table 46 - Quadratic damping coefficient.

Surge	Sway	Heave	Roll	Pitch	Yaw
kN/(m/s)²	kN/(m/s)²	kN/(m/s)²	kN·m/(rad/s)²	kN·m/(rad/s)²	kN·m/(rad/s)²
9.23E+02	9.23E+02	2.30E+03	1.68E+07	1.68E+07	4.80E+07

Source: Author adapted from West et al. (2023).

It is essential to mention that only diagonal terms can be used in OrcaFlex. Moreover, convergence parameters for static analysis have been defined in adherence to the specifications delineated in Table 47, aiming to mitigate instances of non-convergence in static calculations.

Table 47 - Whole System Statics parameters.

Object	Max iterations	Tolerance	Min Damping	Max Damping	Case
System	5000	0.02	20	200	All
Line 1	400	1.00E-06	10	100	0 deg
Line 2	400	1.00E-06	10	100	180 deg
Line 3	400	1.00E-06	10	100	180 deg

Source: Author (2024).

Finally, Table 48 presents the OrcaFlex settings used for both the mean offset and DLC 6.1 tension time history for nylon-based systems and Table 49, for alternative mooring system.

Table 48 - OrcaFlex setup for nylon – based system.

OrcaFlex time step (s)	Top chain discretization (segments)	Synthetic section discretization (segments)	Bottom chain discretization (segment)
0.2	2	70	14

Source: Author (2024).

Table 49 - OrcaFlex set up for the alternative mooring system.

OrcaFlex time step (s)	Top chain discretization (segments)	Spring section discretization (segments)	Synthetic section discretization (segments)	Bottom chain discretization (segment)
0.2	4	5	50	20

Source: Author (2024).

3.5 Results

The optimization framework using NSGA2 was executed with Pymoo's default values, as outlined in Table 50. When optimizing the mooring system using time domain simulation to assess tension constraints, termination was determined by the running metric, configured according to Table 51. Conversely, for optimization using statistical linear learning, termination occurred after 240 generations. It is essential to highlight that the direct simulation took 7.5 days, while the statistical learner required only 1.5 days. A comparison was made between optimizing synthetic-based mooring systems using either time-domain simulations or statistical learning and results obtained by West et al. (2023), alongside outcomes for alternative mooring systems incorporating spring polymer. The analysis began by verifying if the selected seed yielded comparable results to those obtained by West et al. (2023). Subsequently, the Pareto frontier formation in mapped and cost-radius spaces was examined. Designs meeting the target Factor of Safety (FoS) comply with safety standards while minimizing material usage and costs. Balancing safety and economy is critical in engineering design. Thus, the FoS of the entire population is calculated to identify designs achieving this equilibrium. The final part of the analysis focused on evaluating the behavior of each design variable versus the radius, highlighting intriguing trends across the population.

Table 50 - Parameters for the NSGA2.

Parameter	Value
Population size	140
Crossover operator	Exponential
Crossover probability	0.9
Crossover distribution index (η)	15
Mutation operator	Exponential
Mutation probability	0.9
Mutation distribution index (η)	20
Elitism	Implicit to NSGA2

Source: Author (2024)

Table 51 - Running metric parameters.

Parameter	Value
Tolerance ('toll')	0.05
Number of generations not considered ('skip')	2
Period ('period')	10

Source: Author (2024)

3.5.1 OrcaFlex Model Assessment

Due to variations in parameter configurations between OrcaFlex and OpenFAST + MoorDyn, the OrcaFlex model was assessed against the OpenFAST + MoorDyn model. Dynamic simulations were performed using the approximate method for designs A, B, and C to calculate safety factors and cost breakdowns. Table 52 shows that the safety factor for the smaller radius (278 m) exceeds the Target Safety Factor, while for the larger radius, it is smaller. This suggests that the extrapolated tension calculated in this study is lower than that calculated by West et al. (2023) for smaller radii. The cost breakdown comparison in Table 53 indicates a relative change within 1%. However, the anchor cost's relative change is within 3% for the smaller radius (278 m), indicating again a smaller tension magnitude in this work compared to that obtained by West et al. (2023).

Table 52 - Safety Factor for the predefined design A, B, and C.

Rad.	Chain Tension [kN]	nylon tension [kN]	Chain MBS [kN]	Synthetic MBS [kN]	Chain FoS	Synthetic FoS	Target Chain FoS	Target Synthetic FoS
278	5,144	5,130	17,907	11,844	3.48	2.31		
340	5,395	5,393	16,693	11,073	3.09	2.05	3.3	2.18
397	5,104	5,095	15,941	10,429	3.12	2.05		

Source: Author (2024).

Table 53 - Breakdown cost comparison.

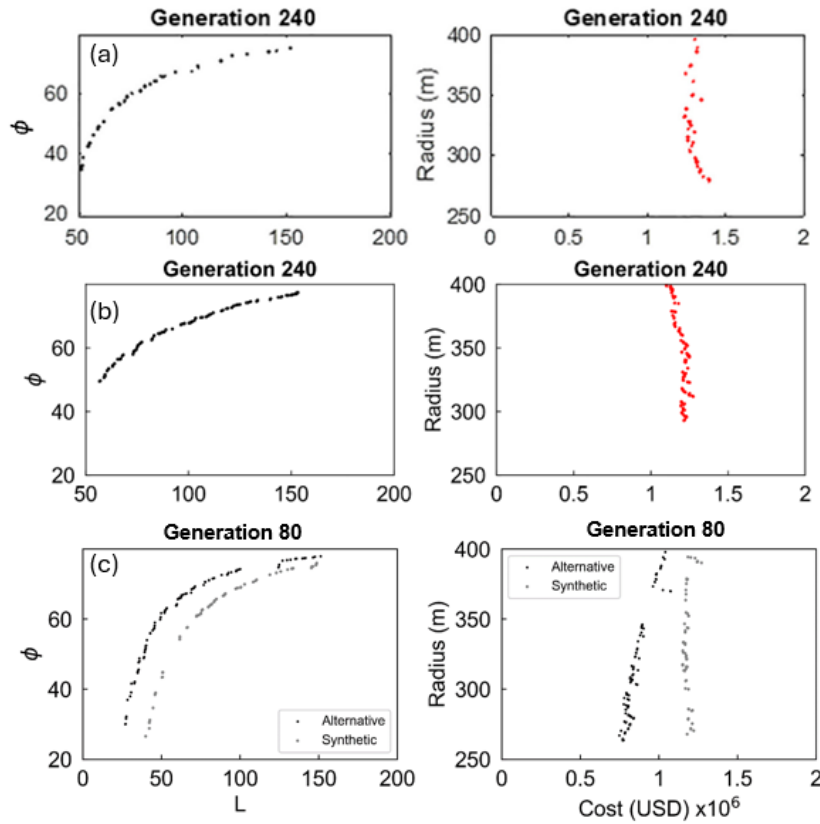
	Radius (m)	Total cost (USD)	Buoy cost (USD)	Synthetic cost (USD)	Chain cost (USD)	Anchor cost (USD)
OpenFAST + MoorDyn	278	1 384 000	478 000	284 000	214 000	408 000
OrcaFlex		1 373 585	484 356	279 862	214 937	394 430
<i>Relative Change</i>		<i>1%</i>	<i>-1%</i>	<i>1%</i>	<i>0%</i>	<i>3%</i>
OpenFAST + MoorDyn	340	1 233 000	305 000	371 000	193 000	364 000
OrcaFlex		1 261 864	309 747	368 694	194 296	389 127
<i>Relative Change</i>		<i>-2%</i>	<i>-2%</i>	<i>1%</i>	<i>-1%</i>	<i>-7%</i>
OpenFAST + MoorDyn	397	1 292 000	310 000	453 000	181 000	348 000
OrcaFlex		1 290 148	312 423	444 429	181 927	351 369
<i>Relative Change</i>		<i>0%</i>	<i>-1%</i>	<i>2%</i>	<i>-1%</i>	<i>-1%</i>

Source: Author (2024).

3.5.2 Objective space analysis

The Pareto fronts of the four simulations are depicted in Figure 35, revealing interesting insights. The cost of the synthetic-based mooring system remains relatively constant at approximately 1.25 million dollars, with the system becoming more economical beyond a radius of 300 m, aligning well with the results obtained by West et al. (2023). In contrast, the cost of the alternative system experiences a significant reduction, indicating the system's potential. Notably, the statistical approach optimization reached a minimum radius of 293 m. This discrepancy can be attributed to the linear regression overestimating tension in the line for smaller radii compared to the values obtained by West et al. (2023). Consequently, the Pareto front in the mapped space is shortened for values of the length L near 50. Conversely, the Pareto front resulting from the direct simulation or time domain simulations extends beyond $L = 50$, suggesting that the estimated tension is lower than that estimated by West et al. (2023), as highlighted in the previous section.

Figure 35 - Pareto frontier in mapped and cost-radius space: (a) West, (b) Statistical Learner, (c) Direct optimization and alternative mooring system optimization.



Source: Author (2024)

Table 54 illustrates the Factor of Safety (FoS) of the final population for the four analyzed methods/systems. In comparison to the FoS obtained by West et al. (2023), the statistical learning approach showed the best adherence. This outcome was expected since the algorithm was run for more generations. On the other hand, optimization using time-domain simulation exhibited greater variability in both the synthetic and alternative systems. For instance, in the synthetic-based system, the coefficient of variation (COV) of the FoS for the chain was 3.51%. This variability can be attributed to using the running metric as a termination criterion, where the maximum generation reached was 80, resulting in a less convergent Pareto frontier. However, by selecting a smaller tolerance in the parameters of the running metric, the COV of the FoS for both systems would be smaller.

Table 54 - Factor of Safety (FoS).

Method/System	Material	Target FoS	Average FoS	Max FoS	Min FoS	FoS COV
OpenFast	Chain	3.30	3.32	3.39	3.30	0.78%
Synthetic-based	Synthetic	2.18	2.19	2.26	2.18	0.62%
Statistical approach	Chain	3.30	3.33	3.46	3.30	0.91%
Synthetic-based	Synthetic	2.18	2.19	2.29	2.18	0.79%
OrcaFlex	Chain	3.30	3.40	3.79	3.30	3.51%
Synthetic-based	Synthetic	2.18	2.20	2.23	2.18	0.58%
OrcaFlex	Chain	3.30	3.47	3.90	3.38	2.21%
Alternative	Synthetic	2.18	2.23	2.35	2.18	1.63%

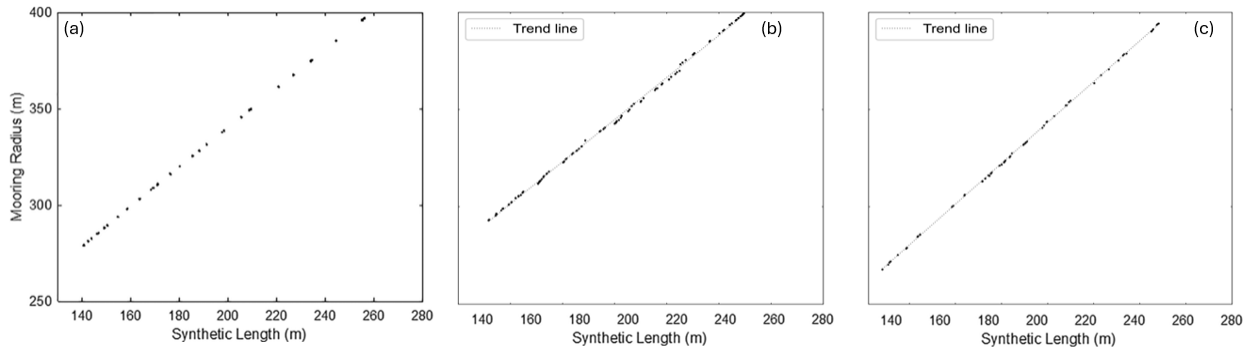
Source: Author (2024)

3.5.3 Design space analysis

3.5.3.1 Synthetic-base mooring system

West et al. (2023) investigated the correlation between the design variables and the mooring radius and cost to understand the relationship between the mooring radius and cost. This investigation served as a basis for comparing the two optimizations of the synthetic-based mooring line conducted in this study. In Figure 36 (a), according to West et al. (2023), the relationship between the radius and the synthetic length appears linear, suggesting the presence of catenary action due to the bottom chain section, which is preserved by the optimizer. Similarly, in Figure 36 (c), a comparable trend is observed for the time-domain simulation. However, Figure 36 (b) shows that using the statistical learner does not capture the catenary behavior well, unlike the time-domain simulations. This discrepancy is likely due to the linear approximation, which may not adequately capture some nonlinearity.

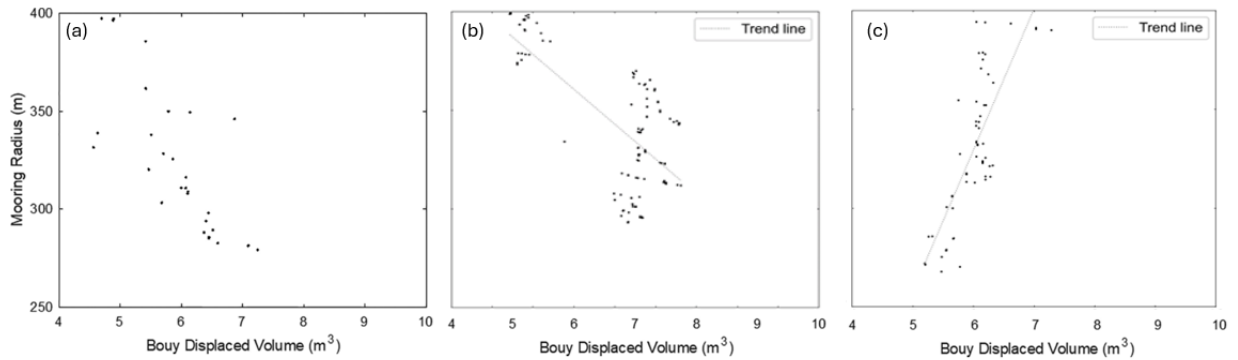
Figure 36 - Radius – synthetic length: (a) West, (b) Statistical learner, (c) Direct optimization.



Source: Author (2024)

From Figure 37 (a), it is evident that West et al. (2023) observed a decrease in buoy displaced volume as the radius decreased. In Figure 37 (b), where the statistical learner approach was employed, a similar trend emerges, albeit with points clustering together, likely due to linear approximation. Figure 37 (c) depicts an inverted trend for the time domain simulation. This deviation may arise from the lower dynamic tension estimated for smaller radii in this study. Consequently, the optimizer favors a shorter line length in such scenarios. It is widely acknowledged that stiffer systems attract more loads. Therefore, when encountering higher loads, the optimizer typically adjusts system stiffness by opting for a longer line length to meet tension constraints. This adjustment was likely observed in optimization by West et al. (2023). Conversely, the optimizer may prefer a shorter line length with smaller tensions or loads, necessitating a smaller buoy to maintain it off the seabed. The observed behavior using the statistical learner approach supports this hypothesis, as the tension or load estimated for smaller radii exceeds that of both the time domain simulation in this study and the analysis conducted by West et al. (2023).

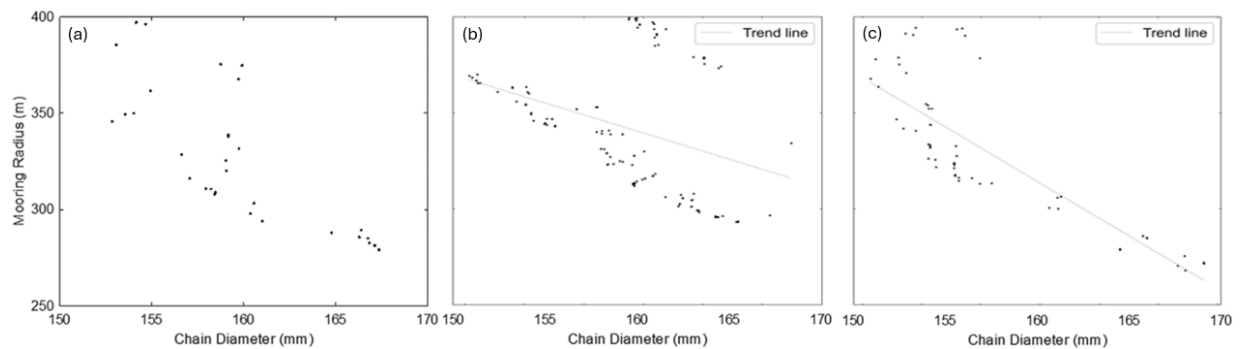
Figure 37 - Radius – buoy displaced volume: (a) West, (b) Statistical learner, (c) Direct optimization.



Source: Author (2024)

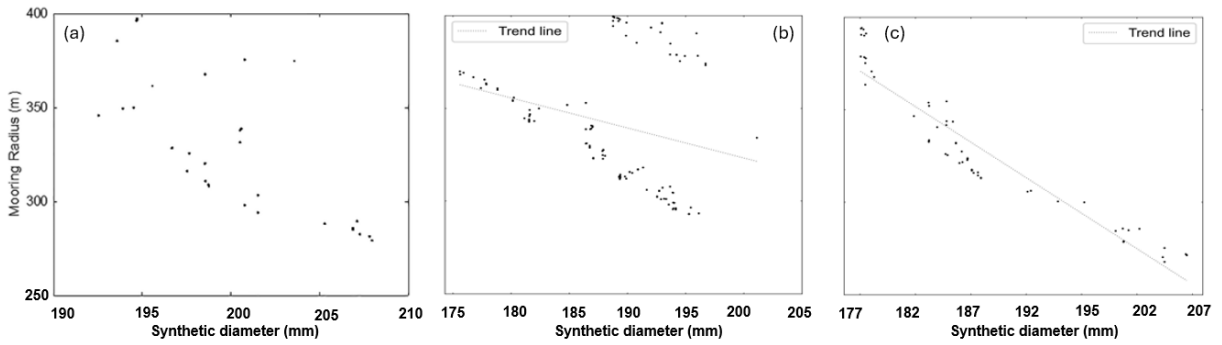
In Figure 38 (a) and Figure 39 (a) West et al. (2023) observed that both the chain diameter and synthetic line decrease with radius. The authors explained that this phenomenon occurs because longer lines have smaller stiffness, thus attracting smaller loads. Consequently, smaller diameters are needed to withstand these reduced loads. Additionally, the line becomes more horizontal as the radius increases, leading to more efficient loading. Figure 38 and Figure 39 both (b) and (c), which depict the statistical learner approach and time domain simulations, respectively, exhibit similar behavior to Figure 38 (a) and Figure 39 (a), respectively.

Figure 38 - Radius – chain diameter: (a) West, (b) Statistical learner, (c) Direct optimization.



Source: Author (2024)

Figure 39 - Radius – Synthetic diameter: (a) West, (b) Statistical learner, (c) Direct optimization.



Source: Author (2024)

3.5.3.2 Constraint assessment of the statistical learner approach

Acknowledging that the constraints $g_6(x)$ and $g_7(x)$ formulated using Equations (28) and (29) might not accurately capture the tension in the line, the results of the statistical learner approach were tested against the violation of these constraints. For this purpose, a six-hour simulation was conducted, each with a different seed, applying the ABS method for the synthetic line, the wave load, and the mean loads for the wave drift, the current, and the wind action to calculate the average maximum dynamic tension in the line. Three representative solutions were chosen, as reported in Table 55:

Table 55 - List of representative design solutions from the statistical learner approach.

Radius (m)	Synthetic Length (m)	Spring Length (m)	Chain Diam (mm)	Synthetic Diam (mm)	Buoy Displaced Volume (m3)	Target Load (kN)
279	133	6	135	175	2.49	3870
340	186	8	136	176	1.67	3910
398	237	12	136	175	2.71	3871

Source: Author (2024)

The results in Table 56 indicate that for a greater radius, the tension is underestimated and violates the constraint $g_6(x)$. This was expected since the linear regression might not capture the behavior of the tension in an accurate manner.

Table 56 - Constraint violation for representative design solutions of the statistical learner.

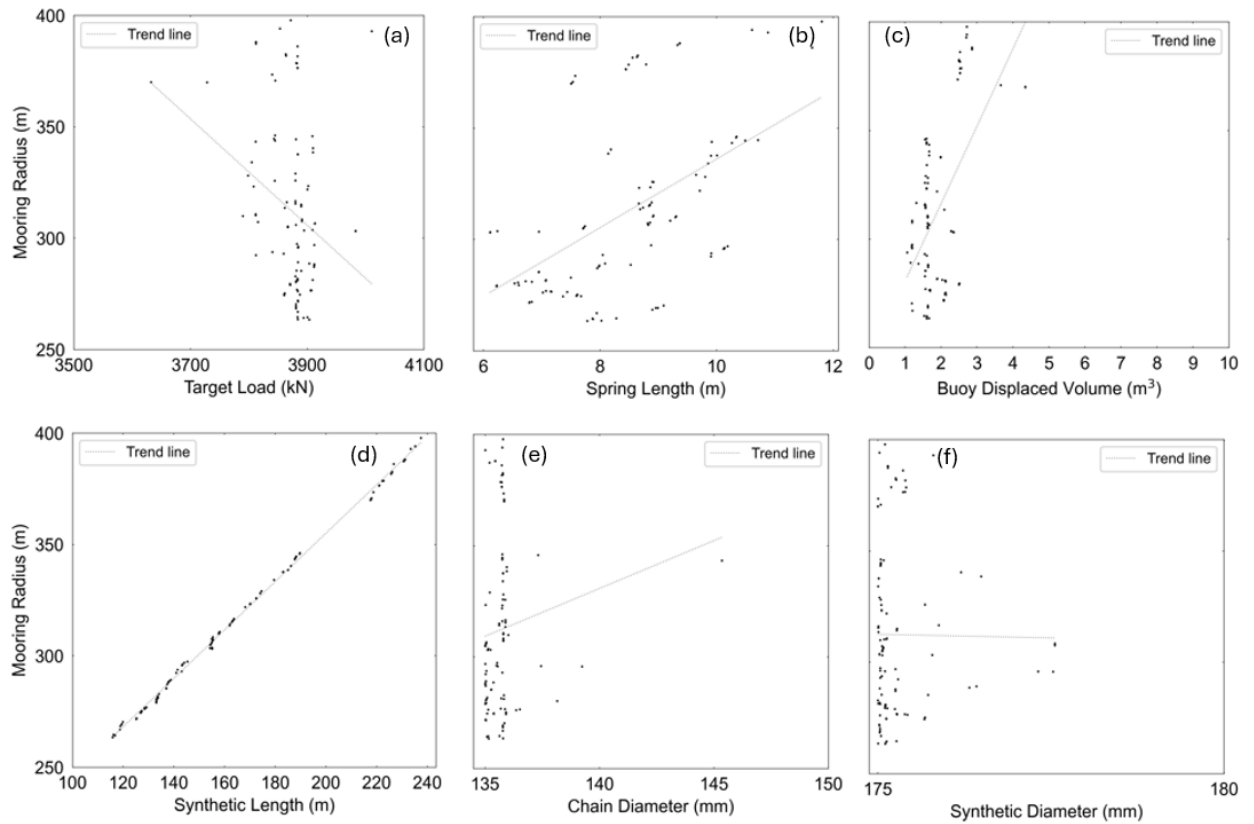
Radius [m]	Diam [mm]	ABS Max Chain Tension [kN]	Chain MBS [kN]	Constraint g₆	FoS	Target FoS
293	158	4900.72	16538.01	-0.0663	3.375	3.3
340	146	4442.71	14754.74	-0.0191	3.321	3.3
397	149	5109.89	15255.2	0.3161	2.985	3.3

Source: Author (2024)

3.5.3.3 Alternative mooring system assessment

In Figure 40 (a), it is observed that the target load converges to around 3900 kN, converging toward the likely maximum static tension associated with the mooring system with the larger radius, according to Table 44. Figure 40 (b) displays a range of spring lengths from 6 to 12 m. Meanwhile, Figure 40 (c) shows the buoy displaced volume converging to 2 m³, primarily influenced by the weight of the bottom chain. Moving on to Figure 40 (d), (e) and (f) show an increasing trend in mooring radius versus synthetic length. Additionally, the convergence of chain and synthetic diameters is seen at 135 mm and 175 mm, respectively. This suggests that the spring component governs line tension, which aligns with expectations. Table 57 shows a representative optimized design geometry consistent with the findings of West et al. (2023). The target load once again reaches 3900 kN, underscoring the dominance of the spring in tension regulation. Moreover, it can be observed that synthetic and spring lengths increase with radius, while the buoy displaced volume converges to 2 m³. Table 58 shows a breakdown of costs, which proportionally increase with radius due to the extended synthetic and spring lengths. Other costs tend to converge toward a constant value. Although greater convergence may be achievable by extending termination criteria periods, the presented results are deemed satisfactory for the purposes of this work.

Figure 40 - Radius vs (a) Target Load, (b) Spring length, (c) Buoy displaced volume, (d) Synthetic length, (e) Chain diameter, (f) Synthetic diameter.



Source: Author (2024).

Table 57 - Representative Design Variable Values.

Radius (m)	Synthetic Length (m)	Spring Length (m)	Chain Diam (mm)	Synthetic Diam (mm)	Buoy Displaced Volume (m³)	Target Load (kN)
279	133	6	135	175	2.49	3,870
340	186	8	136	176	1.67	3,910
398	237	12	136	175	2.71	3,871

Source: Author (2024).

Table 58 - Cost Breakdown.

Mooring radius (m)	Total cost (USD)	Buoy cost (USD)	Synthetic cost (USD)	Chain cost (USD)	Anchor cost (USD)	Spring Cost (USD)
279	837,454	166,831	192,649	138,674	282,087	57,213
340	887,790	111,492	272,530	140,652	287,094	76,022
398	1,040,685	181,555	343,136	140,308	267,092	108,594

Source: Author (2024).

3.6 Conclusion

In this study, the multi-objective optimization framework developed by West et al. (2023) was applied using OrcaFlex to analyze a synthetic-based mooring system, a scenario also examined by West et al. (2023), thereby validating the robustness of the framework's implementation. The method used to select wave loads accounted for the fact that OrcaFlex permits only one seed specification, which may lead to slight sensitivity to the chosen seed.

The primary objective of the optimization framework was to minimize costs across various mooring radii. Two approaches were employed for constraint evaluation: direct optimization via time-domain simulation and a statistical learning method using linear approximation. Analysis of the objective space in length-angle and cost-radius dimensions yielded results consistent with those of West et al. (2023). However, direct optimization showed a leftward shift in the Pareto frontier, indicating potential underestimation of dynamic tension for smaller radii compared to the data from West et al. (2023). Conversely, the statistical approach revealed a 'shortened' Pareto frontier, suggesting a possible overestimation of tension for smaller radii.

Further investigation into the factor of safety across the population revealed greater variability in direct optimization compared to the statistical learning approach, likely due to the fewer generations used in the former. Although the design space generally aligned with the results from West et al. (2023), in direct optimization, an inverted relationship between Radius-Buoy displaced volume was observed, attributed to lower tension estimates for smaller radii in this study. Interestingly, while the statistical learner approach performed reasonably well in terms of the Pareto frontier, an uneven distribution of solutions across the design space was

noted, likely stemming from linear regression inaccuracies. Evaluation of three optimal solutions from the statistical learner approach suggested underestimation of tension for the design with the greater radius, as indicated by a smaller factor of safety compared to the target. This underscores the need for caution in its application, suggesting either analyzing the predominance of design variables that can significantly influence the phenomenon and then utilizing the selected variables for multivariate linear regression. If linear regression is still proven unsatisfactory, employing more sophisticated statistical learning algorithms, such as polynomial regression with a degree greater than 1, or even more advanced methods like Random Forest, Kriging, Neural Network, or XGBoost may be warranted.

Furthermore, direct optimization was conducted for an alternative mooring system incorporating the spring polymer, introducing additional design variables of length and target load. Analysis of the objective space indicated an expected leftward shift in the Pareto frontier due to reduced tension in the line. A linear relationship between cost and radius was observed in the cost-radius dimension, with significantly reduced values compared to the synthetic-based mooring system. Examination of design space variables versus radius revealed convergence of target load, buoy displaced volume, chain diameter, and synthetic diameter toward constant values, consistent with the presumed influence of the polymer spring on tension.

Applying the optimization framework to different systems is not a straightforward task and requires thorough validation. Implementing and validating the framework in OrcaFlex demanded substantial effort and constituted a significant contribution to this study. This process involved meticulous testing and calibration to ensure the accuracy and reliability of the optimization results. Additionally, validating the framework applied to a complex system, such as the one incorporating the polymer spring, represents a novel aspect of this research. Nevertheless, it's crucial to highlight a significant limitation: the framework can solely identify initial design concepts. Once a design is chosen, it must undergo a thorough examination through a complete suite of DLCs recommended by ABS, API, or DNV.

By successfully demonstrating the effectiveness of the optimization framework in analyzing diverse mooring systems, including those with complex components like the polymer spring, this study has paved the way for wider acceptance and utilization of the framework as an automated tool in engineering design. The validation process enhances confidence in the framework's capabilities and establishes a precedent for its application in various real-world scenarios. Ultimately, this contributes to advancing the field of engineering optimization and promoting more efficient and cost-effective design practices.

4 CONCLUSIONS

In this final chapter, a concise summary of the key findings from Chapters 2 and 3 is presented, providing a condensed overview of the research journey. Insights from both chapters are synthesized, elucidating their significance and potential implications. Furthermore, suggestions for future research directions are proposed to inspire further exploration and innovation.

4.1 Summary of Chapter 2

Chapter 2 delves into the promising realm of Floating Wind Energy exploration, particularly focusing on shallow or intermediate water areas. While these environments hold great potential, the key to unlocking their economic viability lies in reducing the levelized cost of energy. This imperative drives the necessity for a substantial decrease in platform and mooring system expenses, which are pivotal cost components in the deployment of floating wind farms.

Anchors and mooring lines emerge as significant contributors to total costs, particularly in shallow waters, where challenges escalate with the scaling up of turbine size. The substantial peak loads experienced by these components not only strain the anchors and lines but also amplify overall project costs. In response to these challenges, synthetic lines such as polyester and nylon have emerged as promising alternatives to traditional catenary chains in mitigating cost burdens in this environment.

However, despite the promise shown by synthetic lines, the existing body of research has predominantly focused on polyester-chain mooring systems, particularly concerning reference 15 MW turbines. This glaring gap in research underscores the need for further investigation. To address this gap, an in-depth exploration into a nylon-chain mooring system, possessing comparable strength to polyester, was undertaken. This investigation centered on a 15 MW turbine positioned atop the VoltturnUS-S platform in the 70-meter-deep waters of the Celtic Sea.

Employing modeling techniques derived from existing literature, the investigation

unveiled a noteworthy 36% reduction in peak loads when utilizing nylon lines compared to polyester. This reduction not only demonstrates the potential for employing smaller anchor and line diameters but also holds the promise of substantially lowering project costs, particularly with the implementation of shared anchor concepts.

While this dissertation contributes valuable insights into the efficacy of materials like nylon in reducing costs and enhancing the economic viability of floating wind energy projects, several challenges persist. These challenges include issues such as excessive rotation and the imperative need for experimental validation of the nylon-line modeling procedure. Addressing these challenges will be instrumental in realizing the full potential of nylon as a viable alternative material in floating wind energy mooring systems, thereby paving the way for greater advancements in the field.

4.2 Summary of Chapter 3

Chapter 3 sheds light on the vast potential of shallow and intermediate waters as ideal settings for floating wind energy projects. However, it also candidly acknowledges the persistent challenges associated with managing peak loads and rotations in such environments. While strides have been made in addressing some of these issues, many still linger, prompting the need for innovative optimization solutions.

In the industrial sector, the optimization of mooring systems remains primarily a manual process, standing in stark contrast to academia's ongoing efforts to automate it, notwithstanding the computational obstacles encountered along the way. This disparity has given rise to the emergence of a multi-objective optimization framework, which aligns more closely with academic pursuits. Within this framework, Load Device Reduction (LDR) has been proposed as a promising avenue for significantly mitigating peak loads and rotations within mooring systems.

This chapter delves into the practical application of the aforementioned framework, utilizing commercial software such as OrcaFlex to implement it. The validation process involves applying it to optimize a 15 MW turbine installed on the VoltturnUS-S platform. Drawing from existing literature, the optimization process employs tools like OpenFast and MoorDyn, necessitating specific seed configurations. However, OrcaFlex's limitation to one

seed configuration presents a unique challenge, requiring a tailored procedure to navigate.

Results from this optimization endeavor encompass both direct optimization through time domain simulation and a statistical learner approach utilizing linear regression. While the statistical approach closely mirrors the baseline, an in-depth analysis of the design space uncovers discrepancies in predicting line tension, underscoring the need for further refinement.

While the framework demonstrates efficacy in optimizing synthetic-based lines, its suitability for more intricate systems incorporating spring polymers remains uncertain. Consequently, the OrcaFlex-implemented framework endeavors to bridge this gap by optimizing an alternative mooring system. This effort reveals promising insights, including the identification of a reasonable Pareto frontier and a discernible linear cost-radius relationship, highlighting the framework's capacity to pinpoint optimized designs at an initial stage.

However, it's imperative to underscore that thorough testing, in accordance with industry standards, is indispensable post-design selection. Additionally, the efficacy of the running metric as a termination criterion is lauded for its ability to provide a nuanced gauge of solution accuracy, complementing traditional visual testing methods.

4.3 Suggestion for future research

The procedure outlined in Chapter 2 for modeling the mechanical behavior of nylon requires testing with either real or scaled-down physical models. However, more advanced implementations of this behavior are underway, incorporating visco-elasto-plastic analytical formulations and an extensive dataset of nylon rope properties. This research is in its initial stages and ongoing, aiming to enhance the dataset, refine analytical formulations, and integrate them into finite element models.

Future research objectives include conducting simulations for other design load cases, such as the Accidental Limit State (ALS) and the Fatigue Limit State (FLS), and considering misaligned wind and wave effects. Additionally, investigating the behavior of a cluster of three turbines sharing an anchor is on the agenda. Control strategy exploration also presents an intriguing avenue for future inquiry.

The optimization carried out in Chapter 3, focusing on the alternative mooring system, can be further evaluated by considering additional design variables, such as elongation-target

load relationships of a different nature or exploring alternative types of load reduction devices. This investigation could extend to deeper waters or involve different line configurations. An analysis to assess the significance of various design variables could help reduce the dimensionality of the design space.

There is still potential for refining the statistical learning approach. Initially, an analysis to identify dominant factors is essential to discard variables with minimal impact on the phenomenon. Then, focusing on the selected variables, exploration of regression methods is advisable for incorporation into a framework customized for reliability-based design optimization. It is recommended to commence with multivariate linear regression before progressing to more advanced techniques, such as polynomial regression with a degree greater than 1. However, evaluating the trade-off between the time required to develop the statistical algorithm and the time saved in conducting reliability-based design optimization is crucial.

5 BIBLIOGRAPHY

ABBAS, N. J. et al. A Reference Open-Source Controller for Fixed and Floating Offshore Wind Turbines. **Wind Energy Science**, v. 7, n. 1, p. 53–73, 2021.

ABS. **Guidance Notes on the Application of Fiber Rope for Offshore Mooring**. ABS: Spring, TX, USA, 2021.

ABS. **Requirements for Position Mooring Systems**. ABS: Spring, TX, USA, 2023.

ACHMUS, M. et al. Un- and reloading stiffness of monopile foundations in sand. **Applied Ocean Research**, v. 84, p. 62–73, 1 Mar. 2019.

ALLEN, C. et al. Definition of the UMaine VoltturnUS-S Reference Platform Developed for the IEA Wind 15-Megawatt Offshore Reference Wind Turbine. National Renewable Energy Laboratory, Golden CO. <https://doi.org/10.2172/1660012>. NREL/TP-5000-76773. 2020.

AL-SOLIHAT, M. K.; NAHON, M. Stiffness of slack and taut moorings. **Ships and Offshore Structures**, v. 11, n. 8, p. 890–904, 16 Nov. 2016.

AMARAL, G. A.; PESCE, C. P.; FRANZINI, G. R. Mooring system stiffness: A six-degree-of-freedom closed-form analytical formulation. **Marine Structures**, v. 84, n. 103189, p. 103189, 1 Jul. 2022.

API. **API RP 2SM: Recommended Practice for Design, Manufacture, Installation, and Maintenance of Synthetic Fiber Ropes for Offshore Mooring**. API: Washington, DC, USA, 2014.

API. **Design and Analysis of Stationkeeping Systems for Floating Offshore Structures**. API: Washington, DC, USA, 2018.

ARYAWAN, I. et al. **Potential Mooring System Optimization Using Polymer Spring Component – Floating Offshore Wind Turbine Application**. Proceedings of the Annual Offshore Technology Conference. **Anais...Offshore Technology Conference**, 2023.

BENASSAI, G. et al. Optimization of Mooring Systems for Floating Offshore Wind Turbines. **Coastal Engineering Journal**, v. 57, n. 4, 1 Dec. 2015.

BLANK, J.; DEB, K. **A Running Performance Metric and Termination Criterion for Evaluating Evolutionary Multi-and Many-objective Optimization Algorithms**. IEEE Congress on Evolutionary Computation (CEC). **Anais...Glasgow, UK.: IEEE**, Jul. 2020. Available online: <<https://pymoo.org>.>

BROMMUNDT, M. et al. **Mooring system optimization for floating wind turbines using frequency domain analysis**. Energy Procedia. **Anais...Elsevier Ltd**, 2012.

BULJAN, A. **offshoreWIND.biz**. Available online: <<https://www.offshorewind.biz/2021/05/14/equinor-funding-shallow-water-floating-wind-mooring-project-in-us/>>. Accessed: 29 Nov. 2022.

BULJAN, A. **offshoreWIND.biz**. Available online: <<https://www.offshorewind.biz/2022/11/16/vestas-15-mw-prototype-turbine-taking-shape-nacelle-arrives-at-test-site/>>. Accessed: 7 Dec. 2022.

CASTILLO, F. T. S. **Floating Offshore Wind Turbines: Mooring System Optimization for LCOE Reduction**. Master of Science Thesis—STOCKHOLM: KTH School of Industrial Engineering and Management, 23 Oct. 2020.

CHEVILLOTTE, Y. et al. Fatigue of improved polyamide mooring ropes for floating wind turbines. **Ocean Engineering**, v. 199, p. 107011, 1 Mar. 2020.

CHEVILLOTTE, Y. **Characterization of the long-term mechanical behavior and the durability of polyamide mooring ropes for floating wind turbines**. Thesis—Brest (Fra): ENSTA Bretagne - École nationale supérieure de techniques avancées Bretagne, 19 jun. 2021.

DEB, K.; AGRAWAL, S. **A Niche-Penalty Approach for Constraint Handling in Genetic Algorithms**. Artificial Neural Nets and Genetic Algorithms. **Anais...** Vienna.: Springer, 1999.

DEPALO, F. et al. Effects of dynamic axial stiffness of elastic moorings for a wave energy converter. **Ocean Engineering**, v. 251, p. 111132, 1 May 2022.

DET NORSKE VERITAS. **DNV RP C205: Recommended practice environmental conditions and environmental loads**. DET NORSKE VERITAS AS, Høvik, Norway, 2010.

DET NORSKE VERITAS. **DNVGL RP E305: Design, testing and analysis of offshore fibre ropes**. DET NORSKE VERITAS AS, Høvik, Norway, 2015.

DEVIN, M. C. et al. Optimizing the Cost and Reliability of Shared Anchors in an Array of Floating Offshore Wind Turbines. **ASCE-ASME Journal of Risk and Uncertainty in Engineering Systems, Part B: Mechanical Engineering**, v. 7, n. 4, p. 1.4051163, 1 Dec. 2021.

DIAZ, B. D. et al. Multiline anchors for floating offshore wind towers. **OCEANS 2016 MTS/IEEE Monterey, OCE 2016**, p. 7761374, 28 Nov. 2016.

EMPRESA DE PESQUISA ENERGÉTICA. **Roadmap Eólica Offshore Brasil**. Available online: <https://www.epe.gov.br/sites-pt/publicacoes-dados-abertos/publicacoes/PublicacoesArquivos/publicacao-456/Roadmap_Eolica_Offshore_EPE_versao_R2.pdf>. Accessed: 24 Jan. 2024.

FERREIRA, F. M. G. et al. Using Design of Experiments and Design Optimization to Determine Statically Equivalent Mooring System on Truncated Water Depth. **Journal of Offshore Mechanics and Arctic Engineering**, v. 139, n. 4, p. 041302, 2017.

FLEMING, P. A. et al. Field-test results using a nacelle-mounted lidar for improving wind turbine power capture by reducing yaw misalignment. **Journal of Physics: Conference Series**, v. 524, n. 1, p. 012002, 2014.

FONTANA, C. M. et al. Multiline anchor force dynamics in floating offshore wind turbines. **Wind Energy**, v. 21, n. 11, p. 1177–1190, 1 Nov. 2018.

GAERTNER, E. et al. Definition of the IEA 15-Megawatt Offshore Reference Wind Turbine. National Renewable Energy Laboratory, Golden, CO. <https://doi.org/10.2172/1603478>. NREL/TP-5000-75698. 2020.

GOV.BR. **Portal vai unificar tramitação de empreendimentos de energia offshore**. Available online: <<https://www.gov.br/pt-br/noticias/energia-minerais-e-combustiveis/2022/10/portal-vai-unificar-tramitacao-de-empreendimentos-de-energia-offshore>>. Accessed: 24 Jan. 2024.

GÖZCÜ, O.; KONTOS, S.; BREDMOSE, H. Dynamics of two floating wind turbines with shared anchor and mooring lines. **Journal of Physics: Conference Series**, v. 2265, n. 4, 2 Jun. 2022.

HALL, M. **MoorDyn User's Guide**. University of Maine, Orono, ME, USA, 2015.

HALL, M. T. J. **Mooring Line Modelling and Design Optimization of Floating Offshore Wind Turbines**. Master Thesis—Victoria, British Columbia, Canada: University of Victoria, 2013.

HUNTLEY, M. B. Fatigue and Modulus Characteristics of Wire-Lay Nylon Rope. **OCEANS 2016 MTS/IEEE Monterey**, p. 7761501, 2016.

IEA. **Renewable Energy Market Update Outlook for 2022 and 2023.**, 2022. Available online: <<https://www.oecd.org/publications/renewable-energy-market-update-faf30e5a-en.htm>>. Accessed: 22 May 2024

IEC. **IEC 61400–3 Design Requirements for Offshore Wind Turbines**. IEC: Geneva, Switzerland., 2019.

IKHENNICHEU, M. et al. **Corewind Review of the state of the art of mooring and anchoring designs, technical challenges and identification of relevant DLCs.**, 2020. Available online: <<https://corewind.eu/wp-content/uploads/files/publications/COREWIND-D2.1-Review-of-the-state-of-the-art-of-mooring-and-anchoring-designs.pdf>>. Accessed: 22 May. 2024

KAI-TUNG MA et al. **Mooring System Engineering for Offshore Structures**. Cambridge, MA, USA: Elsevier, 2019.

KUNAPULI, G. **Ensemble Methods for Machine Learning**. Shelter Island, NY, USA: Manning Publications Co, 2023.

LI, L. et al. Design optimization of mooring system: An application to a vessel-shaped offshore fish farm. **Engineering Structures**, v. 197, 15 out. 2019.

LOZON, E. et al. **Design and Analysis of a Floating-Wind Shallow-Water Mooring System Featuring Polymer Springs**. In: **ASME 2022 4th International Offshore Wind Technical. Ocean, Offshore and Arctic Engineering Division**. 2022. Available online: <<https://www.nrel.gov/docs/fy23osti/83342.pdf>> Accessed: 23 May 2024

MCEVOY, P.; JOHNSTON, E.; MARINE, T. **Polymer Mooring Component for Offshore Renewable Energy**. In **Offshore Technology Conference**. Houston, Texas, USA: 2019.

MCEVOY, P.; KIM, S. **Mooring load management for SR2000 floating tidal device using non-linear polymer components**. In **12th European Wave and Tidal Energy Conference**. URL: https://uploads-ssl.webflow.com/5f8964a5a533790d6cc8820a/5f96cb7a8ba32845a778cb9e_EWTEC-2017.pdf. (Accessed 29 September 2023). 2017. Available online: <https://uploads-ssl.webflow.com/5f8964a5a533790d6cc8820a/5f96cb7a8ba32845a778cb9e_EWTEC-2017.pdf>. Accessed: 28 Sep. 2023

NREL. **OpenFAST Documentation Release v2.3.0**. National Renewable Energy Laboratory, Golden, CO, USA, 2020.

ORCINA. L02 OC4 Semi-sub. Available online: < <https://www.orcina.com/wp-content/uploads/examples/l/l02/L02%20OC4%20Semi-sub.pdf>>. (Accessed 29 September 2023). 2023a.

ORCINA. K03 15MW Semi-sub FOWT. URL: <https://www.orcina.com/wp-content/uploads/examples/k/k03/K03%2015MW%20semi-sub%20FOWT.pdf>. (Accessed 29 September 2023). 2023b.

ORCINA. **OrcaFlex documentation**. Available online: <<https://www.orcina.com/resources/documentation/>>. Accessed: 25 May 2024.

PHAM, H. D. et al. Dynamic modeling of nylon mooring lines for a floating wind turbine. **Applied Ocean Research**, v. 87, p. 1–8, 1 Jun. 2019.

PILLAI, A. C. et al. Anchor loads for shallow water mooring of a 15 MW floating wind turbine — Part I: Chain catenary moorings for single and shared anchor scenarios. **Ocean Engineering**, p. 111816, 2022a.

PILLAI, A. C. et al. Anchor loads for shallow water mooring of a 15 MW floating wind turbine—Part II: Synthetic and novel mooring systems. **Ocean Engineering**, v. 266, 15 Dec. 2022b.

QUIGGIN P.P. **2015 OrcaFlex QA Testing and Validation Document 99/005:7**. Available online: < <https://www.orcina.com/wp-content/uploads/resources/validation/99-005-OrcaFlex-QA-Testing-and-Validation.pdf>>. Accessed: 24 May 2024.

ROSS, A. **Orcina Project 1405 Wind Turbine Validation Report Client**. Available online:< <https://www.orcina.com/wp-content/uploads/resources/validation/R14050101-Wind-Turbine-Validation-Report.pdf>>. Accessed: 24 May 2024.

SPEHT, R. **Windpower Engineering and Development**. Available online: <<https://www.windpowerengineering.com/ready-to-float-a-permanent-cost-reduction-for-offshore-wind/>>. Accessed: 19 May 2024.

THE CROWN ESTATE. **Offshore Engineer**. Available online: <<https://www.oedigital.com/news/500062-uk-the-crown-estate-gives-update-on-celtic-sea-floating-wind-seabed-leasing-process>>. Accessed: 29 Nov. 2022.

VARNEY A. S.; TAYLOR R.; SEELIG W. **Evaluation of Wire-Lay Nylon Mooring Lines in a Wave Energy Device Field Trial**. 2013 OCEANS - San Diego. **Anais...IEEE**, 2013.

VERDE, S.; LAGES, E. N. A comparison of anchor loads, planar displacement, and rotation for nylon and polyester moored systems for a 15 MW floating wind turbine in shallow water. **Ocean Engineering**, v. 280, 15 Jul. 2023.

VRYHOF. **Anchor manual: the guide to anchoring.**, 2018.

WELLER, S. D. et al. Synthetic mooring ropes for marine renewable energy applications. **Renewable Energy**. Elsevier Ltd, 29 Jul. 2015.

WEST, W. et al. Development of a Multi-Objective Optimization Tool for Screening Designs of Taut Synthetic Mooring Systems to Minimize Mooring Component Cost and Footprint. **Modelling**, v. 2, n. 4, p. 728–752, 8 Dec. 2021.

WEST, W. M. et al. The Influence of Synthetic Mooring Line Stiffness Model Type on Global Floating Offshore Wind Turbine Performance. **Journal of Physics: Conference Series**, v. 1452, n. 1, p. 012044, 3 Mar. 2020.

WEST, W. M. et al. Determination of minimum-cost synthetic mooring systems for large floating wind turbines deployed in intermediate water depths. **Journal of Renewable and Sustainable Energy**, v. 15, n. 1, 1 Jan. 2023.

WILLIAMS, R.; MARTINEZ PALACIO, A.; ZHAO, F. **GLOBAL OFFSHORE WIND REPORT**. Available online: <<https://gwec.net/wp-content/uploads/2023/08/GWEC-Global-Offshore-Wind-Report-2023.pdf>>. Accessed: 24 Jan. 2024.

XU, K. et al. Design and comparative analysis of alternative mooring systems for floating wind turbines in shallow water with emphasis on ultimate limit state design. **Ocean Engineering**, v. 219, p. 108377, 1 Jan. 2021a.

XU, S. et al. Experimental evaluation of the dynamic stiffness of synthetic fibre mooring ropes. **Applied Ocean Research**, v. 112, p. 102709, 1 Jul. 2021b.